A multi-color technique for surface temperature measurements in the presence of reflected radiation

Andrew G. Jackson

To the Graduate Council:

I am submitting herewith a thesis written by Andrew G. Jackson entitled "A multi-color technique for surface temperature measurements in the presence of reflected radiation." I have examined the final electronic copy of this thesis for form and content and recommend that it be accepted in partial fulfillment of the requirements for the degree of Master of Science, with a major in Mechanical Engineering.

<div align="right">Firouz Shahrokhi, Major Professor</div>

We have read this thesis and recommend its acceptance:

W. K. McGregor, Roy Schulz

<div align="right">Accepted for the Council:
<u>Carolyn R. Hodges</u></div>

<div align="right">Vice Provost and Dean of the Graduate School</div>

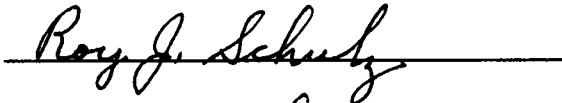(Original signatures are on file with official student records.)

To the Graduate Council:

I am submitting herewith a thesis written by Andrew G. Jackson
entitled "A Multicolor Technique for Surface Temperature
Measurements in the Presence of Reflected Radiation." I have
examined the final copy of this thesis for form and content
and recommend that it be accepted in partial fulfillment of
the requirements for the degree of Master of Science with a
Major in Mechanical Engineering.

_____
Firouz Shahrokhi, Major Professor

We have read this thesis
and recommend its acceptance:

_____

_____

Accepted for the Council:

_____
Vice Provost and Dean
of the Graduate School

STATEMENT OF PERMISSION TO USE

In presenting this thesis in partial fulfillment of the requirements for a Master's degree at The University of Tennessee, Knoxville, I agree that the Library shall make it available to borrowers under rules of the Library. Brief quotations from this thesis are allowable without special permission, provided that accurate acknowledgment of the source is made.

Permission for extensive quotation from or reproduction of this thesis may be granted by my major professor, or in his absence, by the Head of Interlibrary Services when, in the opinion of either, the proposed use of the material in this thesis is for scholarly purposes. Any copying or use of the material in this thesis for financial gain shall not be allowed without my written permission.

Signature _Andrew Jackson_

Date _12/22/90_

A MULTI-COLOR TECHNIQUE FOR SURFACE

TEMPERATURE MEASUREMENTS IN THE

PRESENCE OF REFLECTED RADIATION

A Thesis

Presented for the

Master of Science

Degree

The University of Tennessee, Knoxville

Andrew G. Jackson

May 1991

DEDICATION

To God,

        who gave me life.

To Linda,

        who shares my life.

To Shara,

        whose excitement for life is
        undimmed.

To Joseph,

        whose energy and enthusiasm are a
        model for others.

To Benjamin,

        who derives such joy from the simple
        things in life.

To Spencer,

        whose love and sweetness is
        unsurpassed by mortals.

ACKNOWLEDGMENTS

ABSTRACT

Infrared pyrometry is used as a non-intrusive technique to assess surface temperatures when conventional temperature measurements are not feasible. Turbine engine internal hot part surface temperatures are important in understanding many aspects of the design and operation of aircraft engines such as structural integrity, life, and IR signatures. The problem of assessing engine internal temperatures is similar to the problem of measuring surface temperatures in a non-isothermal cavity. Radiometric measurements made of surfaces within such a cavity include reflected radiation incident to the surface of interest. This incident radiation can cause errors in temperatures determined from the radiometric measurements.

A three-color radiance measurement technique is described for determining the surface temperature of a heated target that is reflecting radiation from an adjacent surface. Radiance measurements are made in three wavelength bands. If the surface behaves as a graybody, the three-color technique can correct for the errors induced by reflected radiation. An experiment was performed to demonstrate the three-color technique for a simple case, and the results are reported.

iv

The three-color technique was shown to be highly sensitive to non-gray behavior. Application of the three-color technique with corrections for non-gray behavior resulted in temperature measurement errors less than 2 percent in the presence of reflected radiation. Conventional ratio pyrometry (two colors) resulted in temperature measurement errors greater than 10 percent in the presence of reflected radiation.

TABLE OF CONTENTS

vi

LIST OF FIGURES

LIST OF TABLES

NOMENCLATURE

a	multiplier in the approximation $N = aT^b$.
b	exponent in the approximation $N = aT^b$.
B	Radiosity, $B = E + pH$.
B.B.	Blackbody
$Bi_{\lambda j}$	Radiosity of surface i measured at wavelength λj.
BRDF	Bidirectional reflectance distribution function.
c	Speed of light in a vacuum.
c_o	Speed of light through a medium.
c1	Planck's first radiation constant.
c2	Planck's second radiation constant.
C	Celsius, an interval temperature scale.
D	Detectivity.
D^*	Normalized Detectivity.
e	Napier's constant, $e = 2.71828$ (base for natural logarithm.
E(T)	Radiant emissive power of a surface at temperature T.
Eb(T)	Radiant emissive power of a blackbody at temperature T.
$Eb(\lambda, T)$	Spectral radiant emissive power of a blackbody at wavelength λ, and temperature T.
FOV	Field of view.
%FOV	Fraction of FOV that is filled by target.
f	Frequency (pertaining to the wavelike nature of electromagnetic radiation).

F_{2-1}	Shape factor (view factor) of surface 2 to surface 1.
F_λ	Filter transmittance at wavelength λ.
g	Geometry factor ($g = pF_{2-1}$).
H	Incident radiation.
I.C.	Influence coefficient.
K	Kelvin, an absolute temperature scale.
ln	Natural logarithm.
m	Slope in the emissivity curve as a function of wavelength.
mv	Millivolts.
n	Index of refraction ($n = c/c_o$).
N	Radiance.
$Nb(\lambda,T)$	Spectral radiance of a blackbody at wavelength λ, and temperature T.
NEP	Noise equivalent power.
N.G.I.	Non-gray index.
N_o	Radiance measured with no reflections present.
N_r	Radiance measured with reflections present.
$N\lambda a,\lambda b$	Inband radiance in the interval λa to λb.
nm	Nanometer (10^{-9} meter).
p	Reflectance.
pH%	Percent reflected energy.
R	Radiance ratio.

R_{ij}	Radiance ratio computed from $N_{\lambda i}/N_{\lambda j}$.
$R\lambda$	Instrument response at wavelength λ.
R_v	Detector responsivity.
S/N	Signal to noise ratio.
sr	Steradian.
T	Temperature.
T_a	Apparent temperature.
T_{true}	Actual or true surface temperature.
λ	Lambda, wavelength of radiation.
λa	Lower half-power point.
λb	Upper half-power point.
λc	Center wavelength.
α	Absorptance.
π	Pi (3.14159).
σ	Stefan-Boltzman constant (5.66925×10^{-8} watts $m^{-2}K^{-4}$).
μm	Micron (10^{-6} meter).
τ	Transmittance.
θ	Angle from surface normal.
δ	Wavelength separation (ratio pyrometry).
ϕ	Azimuth angle.
ϵ	Emissivity
ϵ_λ	Spectral emissivity

CHAPTER I

INTRODUCTION

Internal hot part surface temperatures are impor-
tant in understanding many aspects of the design and
operation of aircraft turbine engines including struc-
tural integrity, life, and IR signatures. The problem
of assessing engine internal temperatures is similar to
the problem of measuring surface temperature in a non-
isothermal cavity.

Infrared pyrometry is used as a non-intrusive tem-
perature measurement technique where high temperatures
are involved and where environmental factors render con-
ventional temperature measurement techniques (i.e. ther-
mocouples, thermistors, etc.) of limited use. The
infrared pyrometry technique, however, can result in
significant measurement errors if the emissive proper-
ties of the surface are not well known and if the sur-
face of interest is reflecting radiation from another
source.

This experiment is part of an effort to develop
turbine engine diagnostic techniques that will provide
meaningful and useful surface temperature measurements.
The focus of the experiment is to consider the errors
that reflected radiation can induce on infrared surface
temperature measurements.

1

The objective of the experiment reported herein is to investigate a surface temperature measurement technique that will not require a priori knowledge of the surface properties and will correct for errors that may be introduced by the presence of radiation originating from a source hotter than the target. The technique requires radiance measurements at three different wavelength bands (three-colors) and will be referred to hereafter as the three-color technique or three-color method. The information gathered through such measurements is sufficient to formulate a correction to the measured surface temperature to account for the reflected radiation from a hotter surface. Absolute temperature measurements within ± 5 percent are desired (± 30 K at 623 K [350 °C]).

The three-color method assumes that the surface to be measured behaves as a graybody and a diffuse emitter. Available data from contemporary engine nozzle surfaces suggest that this assumption may be appropriate over carefully chosen wavelength intervals. It is also assumed that all of the energy incident on the target can be considered to emanate from a single source. It is recognized that these assumptions may not be valid for application of the three-color method to turbine engine hot part measurements, but these assumptions are made in order to simplify the investigation of the

three-color technique and determine whether further investigation is warranted.

This demonstration of the three-color technique used a simple flat plate target. The target surface was a heated aluminum plate that had been instrumented with thermocouples to determine an indicated bulk metal temperature. True target surface temperature was considered to be the bulk metal temperature adjusted for a temperature gradient across the plate. Blackbody radiation is used as a source of reflected energy, providing incident radiation at 900° C and at 1000° C.

A discussion of the fundamentals of radiation theory will be presented in Chapter II. Methods for single-color and two-color radiometric measurements will be discussed. The concept of single-color measurements using the "lowest feasible wavelength" will be discussed. The concept of "minimum wavelength separation" for two-color measurements will be introduced and discussed. The three-color radiometric measurement technique will be introduced and explained in Chapter III. The apparatus and procedure used to demonstrate the three-color technique will be presented in Chapters IV and V. Solutions with the three color technique will be compared with two-color solutions and single-color solutions in Chapter VI, followed by conclusions and recommendations in Chapter VII.

CHAPTER II

RADIOMETRIC TEMPERATURE MEASUREMENT THEORY

Review of Radiation Theory

Any object that is at a temperature above absolute zero (0 K or -273° C) radiates energy in the form of electromagnetic radiation to its surroundings. The surroundings in turn (if above 0 K) radiate energy to the object. The object is said to be in equilibrium if the energy leaving the object is equal to the energy entering the object. Equilibrium also implies that the temperature of the object is not changing with time. For the purpose of this discussion, objects will be considered to be in equilibrium unless otherwise specified.

Electromagnetic radiation is typically characterized by the wavelength of the radiation from the relation:

$$\lambda = \frac{c}{f} \qquad \text{eq. 2.1}$$

where:

λ = wavelength
f = frequency
c = speed of light

The units for wavelength are typically microns

(μm = 10^{-6} meters) or nanometers (nm = 10^{-9} meters).
Thermal radiation is commonly defined as the electromag-
netic radiation in the band from 0.3 to 50 μm and
includes all or part of three sub-ranges, the ultravio-
let, the visible, and the infrared. These sub-ranges
are illustrated in Figure 2.1. (Sparrow, p.4).

In the year 1900, Max Planck ushered in the era of
quantum physics by successfully deriving a formula for
the radiation emitted by an object. (Halliday, p. 762).
The total amount of radiation emitted from a surface
into the hemisphere above the surface at all wavelengths
is referred to as the total hemispherical radiation
given by the equation:

$$E(T) = \int_0^{\infty} \epsilon_\lambda E_b(\lambda T)\, d\lambda \qquad \text{eq. 2.2}$$

where:

$$E_b(\lambda T) = \frac{c1}{n^3 \lambda^5 (e^{c2/n\lambda T} - 1)} \qquad \text{eq. 2.3}$$

ϵ_λ = spectral emissivity of the surface
$E_b(\lambda T)$ = Planck's equation
c1 = first radiation constant
c2 = second radiation constant
n = index of refraction
λ = wavelength

5
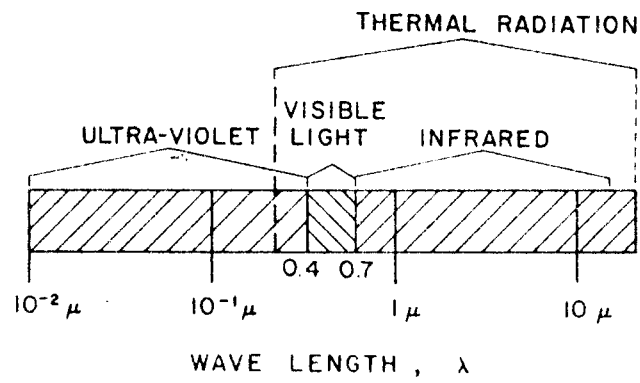
Figure 2.1 Classifications of Radiation.

Values for Planck's first and second radiation constants are given in Table 2.1. (Gubareff p.10,11).

The index of refraction for a given medium is: (Sparrow, p. 4).

$$n = \frac{c}{c_o}$$ eq. 2.4

c = speed of light in a vacuum
c_o = speed of light through the medium

Since the value of n is exactly 1.0 in a vacuum and approximately 1.0003 in air (Halliday p. 670), n is often omitted from Planck's equation. The output of equation 2.2 is referred to as Radiance, Radiancy, Radiant Power, Radiant Emissive Power, Emittance, ad infinitum and similarly it seems that many symbols have been used to represent this quantity. The author prefers the term Radiant Power (E) to describe radiation into a hemisphere above a surface, and the term Radiance (N) to describe the Radiant Power per unit solid angle (steradian). The units for Radiant Power depend on the form of Planck's first radiation constant used as shown in Table 2.1.

The Planck function can be generalized as a function of the single variable $(n\lambda T)$. (Sparrow p. 6).

Table 2.1   Planck's First and Second Radiation
Constants

c1	c2	Output Units	Reference
$1.187 \cdot 10^8$ $\dfrac{Btu \cdot \mu m^4}{hr \cdot ft^2}$	$2.5896 \cdot 10^4$ $\mu m \cdot {}^\circ R$	$\dfrac{Btu}{hr \cdot ft^2 \cdot \mu m}$	Holman p. 289
$3.74126 \cdot 10^{-5}$ $\dfrac{erg \cdot cm^2}{sec}$	1.4388 $cm \cdot K$	$\dfrac{erg}{cm^3}$	Gubareff p. 8
$3.740 \cdot 10^{-5}$ $\dfrac{erg \cdot cm^2}{sec}$	1.4387 $cm \cdot K$	$\dfrac{erg}{cm^3}$	Sparrow p. 5
$1.191062 \cdot 10^8$ $\dfrac{watts \cdot \mu m^4}{sr \cdot m^2}$	1.438786 $\mu \cdot K$	$\dfrac{watts}{\mu m \cdot sr \cdot m^2}$	Nutter p. 8

8

$$\frac{Nb(\lambda T)}{n^3 T^5} = \frac{c1}{(n\lambda T)^5 (e^{c2/n\lambda T} - 1)} \qquad \text{eq. 2.5}$$

or if n = 1.0

$$\frac{Nb(\lambda T)}{T^5} = \frac{c1}{(\lambda T)^5 (e^{c2/\lambda T} - 1)} \qquad \text{eq. 2.6}$$

This form of the Planck function is shown in Figure 2.2.

Radiation properties

Planck's equation describes the theoretical maximum energy that can be emitted by a surface at a given temperature (T). An object emitting this amount of energy is called a blackbody. The ratio of energy emitted by a given surface to the energy emitted by a blackbody is called the emissivity (ϵ).

$$\epsilon = E/E_b \qquad \text{eq. 2.7}$$

E = energy emitted by real surface at T

E_b = energy emitted by blackbody at T

Three additional terms used to describe the radiative properties of surfaces are absorptance α, the fraction of incident radiation absorbed by the surface;

9
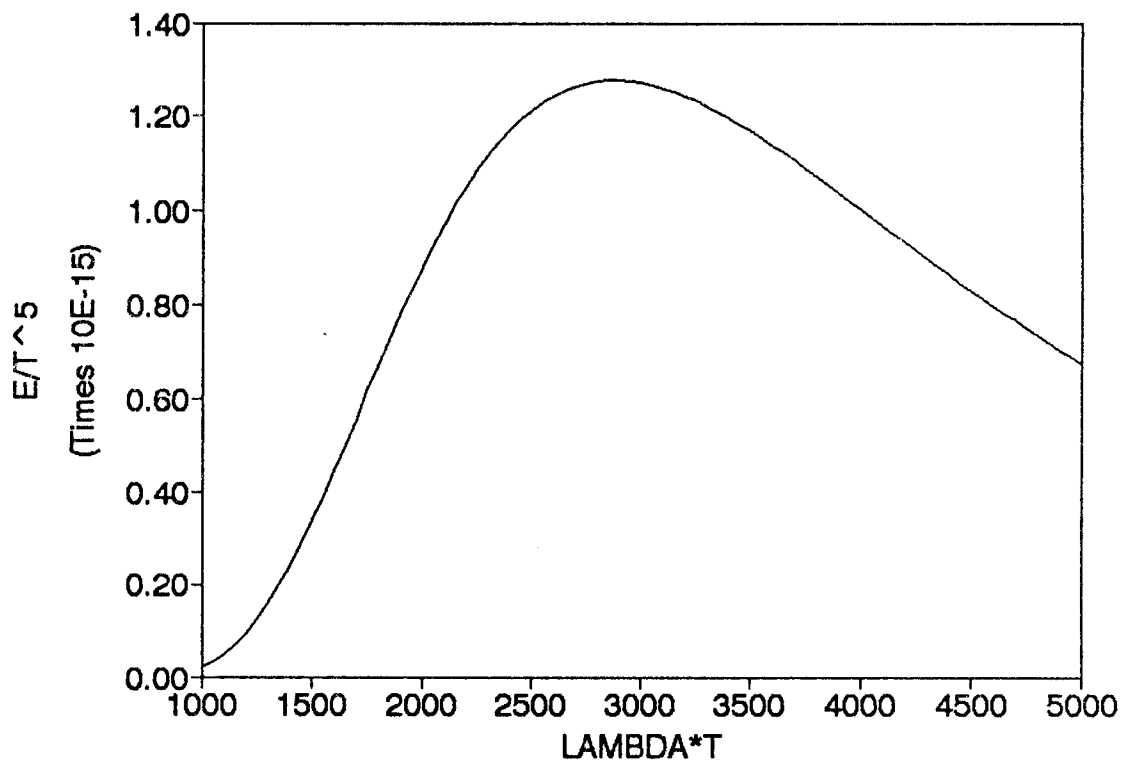
Figure 2.2   Planck's Law as a Function of the Single
             Variable (λT).

reflectance p, the fraction of incident energy reflected by the surface; and transmittance r, the fraction of incident energy transmitted through the surface. From the principle of conservation of energy it follows that:

$$\alpha + p + r = 1 \qquad \text{eq. 2.8}$$

If an object is opaque then:

$$\alpha + p = 1 \qquad \text{eq. 2.9}$$

Furthermore, Kirchoff's Law states that for a special case called a diffuse graybody, absorptance equals emissivity. (Sparrow, p. 41).

$$\alpha = \epsilon \qquad \text{eq. 2.10}$$

Blackbody radiation

A blackbody is defined as a body with a surface that has the characteristics

$$\alpha = \epsilon = 1$$

A true blackbody can not be constructed but a reasonable approximation is found in an isothermal cavity with a relatively small aperture. A ray of radiant energy entering the cavity through the aperture will be reflected and re-reflected within the cavity

until most of the energy is absorbed as shown in Figure 2.3. (Gubareff, p. 4).

Blackbodies are sometimes referred to as cavity radiators; however, the blackbody radiation is considered to emanate from an imaginary surface in the plane of the blackbody aperture. This imaginary surface can be referred to as a black surface. At low temperatures it will appear black since it absorbs all incoming radiation.

Commercial blackbodies are constructed using heated cavities such as shown in Figure 2.4. (Holman, p. 409). Such blackbodies can attain effective emissivities of about 0.99. The temperature uncertainty of such a blackbody is estimated to be ± 2 K.

Most real objects are opaque ($\tau = 0$). Even glass and water are opaque throughout most of the infrared spectrum. The absorption of radiation in opaque objects is generally considered to take place almost wholly in the first few molecular layers. For these reasons, radiation emission and absorption in solid objects are considered to be surface phenomena. Hence we will generally refer to surfaces rather than objects. It should also be noted however, that radiometric temperature measurements are surface temperature measurements and are not capable of assessing the temperature at any immersion depth into the solid.

12
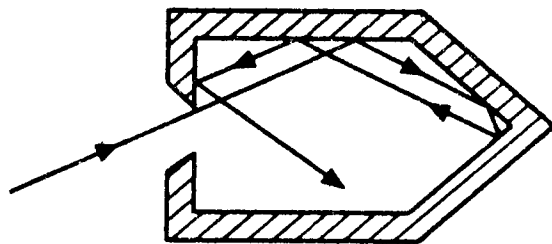
Figure 2.3 A Cavity Approximation of a Blackbody.
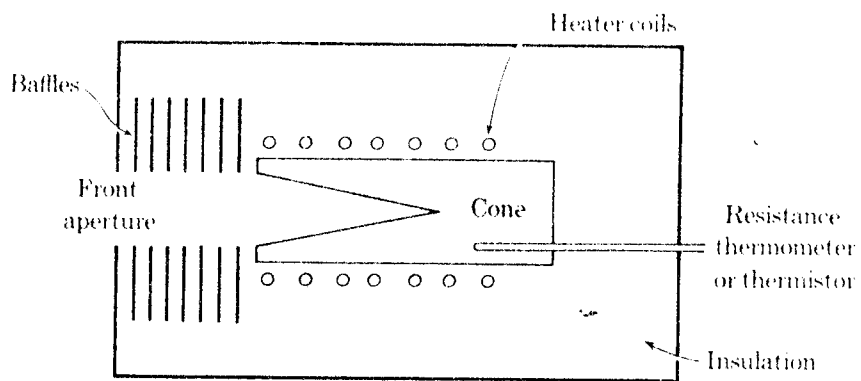
Figure 2.4 Typical Construction of a Blackbody Source.

14

Radiosity

Consider a surface at temperature T as in Figure
2.5. In addition to emitting radiation, the surface may
also be reflecting radiation that is incident on the
surface. Incident radiation will be referred to as irra-
diance (H). The total radiation leaving the surface is
the sum of the emitted radiation and the reflected
radiation and is given the name radiosity (B).

$$B = \epsilon E_b + pH \qquad \text{eq. 2.11}$$

ϵ = emissivity
E_b = blackbody radiant power
p = reflectance
H = incident radiation (irradiance)

It is important to note that conventional radiation
detectors sense radiosity per steradian and not
radiance! In most measurements, pH is assumed to be
negligible and radiosity measurements are referred to
throughout radiation literature as radiance measure-
ments. In the discussion that follows, radiation
measurements will be referred to as radiance measure-
ments, but the reader should understand that radiosity
is really the quantity being measured. According to
Nutter (p. 40,41):
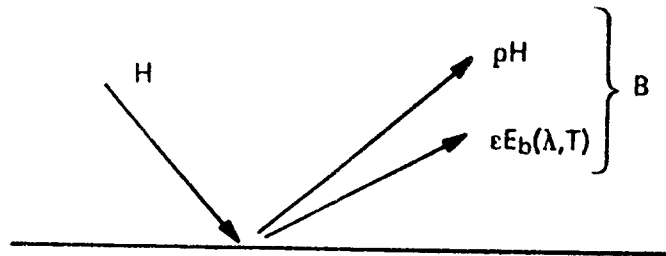
Figure 2.5 Radiosity (B).

"At target temperatures below about 100-150 deg. C, reflected radiation is usually the dominant source of error in radiation thermometry....The trend in recent years has been toward trying to develop techniques for dealing with reflected radiation ..."

The radiation properties discussed up to this point have been total (over all wavelengths) hemispherical (in all directions) properties. In many practical cases, the radiation in a given wavelength band (spectral) and in a given direction (directional) must be considered. The subscript λ will be used to denote spectral surface properties; absence of the subscript λ will denote total properties. The subscript $\theta\phi$ will denote directional properties; absence of the subscript $\theta\phi$ will denote hemispherical properties. (i.e. $\epsilon_{\lambda\theta\phi}$ is spectral directional emissivity, while ϵ is the total hemispherical emissivity). Gray, diffuse surfaces have spectral directional properties that are equal to total hemispherical properties.

$$\epsilon_{\lambda\theta\phi} = \epsilon \text{ (gray and diffuse)}$$

Directional versus hemispherical properties

Radiance (N) is the amount of energy radiated from a surface per unit time and unit area normal to a given direction per unit solid angle (sr). Hemispherical integration of radiance will yield radiant power (Sparrow

17

p.9). For special cases where radiance is isotropic
(independent of direction), hemispherical integration
leads to:

$$E = \pi N \qquad \text{eq. 2.12}$$

It is often not clear from literature whether
radiant power or radiance is being discussed. The units
and value of Planck's first radiation constant (c1 =
3.741×10^8 watts$\cdot\mu m^4/m^2$ for radiant power, c1/π = 1.191
$\times 10^8$ watts$\cdot\mu m^4/m^2\cdot$sr for radiance) will indicate which
quantity is being addressed. The special case of an
isotropic surface is usually referred to as a diffuse
surface. The radiation leaving a diffusely emitting and
diffusely reflecting surface is uniform in all direc-
tions. It can be seen from Figure 2.6 (Sparrow p. 54)
that nonmetals can be considered diffuse emitters to
about 50 or 60 deg. from a normal to the surface. Met-
als (Figure 2.7) (Sparrow p. 55) can be treated as dif-
fuse emitters out to about 30 deg. from normal.

The situation with reflectance is somewhat more
complex since one must consider the directional charac-
teristics of incoming (incident) and outgoing
(reflected) radiation. Three directional reflectances
to be considered are: (Sparrow p. 56).

1. Directional-hemispherical reflectance

2. Hemispherical-directional reflectance
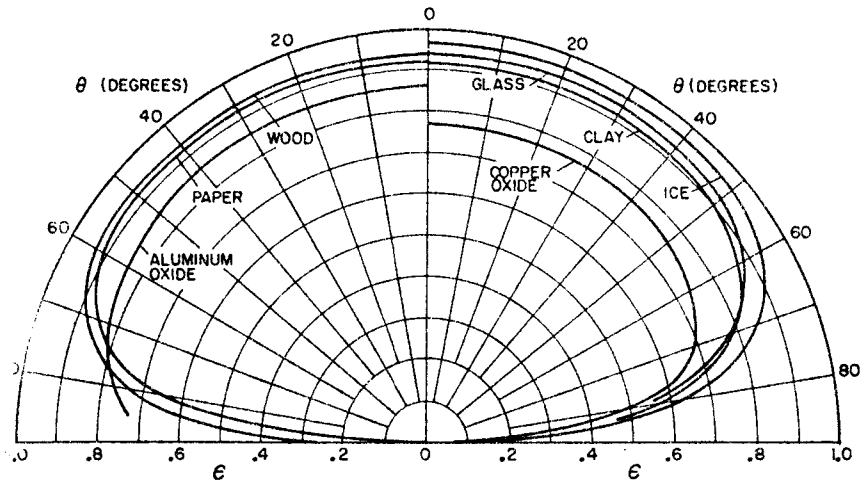
Figure 2.6   Distribution of the Total Directional Emissi-
vity for Several Electric Nonconductors.
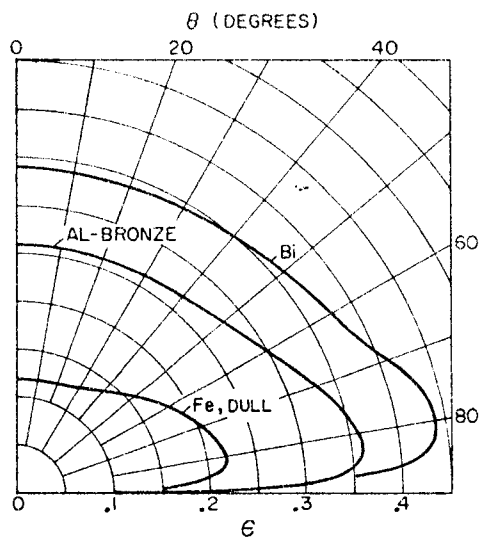
Figure 2.7   Distribution of the Total Directional
Emissivity for Several Metals.

19

3. Bidirectional reflectance

Directional-hemispherical reflectance relates the energy reflected in all directions (into the hemisphere above the surface) from an incident beam at a specific angle.

Hemispherical-directional reflectance relates how the surface reflects all of the incident (incoming) radiation (from the hemisphere above the surface) to a viewer situated at a particular direction from the surface.

Bidirectional reflectance denotes a specific angle of incident radiation and specific angle of collected reflected radiation. A diffuse bidirectional reflector will reflect equally in all directions even though all incident radiation may strike the surface at a particular angle. On the other hand, a perfectly specular (mirror-like) surface will reflect all radiation at an angle equal (but opposite from normal) to the angle of incidence. An illustration of specular and diffuse reflections is shown in Figure 2.8. While no real surface is truly perfectly specular, metals generally tend to be specular while non-metals tend to be diffuse, and smooth surfaces tend to be specular while rough surfaces tend to be diffuse.

a = θ

90 deg

Incident Radiation | Reflected Radiation

α

θ

Specular Reflecting Surface

a. Specular reflections

Incident Radiation

Reflected Radiation

Diffuse Reflecting Surface

b. Diffuse reflections
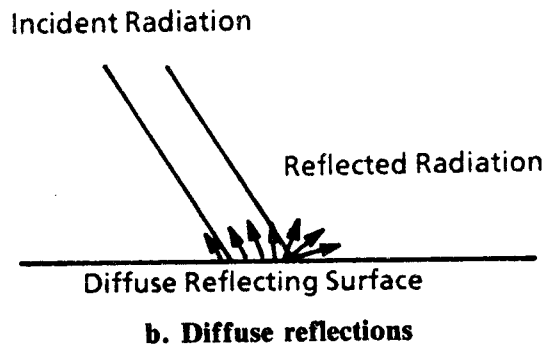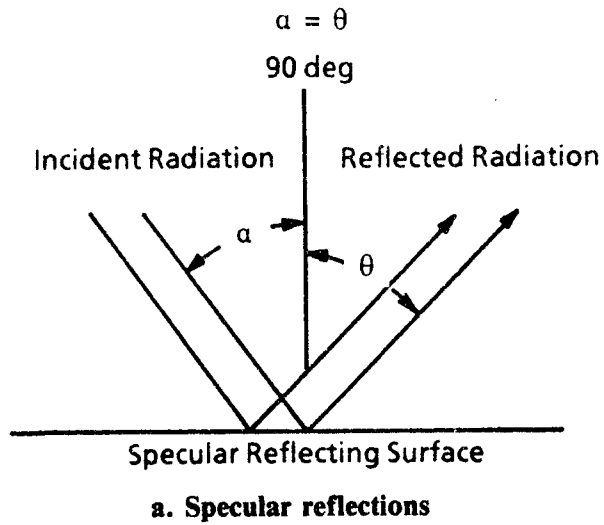
Figure 2.8   Comparison of Specular and Diffuse Reflec-
tions.

Spectral versus total properties

Spectral or monochromatic properties refer to properties at a given wavelength. Spectral radiant power as given in equation 2.3 has units of energy per time, per area, per wavelength, and has little physical meaning unless integrated over a particular wavelength band λa to λb. For very small intervals of λa to λb the Planck function can be approximated without integration:

$$\int_{\lambda a}^{\lambda b} Eb(\lambda T)d\lambda \approx Eb(\lambda c, T)(\lambda b - \lambda a) \qquad \text{eq. 2.13}$$

where:

$$\lambda c = \frac{\lambda a + \lambda b}{2}$$

The integral of the Planck function from zero to infinity yields the Stefan-Boltzmann equation (Sparrow p. 8) which gives the total radiation at all wavelengths or total radiant power:

$$\int_{0}^{\infty} Eb(\lambda T)d\lambda = n^2 \sigma T^4 \qquad \text{eq. 2.14}$$

σ = Stefan-Boltzmann constant
(5.66925×10^{-12} watts $cm^{-2} sec^{-1} K^{-4}$)

22

In the discussion that follows we will primarily be concerned with spectral properties. It is important to note that spectral properties can be easily related to total properties only under special circumstances. The most important special case is graybody behavior. A graybody is defined as one whose surface properties are independent of wavelength.

$$\epsilon_\lambda = \epsilon$$
$$\alpha_\lambda = \alpha$$
$$p_\lambda = p$$
$$\tau_\lambda = \tau$$

Kirchoff's Law states that directional spectral absorptance equals directional spectral emissivity:

$$\alpha_\lambda = \epsilon_\lambda \qquad\qquad \text{eq. 2.15}$$

so that for diffuse gray behavior:

$$\alpha = \epsilon \qquad\qquad \text{eq. 2.16}$$

It must be emphasized that the above relation is only true for diffuse graybody behavior. This means that although:

$$\alpha_\lambda + p_\lambda = 1 \qquad\qquad \text{eq. 2.17}$$

for any opaque surface, the relation:

$$\epsilon_\lambda + p_\lambda = 1 \qquad\qquad \text{eq. 2.18}$$

23

is true only for a diffuse surface. This distinction
will be very important later on.

Few real surfaces exhibit true graybody behavior
but as long as the surface properties are constant
within the wavelength band of interest, graybody behav-
ior can be assumed.

Radiance Measurements

Many devices have been devised to measure radiant
energy. These devices are typically called photodetec-
tors and are subdivided into two categories: Quantum
(photoelectric) detectors that convert photons into
charge carriers, and thermal detectors that sense the
heating effect of absorbed radiation. (Nutter p. 49).
Two types of thermal detectors, the thermopile radio-
meter and the thermistor bolometer are described by
Holman. (p. 406-409).

Several photoelectric detectors designed to
operate at room temperature are shown in Figure 2.9.
(Nutter p. 51). In order to reduce detector noise, many
instruments provide for cooling the detector down to
liquid nitrogen temperatures.

Determination of inband radiance

The inband radiance describes the total radiance
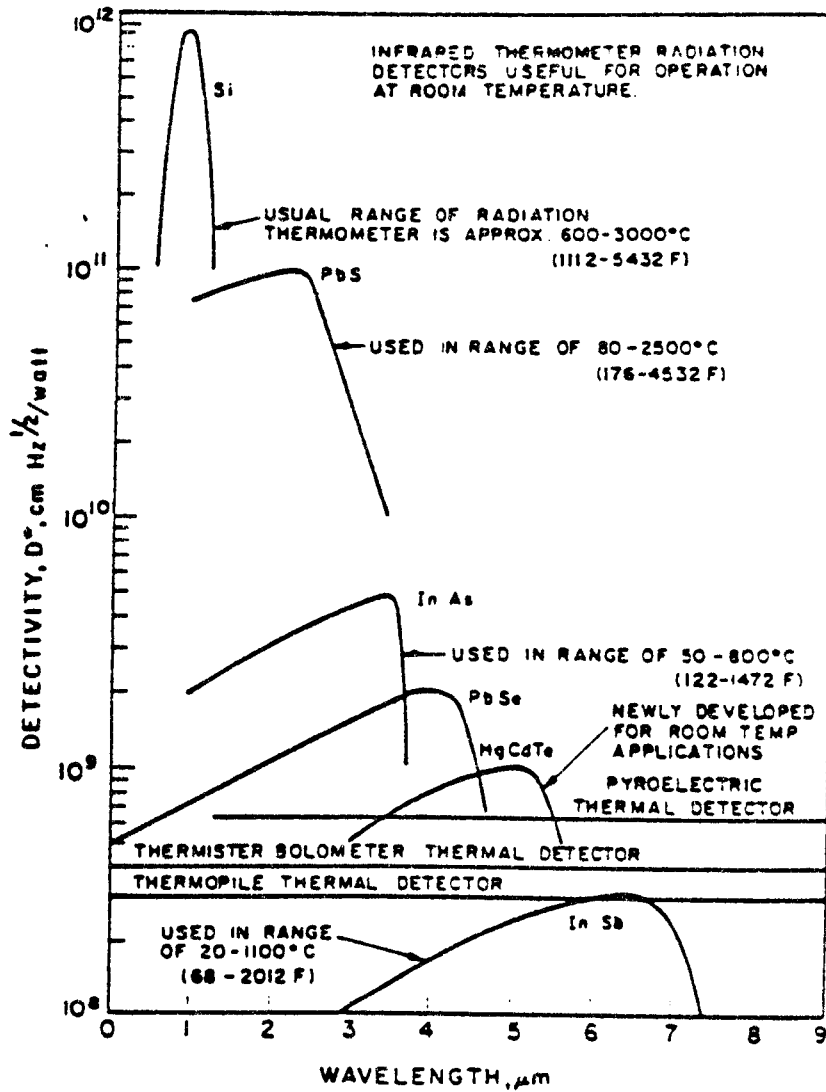
Figure 2.9   Photodetectors Commonly Used in Radiation
Thermometry, for Room Temperature Operation.

measured by an instrument that has been designed to make measurements in a particular wavelength band. The wavelength band is typically specified by the lower half-power point (λa) and the upper half-power point (λb). Alternatively, the band can be specified by a center wavelength and a bandwidth ($\lambda b - \lambda a$). The half-power points are the wavelengths between which the filter relative transmittance is 50 percent or greater (Figure 2.10).

The millivolt response of an instrument is described by the following relation:

$$mv = K \int_{0}^{\infty} F_{\lambda} R_{\lambda} \epsilon_{\lambda} Nb(\lambda T) d\lambda \qquad \text{eq. 2.19}$$

mv = millivolt response
$F\lambda$ = Filter transmission
$R\lambda$ = Instrument response (including relative spectral response of all optics plus the detector)
$\epsilon\lambda$ = target spectral emissivity
K = instrument gain

Calibration with a blackbody source allows K to be calculated:

$$K = \frac{mv}{\int_{0}^{\infty} F_{\lambda} R_{\lambda} \epsilon_{\lambda} Nb(\lambda T) d\lambda} \qquad \text{eq. 2.20}$$

26
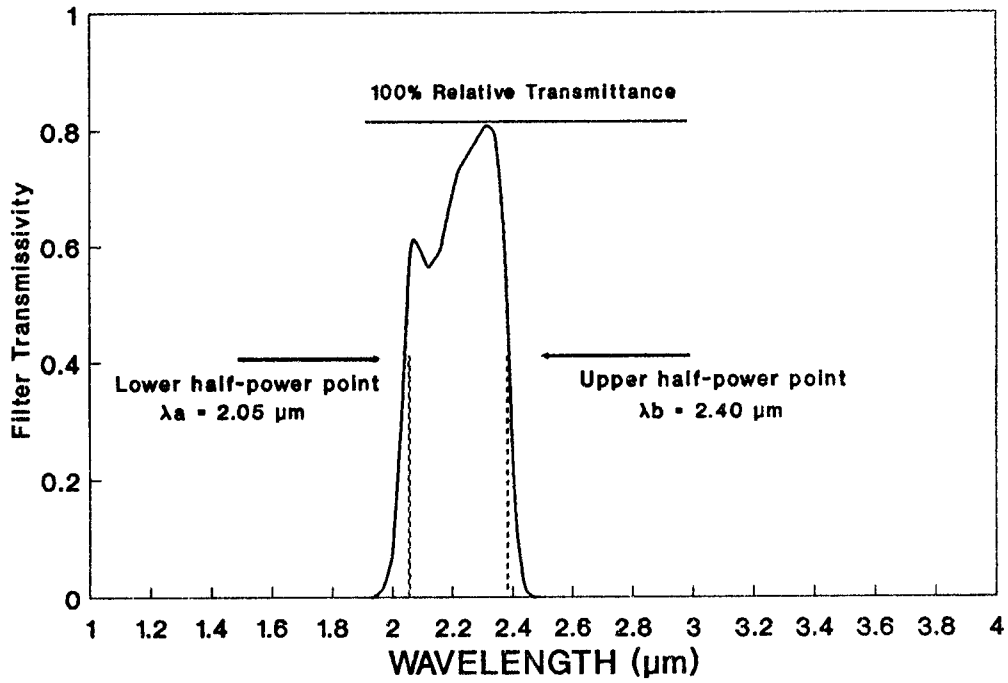
Figure 2.10   Half-power Points for a Typical Band-pass
              Filter.

and inband radiance from λa to λb from an unknown source can then be computed:

$$N_{\lambda a, \lambda b} = \frac{mv}{K} \qquad \text{eq. 2.21}$$

Temperature determination from radiance

If we assume that graybody behavior holds over the band-pass of the filter (i.e. ϵ is constant between λa and λb):

$$\frac{mv}{\epsilon} = K \int_{0}^{\infty} F_\lambda R_\lambda \, Nb(\lambda T) d\lambda \qquad \text{eq. 2.22}$$

Knowing F_λ and R_λ and using K from the blackbody calibration a curve can be generated that relates inband radiance to temperature (Figure 2.11). However, since F_λ and R_λ are not always precisely known it is usually simpler to generate a calibration curve from a multi-step blackbody calibration. The radiometer can then be calibrated directly in millivolts (Figure 2.12).

To determine the temperature of a heated surface, radiometer millivolt readings are taken. An apparent surface temperature can then be read directly from the calibration curve. If the value of ϵ is not known, ϵ =
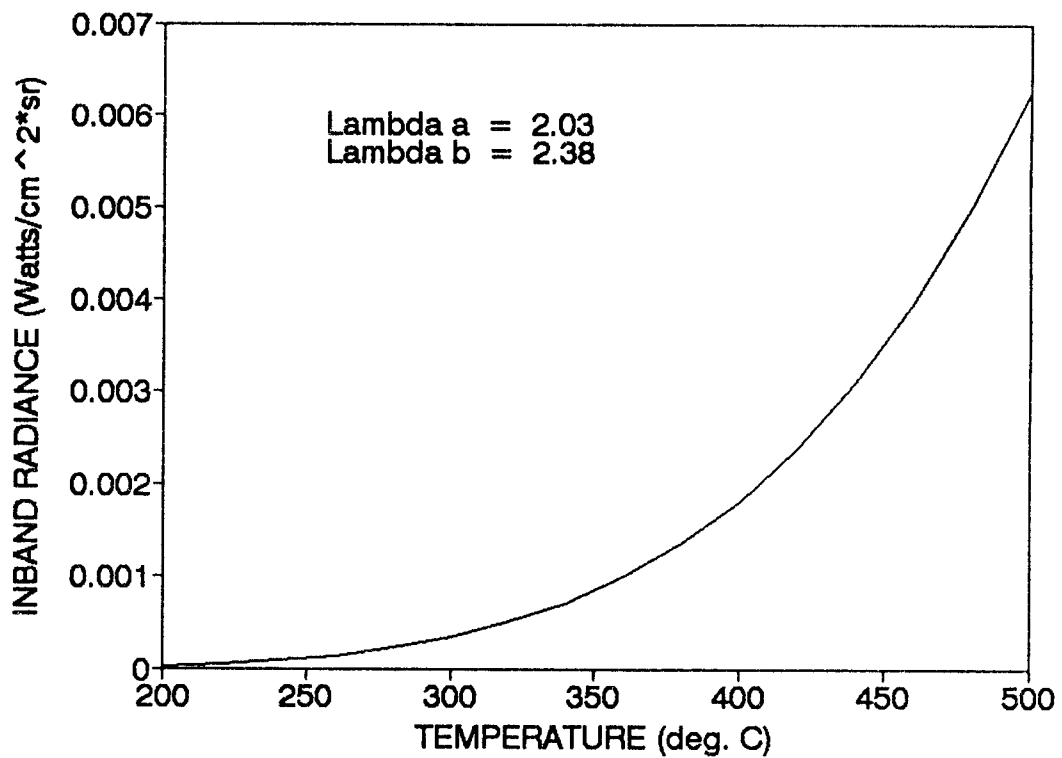
Figure 2.11   Single-color Temperature Calibration
(Radiance versus Temperature).

29
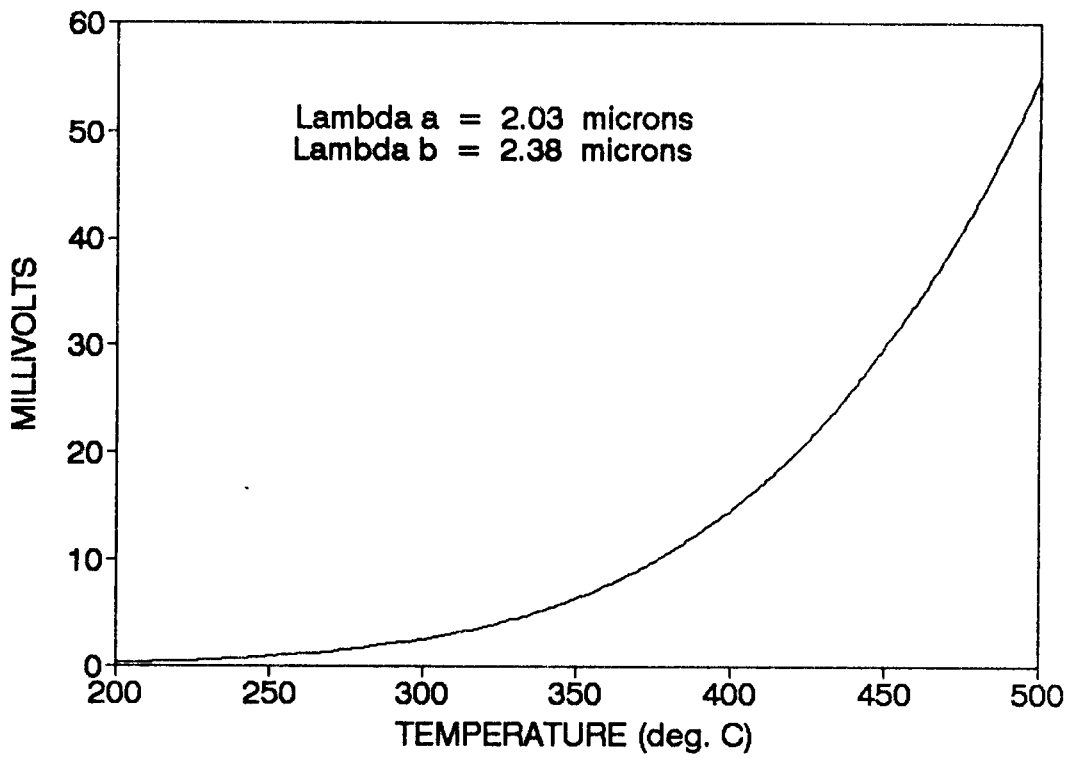
Figure 2.12   Single-color Temperature Calibration
(Millivolts versus Temperature).

1 is commonly assumed. Solving for T with ϵ = 1 yields
an apparent blackbody temperature T_a that represents the
temperature of a blackbody that is emitting the same
radiance as the target surface. Note that if all other
sources of error are negligible:

$$T_a \leq T_{true}$$

Influence coefficient of radiance to temperature

The influence coefficient or sensitivity of
Radiance to temperature can be determined from differ-
entiation of Wein's approximation to the Planck function
given as:

$$Nb(\lambda, T) = \frac{c1}{\lambda^5 (e^{c2/\lambda T})} \qquad \text{eq. 2.23}$$

differentiating with respect to T we have:

$$\frac{dN}{T} = \frac{c1}{\lambda^5} \frac{-(e^{c2/\lambda T})(-c2/\lambda T^2)}{(e^{c2/\lambda T})^2}$$

$$= N \frac{c2}{\lambda T^2} \frac{(e^{c2/\lambda T})}{(e^{c2/\lambda T})} \qquad \text{eq. 2.24}$$

$$\frac{dN}{N} = \frac{c2}{\lambda T} \frac{dT}{T} \qquad \text{eq. 2.25}$$

or:

31

$$\frac{dT}{T} = \frac{\lambda T}{c2} \frac{dN}{N} \qquad \text{eq. 2.26}$$

From equation 2.23 we can say that for small increments of dT/T we can approximate radiance by the relation:

$$N = aT^b \qquad \text{eq. 2.27}$$

where:

$$b = \frac{c2}{\lambda T} \qquad \text{eq. 2.28}$$

This is sometimes referred to as the "power of T" relationship of radiance (Nutter p. 54). The influence coefficient of radiance to temperature is the reciprocal of equation 2.26:

$$I.C. = \frac{\lambda T}{c2} \qquad \text{eq. 2.29}$$

It is clear from equation 2.29 that a smaller value of (λT) will produce a lower influence coefficient of radiance to temperature. A lower influence coefficient means that lower errors in the temperature calculation will result from given errors in the radiance measurement.

Minimizing temperature error

The temperature error due to error in the value of ϵ can be minimized by tailoring the instrument to the measurement, that is, by selecting a wavelength to minimize the influence coefficient of radiance to temperature. It can be shown (Appendix A) that the error in temperature measurement due to non-blackbody behavior is represented by:

$$\frac{dT}{T} = \frac{\lambda T}{c2} \frac{\epsilon - 1}{\epsilon} \qquad \text{eq. 2.30}$$

This temperature error is shown in Figure 2.13 for 4 values of (λT). Obviously the lower values of (λT) lead to lower error due to non-blackbody behavior.

If an emissivity less than one is used in the temperature determination, the temperature error due to an error in the assumed emissivity value is:

$$\frac{dT}{T} = \frac{\lambda T}{c2} \frac{d\epsilon}{\epsilon} \qquad \text{eq. 2.31}$$

To minimize errors in temperature due to unknown emissivity, temperature measurements should be made at the "shortest feasible wavelength" (Ibid p. 55).
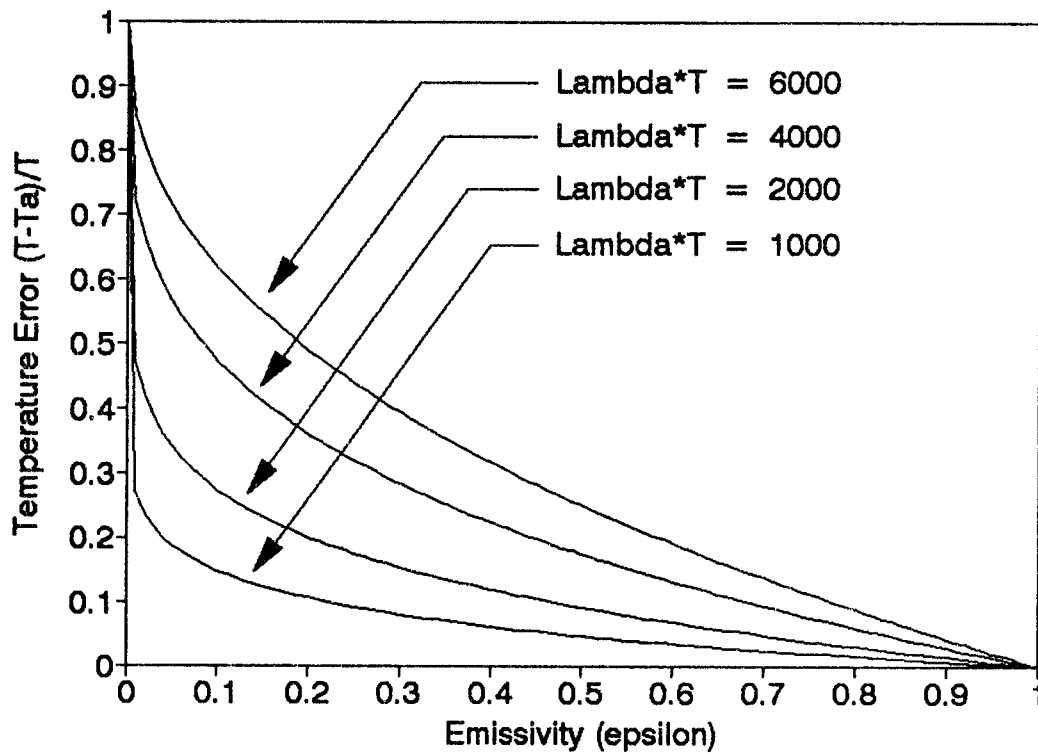
Figure 2.13   Temperature Error due to Non-black
              Behavior.

34

Shortest feasible wavelength

Detector sensitivity and other constraints must be considered in selecting the shortest feasible wavelength. Also note that instrument sensitivity is gained at the expense of dynamic range. However, the most serious consideration in tailoring an instrument to the shortest feasible wavelength is that for any given target temperature, there is a wavelength below which the emitted radiation from the target is negligible. Negligible radiation in this context means radiation that is indistinguishable from detector noise.

If the magnitude of the detector noise is known, the error in the radiance measurement due to noise can be estimated. An example of the error in the radiance measurement due to detector noise in a typical blackbody receiver (see Appendix B) is shown in Figure 2.14. The temperature error due to detector noise is:

$$\frac{dT}{T} = \frac{\lambda T}{c2} \frac{dN}{N \text{ (noise)}} \qquad \text{eq. 2.32}$$

and is shown in Figure 2.15.

In order to compute the shortest feasible wavelength, the temperature of the surface of interest must be known in advance. However, for measurements at a given temperature, proper choice of wavelength can lead

35
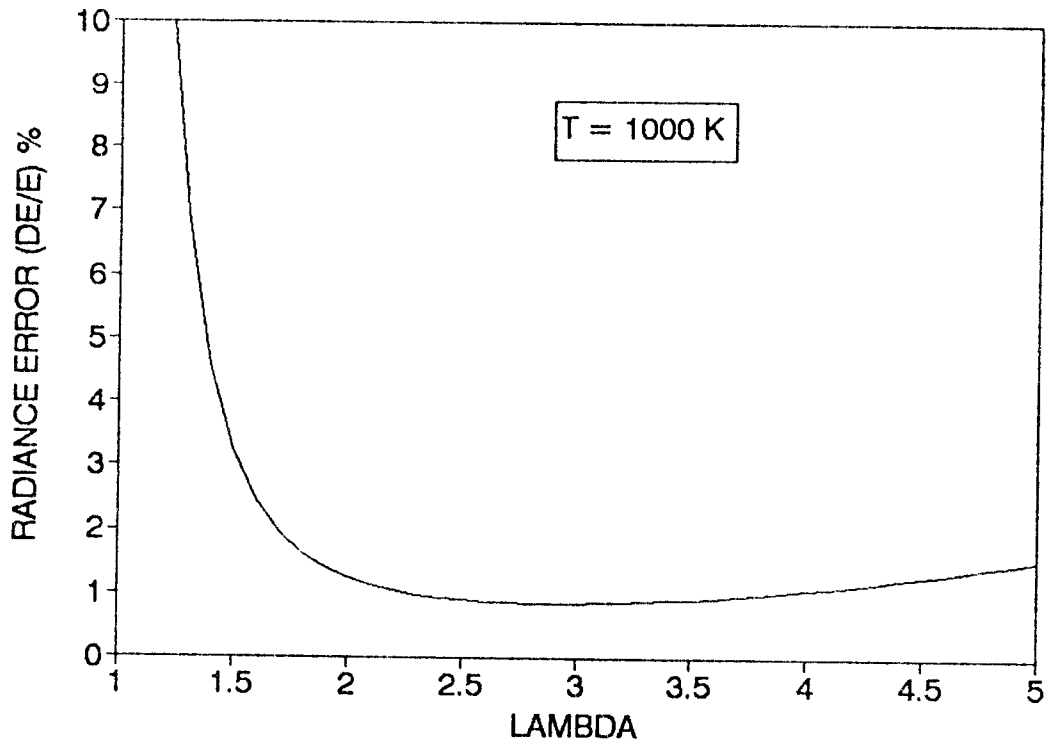
Figure 2.14   Radiance Error due to Detector Noise
(Typical Blackbody Receiver).
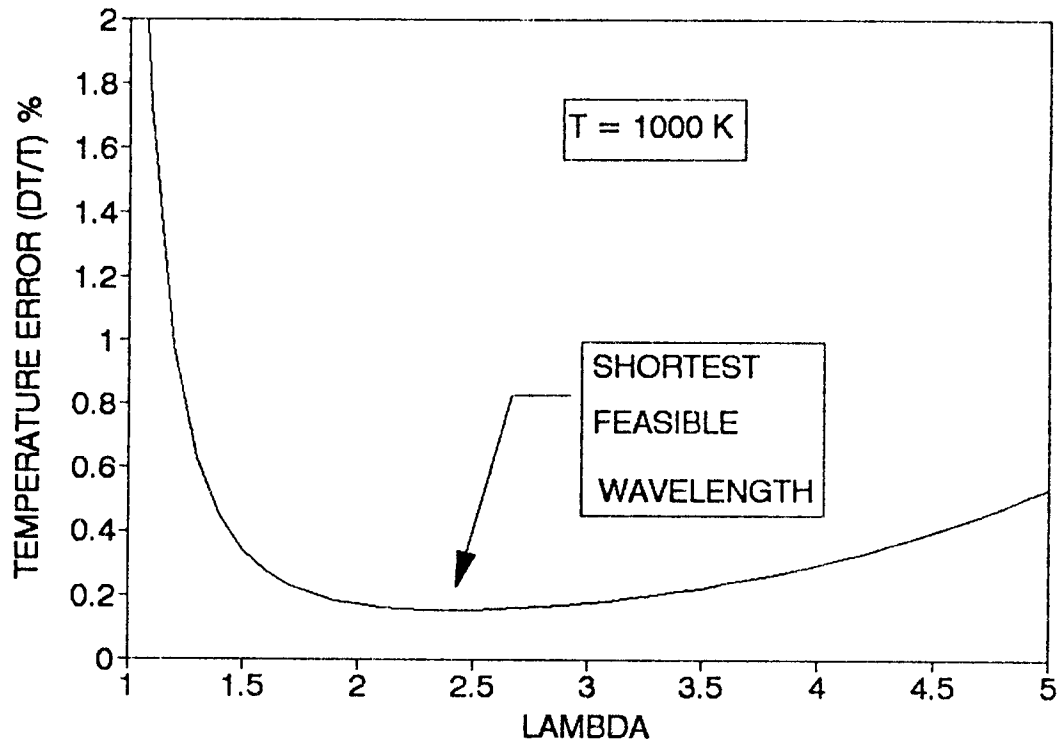
Figure 2.15   Shortest Feasible Wavelength for a Typical
Blackbody Receiver.

to surface temperature measurements that are relatively insensitive to errors in the assumed emissivity value. Unfortunately, temperature determination from radiance measurements at the lower wavelengths are increasingly sensitive to errors induced by radiation incident on the target originating from a surface at higher temperatures.

Surface Temperature from Radiance Ratio Measurements

Two-color or ratio measurements are useful for surface temperature measurements when the spectral emissivities are unknown but graybody conditions are known to exist, when the target does not fill the field of view of the instrument, and when significant radiance attenuation occurs in the medium separating the target and the instrument. Ratio pyrometers have been successfully used in the steel industry where graybody conditions can often be shown to exist. (Nutter p. 57) For the purpose of this discussion, the term "two-color" will denote measurements made in two discrete wavelength bands. The ratios of these measurements can be computed and used to infer a surface temperature value. Both ratio and spectral information is available. "Ratio" measurements will denote those which measure or record only the radiance ratio itself. Spectral information in such cases is not available.

A common method used to build a ratio or two-color pyrometer is to use a beam splitter with selected filters to obtain the spectral measurements desired. One such instrument is shown in Figure 2.16. (Gardner, p. 410).

The two-color temperature measurement technique relies on the fact that for a perfect graybody, the ratio of the radiances at two wavelengths defines a unique blackbody curve. The temperature of such blackbody curve is equal to the surface temperature of the graybody (see Figure 2.17).

The radiance ratio, R, is computed at the two wavelength bands with the shorter wavelength typically in the numerator:

$$R \quad = \quad \frac{N\lambda 1(T)}{N\lambda 2(T)} \quad = \quad \frac{\epsilon_{\lambda 1} Nb\lambda 1(T)}{\epsilon_{\lambda 2} Nb\lambda 2(T)} \qquad \text{eq. 2.33}$$

for a graybody $\epsilon_{\lambda 1} = \epsilon_{\lambda 2}$, therefore:

$$R \quad = \quad \frac{N\lambda 1(T)}{N\lambda 2(T)} \quad = \quad \frac{Nb\lambda 1(T)}{Nb\lambda 2(T)} \qquad \text{eq. 2.34}$$

A calibration curve is determined for the two-color pyrometer by measuring the radiance ratio of the blackbody at different temperatures. A typical calibration curve is shown in Figure 2.18.

Note that the actual ratio measurements involve

39
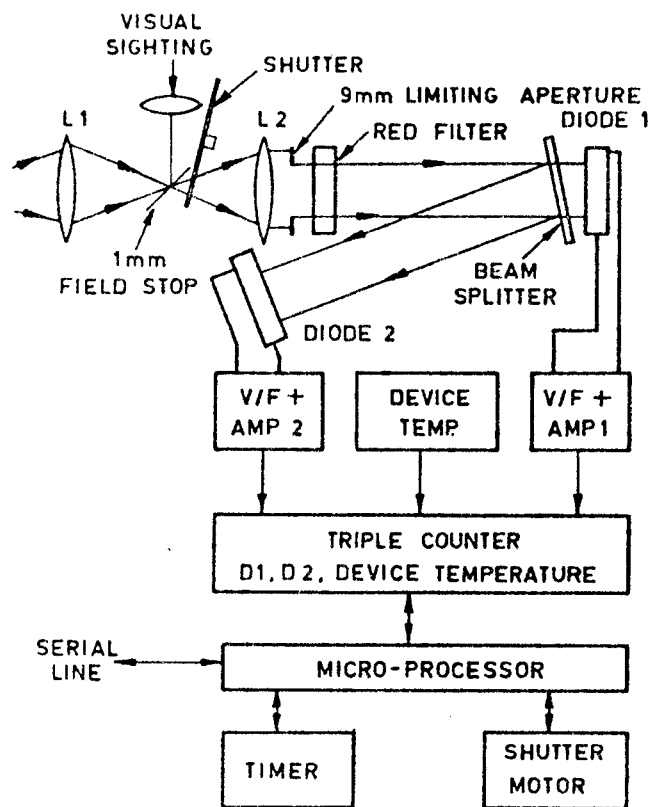
Figure 2.16   Optical diagram and electronic block
diagram of ratio pyrometer.
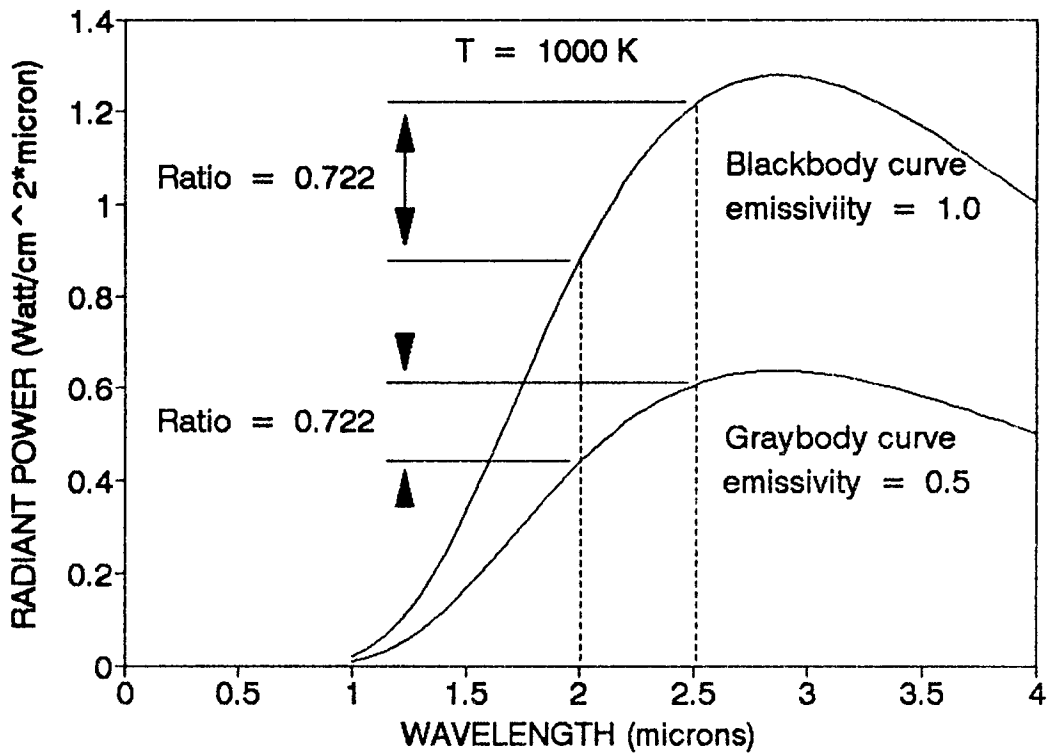
Figure 2.17   Radiance Ratio Comparison for Blackbody
and Graybody Curves.
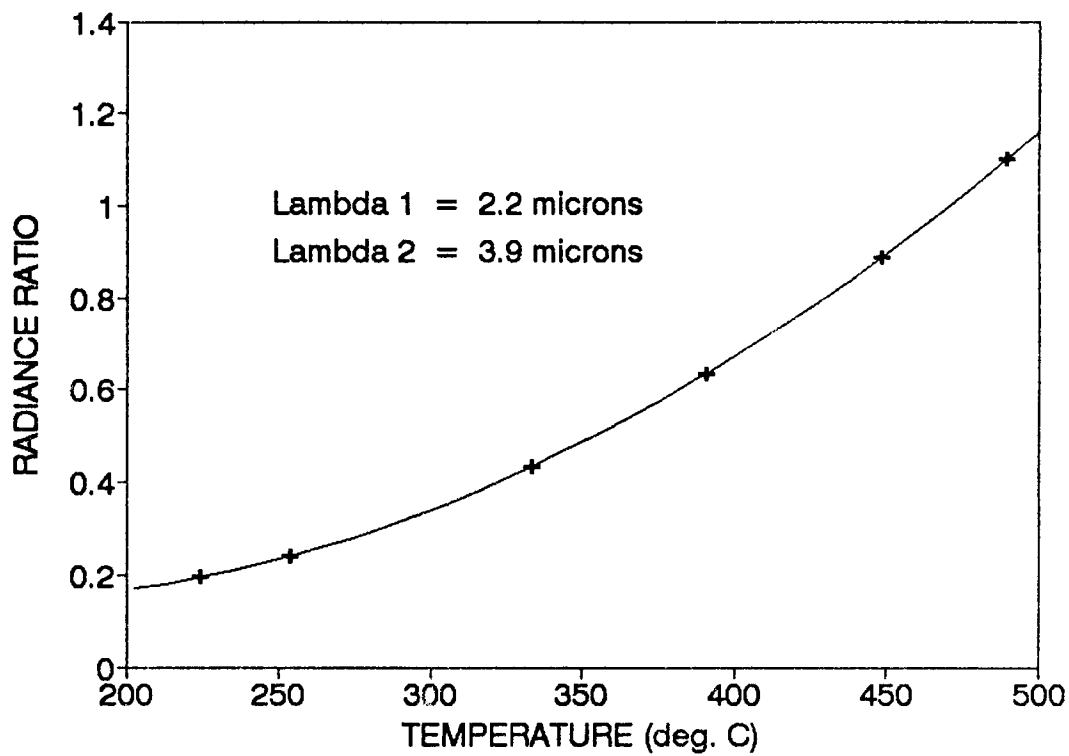
Figure 2.18 Typical Radiance Ratio Calibration Curve.

42

inband radiance measurements rather than spectral
measurements.

$$R = \frac{Nb_{\lambda 1a, \lambda 1b}}{Nb_{\lambda 2a, \lambda 2b}}$$

As long as the bandpass is narrow, and the surface
is gray, the inband radiance ratios will be proportional
to the spectral radiance ratios. Spectral ratios and
properties will be indicated throughout the remainder of
this discussion for the sake of simplicity, unless
otherwise noted. When non-gray surfaces are discussed,
the spectral properties within the filter bandpass will
be assumed constant.

Advantages of Ratio Pyrometry

For certain applications, two-color pyrometry has
clear advantages over single-color pyrometry:
1. Field of view need not be filled
2. Known emissivity values not necessary
3. Relative insensitivity to attenuation

A discussion of each of these advantages and the errors
that can result in each case follows.

Field of view

The independent parameter in the ratio measurement

43

is the ratio of the energy in the two wavelength bands.
If the background area (that area of the FOV that is not
filled by the target) is at a temperature much lower
than the target temperature, the emitted energy from the
background can be neglected. If the background energy
is negligible, the radiance ratio will be constant
regardless of the fraction of the field of view that is
filled. An example of the error introduced by a non-
filled field of view is discussed in Appendix C and is
illustrated in Figure 2.19 for a graybody at 1000 K.

Unknown Emissivity Values

The errors due to incorrect value of emissivity
cancel out in the ratio technique if the surface behaves
as a graybody. If the target surface is not gray, an
error is introduced in the ratio measurement. This error
can be corrected if the ratio of the emissivities is
known.

$$R \times \frac{\epsilon_{\lambda 2}}{\epsilon_{\lambda 1}} = \frac{\epsilon_{\lambda 2}}{\epsilon_{\lambda 1}} \times \frac{\epsilon_{\lambda 1} N b_{\lambda 1}(T)}{\epsilon_{\lambda 2} N b_{\lambda 2}(T)} \qquad \text{eq. 2.35}$$

If the ratio of the emissivities is not known, the
error due to non-gray behavior can be minimized by
reducing the interval between $\lambda 1$ and $\lambda 2$, the wavelength
separation. The degree of non-grayness can be charac-

44
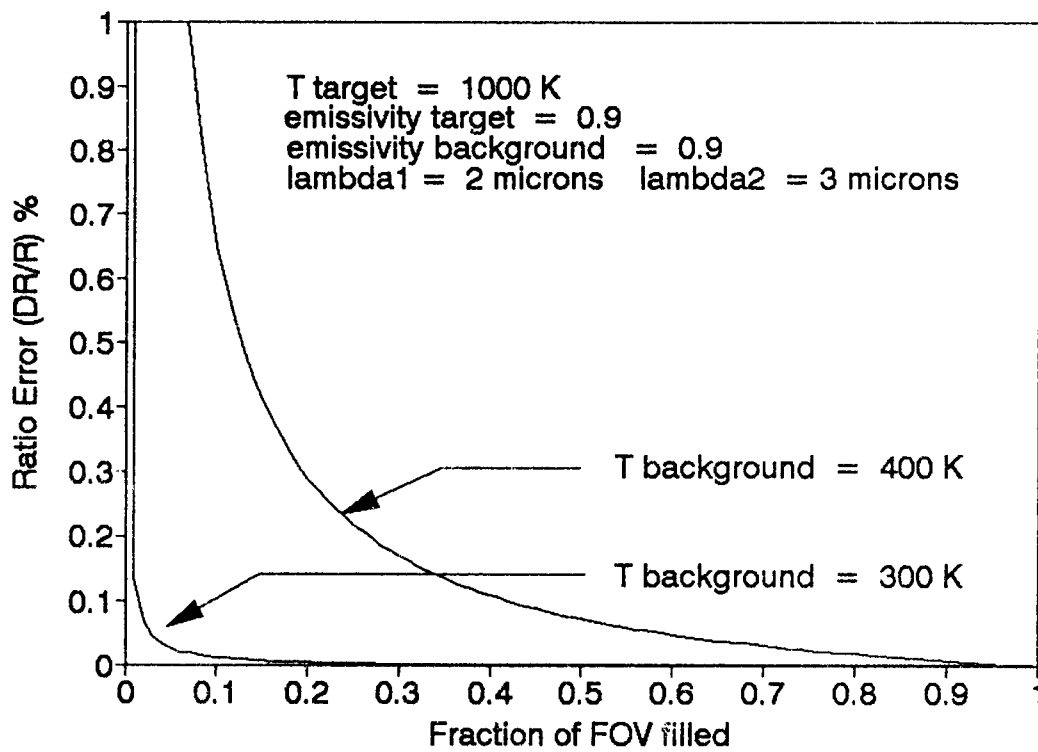
Figure 2.19   Ratio Pyrometry Error due to Non-filled
             Field of View.

terized by the slope of the straight line through the emissivities at $\lambda 1$ and $\lambda 2$. (Gardner p.409) The ratio of the emissivities at $\lambda 1$ and $\lambda 2$ can now be defined as:

$$\frac{\epsilon_{\lambda 2}}{\epsilon_{\lambda 1}} = \frac{m\ (\lambda 2 - \lambda 1)}{\epsilon_{\lambda 1}} + 1 \qquad \text{eq. 2.36}$$

where   slope $m = (\epsilon_{\lambda 2} - \epsilon_{\lambda 1})/(\lambda 2 - \lambda 1)$

If we have assumed graybody behavior ($\epsilon_{\lambda 1}/\epsilon_{\lambda 2} = 1$), then the error in emissivity ratio is given by:

$$\frac{1 - \epsilon_{\lambda 1}/\epsilon_{\lambda 2}}{\epsilon_{\lambda 1}/\epsilon_{\lambda 2}} = (\epsilon_{\lambda 2}/\epsilon_{\lambda 1} - 1) \qquad \text{eq. 2.37}$$

substituting we have:

$$\frac{d\epsilon}{\epsilon} = \frac{m\ (\lambda 2 - \lambda 1)}{\epsilon_{\lambda 1}} \qquad \text{eq. 2.38}$$

and since the influence coefficient between radiance ratio and emissivity ratio is 1.0:

$$\frac{dR}{R} = \frac{m\ (\lambda 2 - \lambda 1)}{\epsilon_{\lambda 1}} \qquad \text{eq. 2.39}$$

The relationship between radiance ratio error and temperature error for a ratio pyrometer (see Appendix D) is:

46

$$\frac{dT}{T} = \frac{(\lambda_1\lambda_2)T}{(\lambda_2-\lambda_1)c_2}\frac{dR}{R} \qquad \text{eq. 2.40}$$

so we see that the contribution of non-gray behavior
to the temperature error is:

$$\frac{dT}{T} = \frac{(\lambda_1\lambda_2)mT}{c_2\epsilon_{\lambda 1}} \qquad \text{eq. 2.41}$$

Equations 2.40 and 2.41 can be written in terms of
wavelength separation (δ) where:

$$\delta = \frac{\lambda_2 - \lambda_1}{\lambda_1}$$

$$\frac{dT}{T} = \frac{\delta + 1}{\delta}\frac{\lambda_1 T}{c_2}\frac{dR}{R} \qquad \text{eq. 2.42}$$

$$\frac{dT}{T} = \frac{(\delta + 1)\lambda_1^2 \, m}{\epsilon_{\lambda 1}}\frac{T}{c_2} \qquad \text{eq. 2.43}$$

The temperature error due to non-gray behavior is
shown in Figures 2.20 and 2.21 for a sample case where
the surface temperature (T) is 1000 K and the emissivity
slope divided by the emissivity at lambda 1 ($m/\epsilon_{\lambda 1}$) is
0.1. The term ($m/\epsilon_{\lambda 1}$) will be referred to hereafter as
the Non-gray Index (N.G.I.) (see Appendix D). While it
is clear that this error is minimized by reducing the
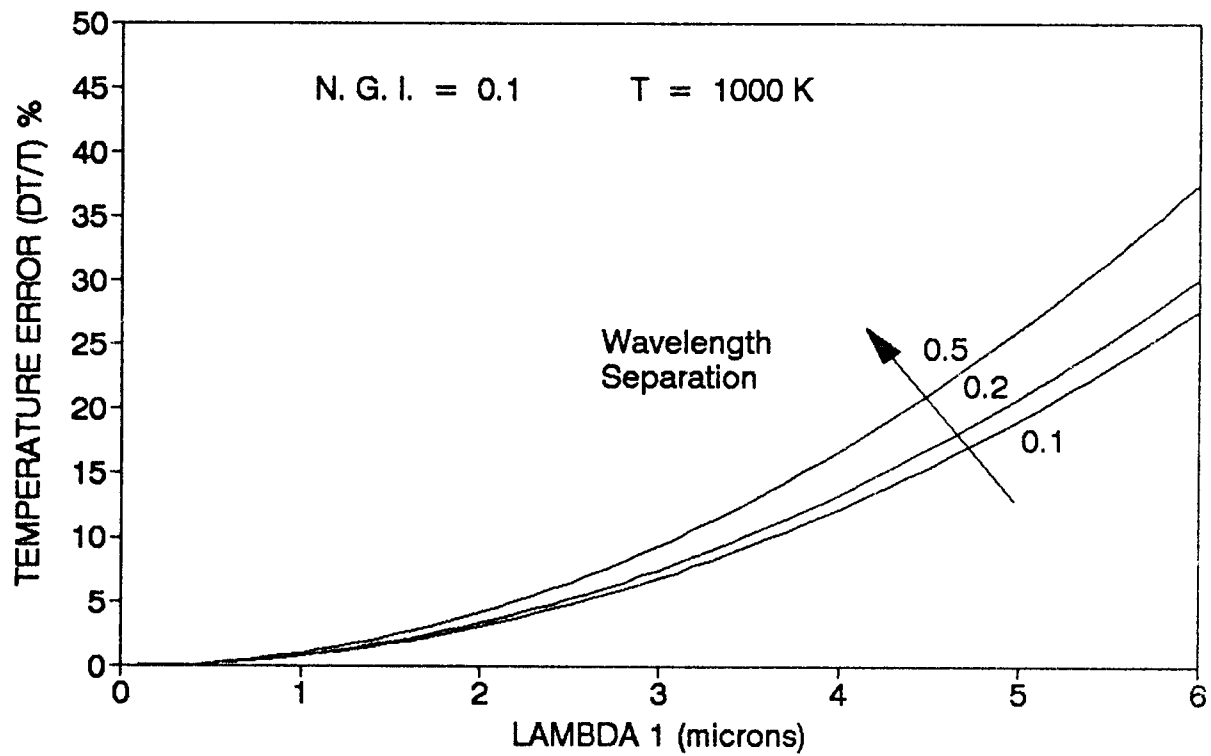
Figure 2.20   Ratio Pyrometry Error due to Non-gray
             Behavior as a Function of Wavelength.

48
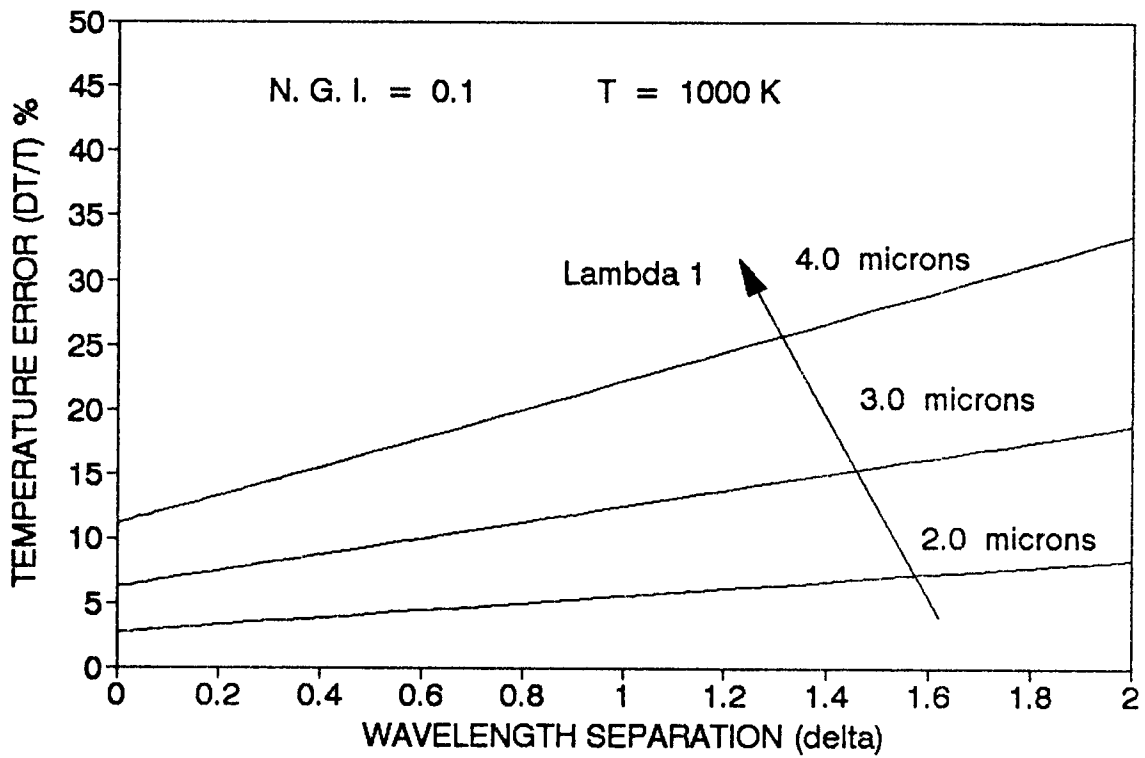
Figure 2.21   Ratio Pyrometry Error due to Non-gray
             Behavior as a Function of Wavelength
             Separation.

wavelength separation, one should note that this error is only that attributable to non-gray behavior of the surface and does not account for other sources of error in the radiance ratio such as detector noise. By examining the effect that wavelength separation has on these errors, a "minimum feasible wavelength separation" can be determined for a given measurement.

Minimum Feasible Wavelength Separation

The relationship between radiance ratio error and the temperature error or influence coefficient (I.C.) from equation 2.40 is:

$$I.C. = \frac{\delta + 1}{\delta} \frac{\lambda 1 T}{c2} \qquad \text{eq. 2.44}$$

or in generalized form:

$$\frac{I.C.}{\lambda 1 T} = \frac{\delta + 1}{\delta} \frac{1}{c2} \qquad \text{eq. 2.45}$$

This relationship is shown in Figure 2.22 for the generalized case (equation 2.45) and in Figure 2.23 (equation 2.44) for four specific cases. Note that for small values of wavelength separation, the influence coefficient is very high. The noise induced radiance ratio error for a typical blackbody receiver is shown in

50
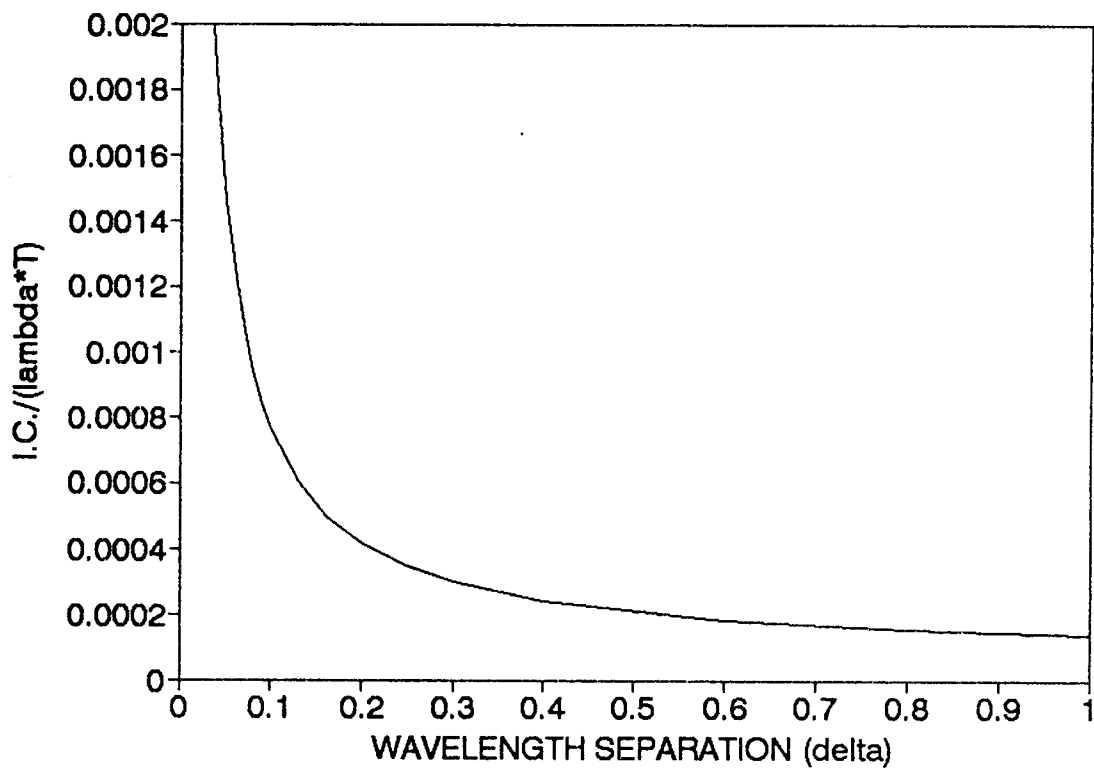
Figure 2.22   Generalized Influence Coefficient of
              Radiance Ratio Error to Temperature Error.
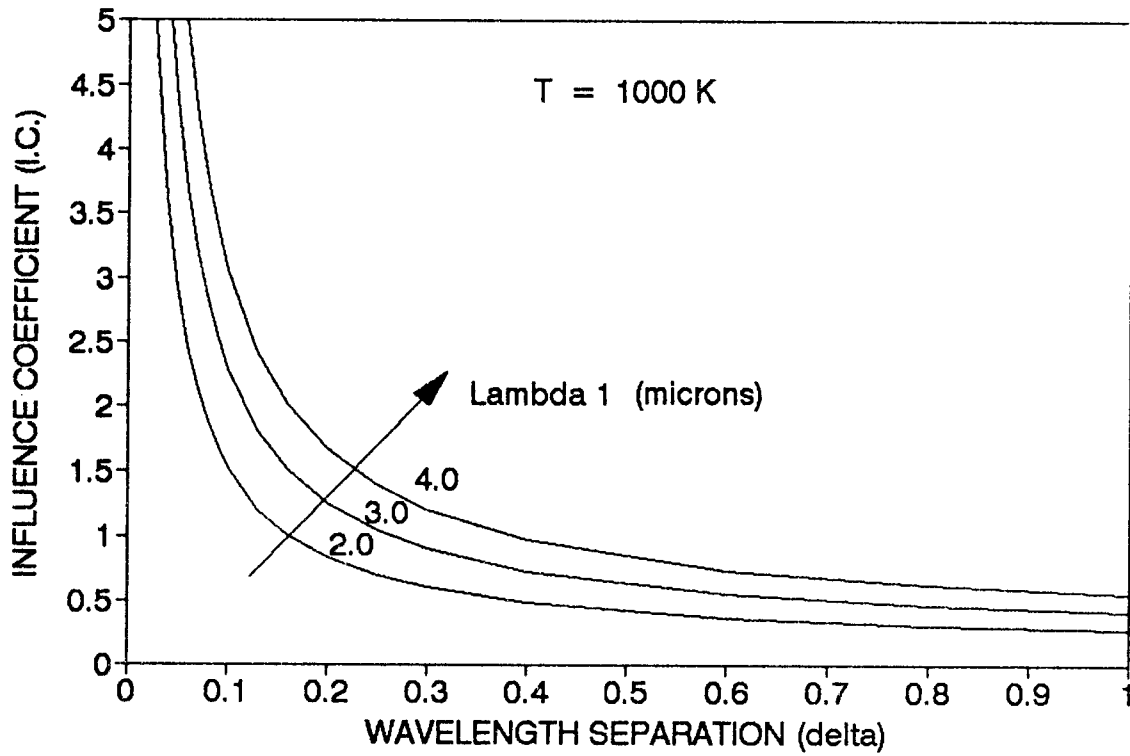
Figure 2.23   Influence Coefficient of Radiance Ratio
Error to Temperature Error for a Surface
at 1000 K.

Figure 2.24. The noise induced temperature error is shown in Figure 2.25.

It is clear that there is a "minimum feasible wavelength separation" below which the influence coefficient of radiance ratio error to temperature error is so high that the noise induced errors become unacceptable. Since the error due to non-gray behavior must be considered a systematic error rather than a random error, the combined error due to noise and non-gray behavior is simply the sum of the two errors (Figure 2.26) and can be used to compute the "minimum feasible wavelength separation" which yields the lowest temperature error for a given measurement.

Attenuation

The ratio technique is relatively insensitive to errors introduced by attenuation of the target radiance from clouds, dust, smoke, etc. as long as the attenuation is equal in the two wavelength bands. If the attenuation is not equal, an error will be introduced similar to the non-gray error discussed previously.

Disadvantages of ratio pyrometry

Disadvantages of the two-color technique include:

1. Lower inherent accuracy

2. Increased sensitivity to incident radiation
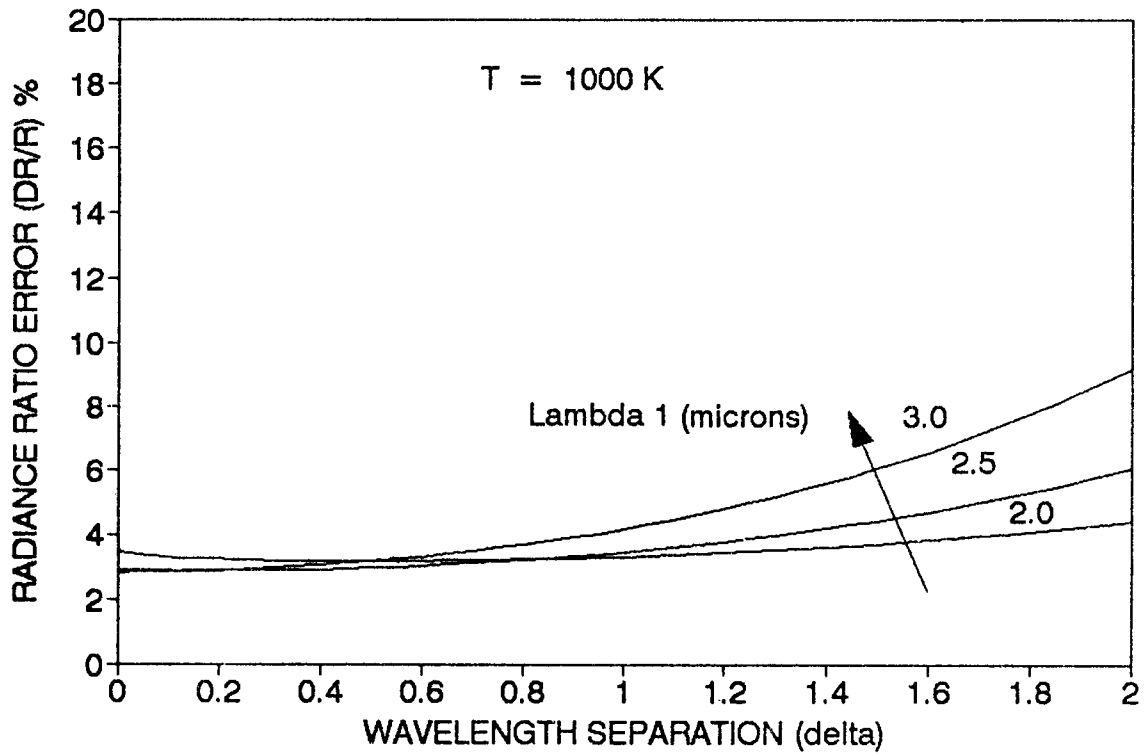
Figure 2.24   Noise Induced Radiance Ratio Error
              (Typical Blackbody Receiver).
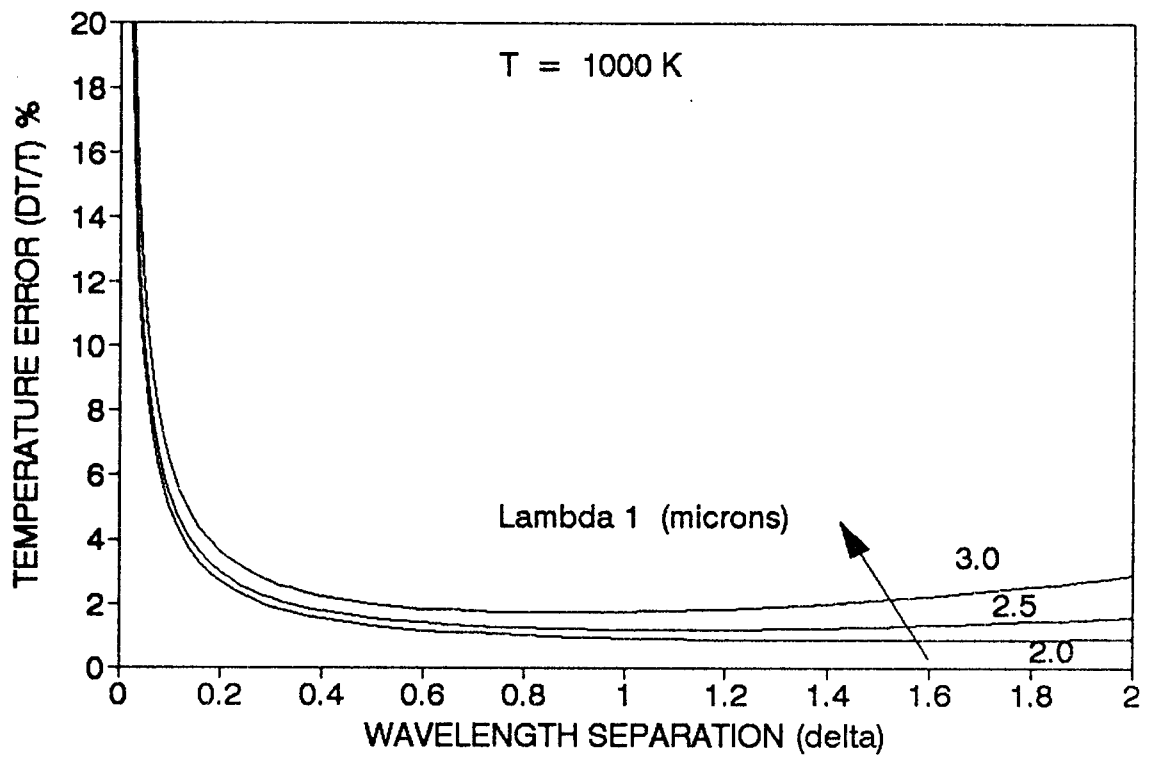
Figure 2.25   Noise Induced Temperature Error
(Typical Blackbody Receiver).
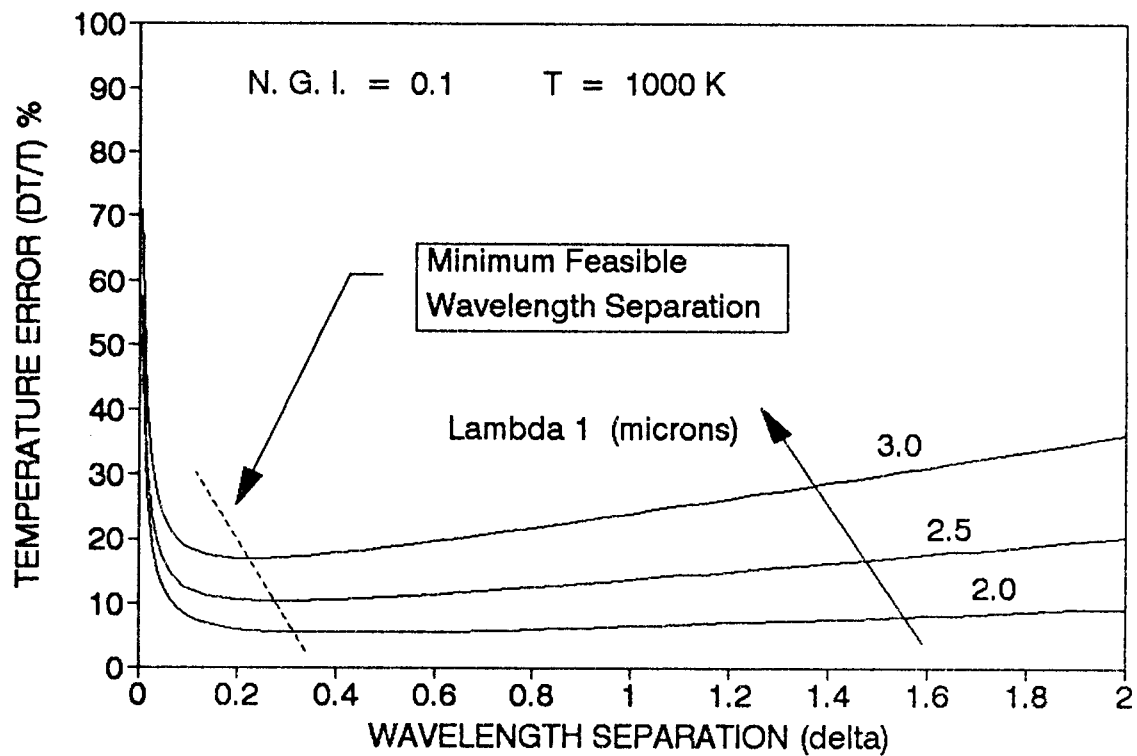
Figure 2.26   Minimum Feasible Wavelength Separation
(Typical Blackbody Receiver).

Inherent Accuracy

Aside from advantages in specific applications men-
tioned already, it is important to recognize that:

> ... for a constant uncertainty in the
> [radiance] measurement, a two-color pyrometer
> always has a greater error than the one color
> temperature calculated from the shorter wave-
> length signal, and the closer together the
> wavelengths are, the worse the error. (Spjut,
> p. 186) (emphasis added)

Spjut further states that two-color pyrometry is
justified only in those three instances already men-
tioned, and for non-gray behavior, the known emissivity
ratio ($\epsilon_{\lambda 1}/\epsilon_{\lambda 2}$) must be at least

$$\frac{1/\lambda 1}{1/\lambda 2 - 1/\lambda 1}$$

times as accurate as $\epsilon_{\lambda 1}$. (Ibid, p. 186).

Sensitivity to Incident Radiation

Two-color pyrometers are also subject to increased
sensitivity to errors from incident radiation reflected
into the instrument. The error due to reflected radia-
tion for a sample case is shown in Figure 2.27 for a
single-color pyrometer and in Figure 2.28 for a two-
color pyrometer. Note that the two-color pyrometer is
particularly sensitive to reflections originating from a
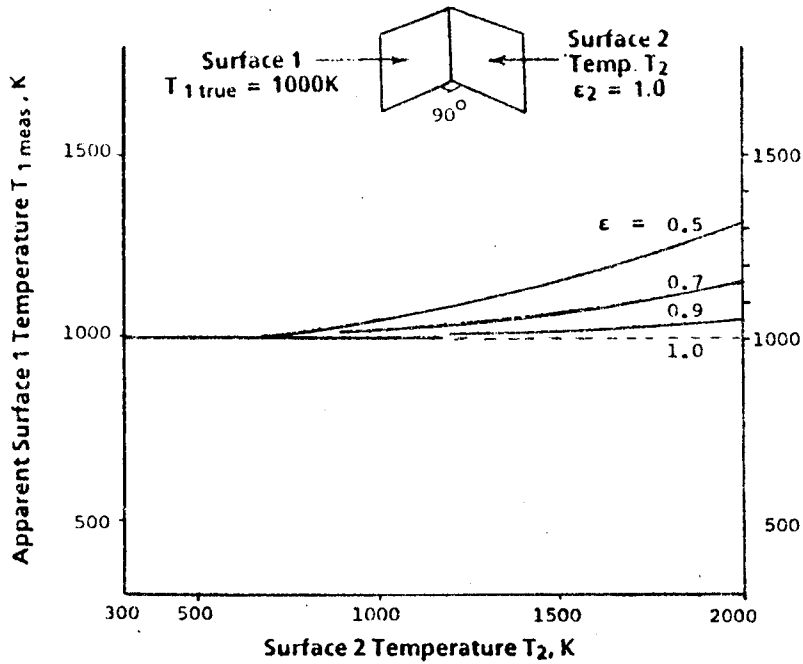
Figure 2.27   Measurement error due to reflection
(single-color system).
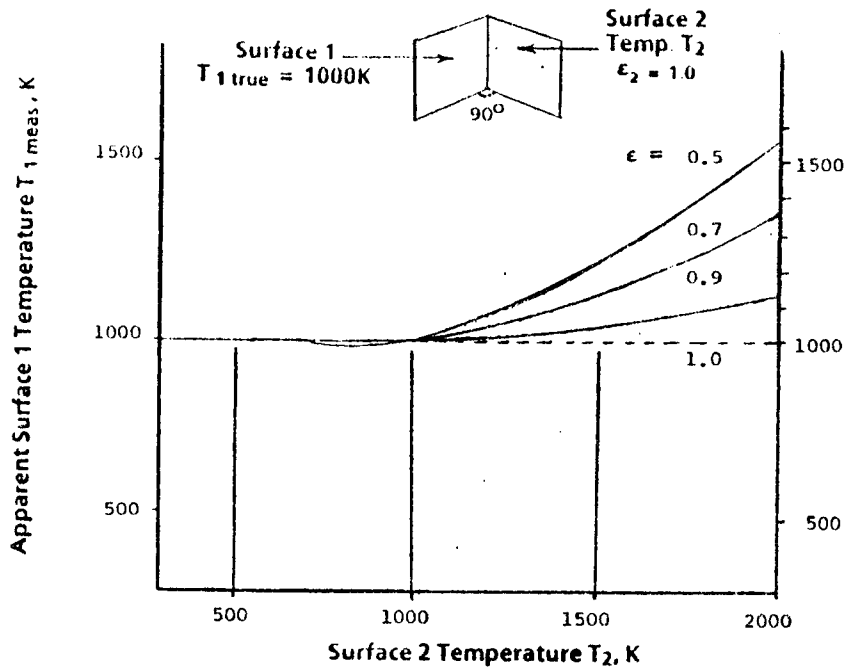
Figure 2.28   Measurement error due to reflection
(two-color system).

58

hotter surface.   The advantages of ratio pyrometry make it suited to the problem of measuring hot part temperatures inside the tailpipe of an aircraft turbine engine. However, the sensitivity of the ratio pyrometer to errors introduced by radiation reflected by the target illustrates the need for a measurement technique that can capitalize on the advantages of the ratio technique yet remain insensitive to errors induced by reflections.

CHAPTER III

A THREE-COLOR METHOD OF DETERMINING SURFACE
TEMPERATURE IN THE PRESENCE OF
REFLECTED RADIATION

Problem Statement

Surface temperature measurements using infrared
techniques are subject to error if the area of interest
(target) is reflecting radiation from a hotter source.
The magnitude of this error is a function of the temper-
ature ratio between the target and the hotter source,
the view factor between them, and the spectral surface
properties of the target and the hotter source.

Infrared temperature measurement techniques deter-
mine surface temperature by measuring the radiation from
the target surface. The fundamental principles behind
infrared temperature measurements including single-color
and two-color measurements were explained in Chapter II.
It was noted, however, that radiation detectors cannot
distinguish between reflected radiation and emitted
radiation. The quantity that is really being measured
is not radiance, but directional radiosity which is the
sum of the radiance and the reflected incident radiation
(see Figure 2.5). The assumtion that pH is zero is suf-
ficiently accurate for many applications, however, an

attempt to measure surface temperatures accurately inside a large radiating cavity such as a furnace, or an aircraft turbine engine exhaust nozzle, or a turbine engine combustor, can lead to significant errors due to reflected radiation.

Atkinson and Strange have done extensive work using a two-color method to determine aircraft turbine blade temperatures in the presence of reflected radiation. They have proposed several methods of improving the accuracy and utility of their two-color method. Among their recommended approaches is a multi-color method although no specifics are mentioned. Multi-color methods have been explored for determining surface temperatures of molten gas-tungsten arc weld pools (Hunter p. 1081-1085). This approach uses up to 500 measurements at discrete wavelength bands between 0.60 and 0.80 μm. This method however, assumes that only emitted radiation is being measured.

The need exists for an improved radiometric technique that can, without detailed knowledge of surface emissivities, be applied to the measurement of hot surfaces that may also be reflecting energy from another source.

Three-color Method

This work proposes a three-color infrared measure-

ment technique for determining surface temperature using a radiometer with filters at three different wavelength bands (three-colors). It will be shown that the information gathered through such measurements is sufficient to formulate a correction to the measured surface temperature to account for reflected radiation from a hotter surface.

The three-color approach assumes that the surface to be measured is gray and diffuse. It is also assumed that all of the energy incident on the target can be considered to emanate from a single source.

The radiosity (B1) from surface 1 (the target) in the presence of reflection from surface 2 measured in three different wavelength bands is:

$$B1_{\lambda 1} = \epsilon_{\lambda 1} Eb(\lambda 1, T1) + p_{\lambda 1} F_{2-1} B2_{\lambda 1} \qquad \text{eq. 3.1}$$

$$B1_{\lambda 2} = \epsilon_{\lambda 2} Eb(\lambda 2, T1) + p_{\lambda 2} F_{2-1} B2_{\lambda 2} \qquad \text{eq. 3.2}$$

$$B1_{\lambda 3} = \epsilon_{\lambda 3} Eb(\lambda 3, T1) + p_{\lambda 3} F_{2-1} B2_{\lambda 3} \qquad \text{eq. 3.3}$$

where B1 and B2 are measured radiosities of surface 1 and 2, ϵ is the emissivity and p is the reflectivity of surface 1, F_{2-1} is the shape factor of surface 2 to surface 1, and $Eb(\lambda, T1)$ is the spectral emissive power of a blackbody at temperature T1 and wavelength λ.

The radiosities of surface 1 and surface 2 at the three wavelengths can be determined by measurements made

62

in the three wavelength bands. If we assume that surface 1 behaves as a graybody ($\epsilon_{\lambda 1} = \epsilon_{\lambda 2} = \epsilon_{\lambda 3} = \epsilon$ and $p_{\lambda 1} = p_{\lambda 2} = p_{\lambda 3} = p$), this leaves three equations in four unknowns (p, F_{2-1}, ϵ, and $Eb(\lambda, T1)$). By combining p and F_{2-1} into a single unknown g, we now have three equations in three unknowns which can be solved to yield T1. However, since T1 is implicit in $Eb(\lambda, T1)$, the solution is not straightforward. The following solution is proposed.

By algebraic manipulation, equations 3.1, 3.2, and 3.3 can be rewritten in the form:

$$\frac{Eb(\lambda 1, T1)}{Eb(\lambda 2, T1)} = \frac{B1_{\lambda 1} - gB2_{\lambda 1}}{B1_{\lambda 2} - gB2_{\lambda 2}} = R12 \qquad \text{eq. 3.4}$$

$$\frac{Eb(\lambda 1, T1)}{Eb(\lambda 3, T1)} = \frac{B1_{\lambda 1} - gB2_{\lambda 1}}{B1_{\lambda 3} - gB2_{\lambda 3}} = R13 \qquad \text{eq. 3.5}$$

$$\frac{Eb(\lambda 2, T1)}{Eb(\lambda 3, T1)} = \frac{B1_{\lambda 2} - gB2_{\lambda 2}}{B1_{\lambda 3} - gB2_{\lambda 3}} = R23 \qquad \text{eq. 3.6}$$

where g is a geometry factor ($g = pF_{2-1}$)

This represents three equations describing the blackbody radiance ratios of surface 1 at the true temperature computed at the specified wavelengths. There appears to be four unknowns (g, R_{12}, R_{13}, and R_{23}) in equations 3.4, 3.5, and 3.6, but R_{12}, R_{13}, and R_{23} are

functions of T1. The relationship between these ratios (R_{12}, R_{13}, and R_{23}) and T1 can be determined through calibration with a blackbody (as outlined in Chapter V). Three solutions for geometry factor (g) can be derived from equations 3.4, 3.5, and 3.6 yielding the following three expressions:

$$g1 = \frac{R_{12}B1_{\lambda 2} - B1_{\lambda 1}}{R_{12}B2_{\lambda 2} - B2_{\lambda 1}} \qquad \text{eq. 3.7}$$

$$g2 = \frac{R_{13}B1_{\lambda 3} - B1_{\lambda 1}}{R_{13}B2_{\lambda 3} - B2_{\lambda 1}} \qquad \text{eq. 3.8}$$

$$g3 = \frac{R_{23}B1_{\lambda 3} - B1_{\lambda 2}}{R_{23}B2_{\lambda 3} - B2_{\lambda 2}} \qquad \text{eq. 3.9}$$

Now if the graybody assumption is true, then $g_1 = g_2 = g_3$ and hence:

$$\frac{R_{12}B1_{\lambda 2} - B1_{\lambda 1}}{R_{12}B2_{\lambda 2} - B2_{\lambda 1}} - \frac{R_{13}B1_{\lambda 3} - B1_{\lambda 1}}{R_{13}B2_{\lambda 3} - B2_{\lambda 1}} = 0 \qquad \text{eq. 3.10}$$

$$\frac{R_{12}B1_{\lambda 2} - B1_{\lambda 1}}{R_{12}B2_{\lambda 2} - B2_{\lambda 1}} - \frac{R_{23}B1_{\lambda 3} - B1_{\lambda 2}}{R_{23}B2_{\lambda 3} - B2_{\lambda 2}} = 0 \qquad \text{eq. 3.11}$$

$$\frac{R_{13}B1_{\lambda 3} - B1_{\lambda 1}}{R_{13}B2_{\lambda 3} - B2_{\lambda 1}} - \frac{R_{23}B1_{\lambda 3} - B1_{\lambda 2}}{R_{23}B2_{\lambda 3} - B2_{\lambda 2}} = 0 \qquad \text{eq. 3.12}$$

All of the parameters in equation 3.10 can be measured (assuming that surface 2 can be viewed by manipulation of the three-color instrument) except the radiance ratios, R_{12} and R_{13}. They are implicit functions of the single unknown T1. For a given value of T1, corresponding values of R_{12} and R_{13} have been determined from the blackbody calibration. Equation 3.10 can be solved iteratively by assuming a value for T1 which then determines R_{12} and R_{13}. A non-zero result of equation 3.10 indicates that the assumed value for T1 was in error. By raising or lowering T1 and solving iteratively, equation 3.10 can be made to converge on a solution close to zero. T1 at the point of convergence is the three-color solution for T1. Solutions for equations 3.11 and 3.12 can be derived similarly. In the ideal case these solutions will yield a single value for T1 as shown in Figure 3.1a. When real data are used, each solution may yield a slightly different value for T1 as illustrated in Figure 3.1b. Unless otherwise specified in the discussion that follows, the three-color temperature solution will be represented by the average of the three values derived for T1 from equations 3.10, 3.11, and 3.12.

As this work was nearing completion, the author was apprised of a paper by M. H. Horman published in 1976 in which a technique was introduced that uses the
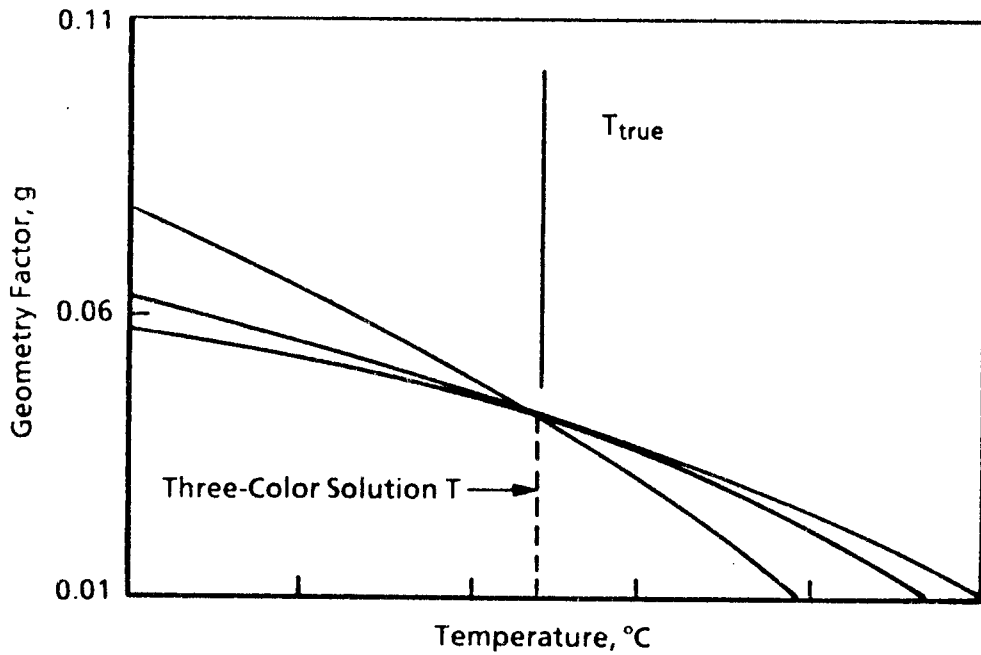
a. Ideal solution (synthesized data)
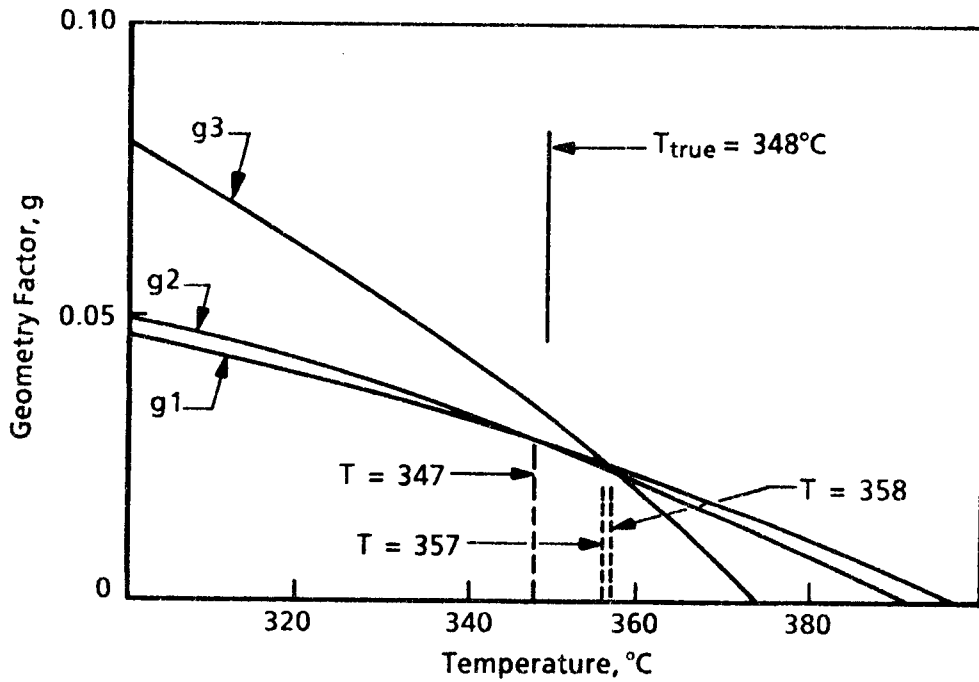
b. Real solution (experimental data)

Figure 3.1   Geometry factor (g) convergence leading to three-color solutions.

ratio outputs of a multispectral IR sensor to determine the true temperature of an object and the relative amounts of reflected and emitted flux. Horman's technique is similar to the three-color technique described herein.

CHAPTER IV

APPARATUS

An experiment was devised to investigate the three-color measurement technique described in Chapter III. The apparatus used in this experiment include three major components; an infrared radiation detection system (radiometer), a heated target surface, and a high temperature radiation source of reflected energy.

Infrared Radiation Detection System

The infrared radiation detection system chosen for this investigation was a Barnes ® Spectral Master Radiometer, model 12-660 Serial Number (S/N) 119, manufactured by Barnes Engineering Company, 30 Commerce Road, Stamford Connecticut. The Barnes radiometer was chosen because it incorporated a remotely controlled eight-position filter wheel (the ability to detect radiation in at least 3 discrete wavelength bands was critical in this experiment) and because it uses a variable gain amplifier which gives the instrument a large dynamic range. The Barnes Radiometer incorporates an immersed thermistor bolometer detector with a anti-reflection coated germanium lens. Operating principles of a thermistor bolometer are described in Holman (p. 408,409).

Radiometer Characteristics

The Barnes Radiometer is shown in Figure 4.1. The bolometer detector spectral response ranges from 1.8 to 28 microns as reported in the operator's manual that accompanied the instrument (Figure 4.2). The total response of the radiometer will be affected by the spectral transmission characteristics of all lenses, filters, and other optical devices in the optical path. An eight position filter wheel is mounted in front of the detector (Figure 4.3). The filter wheel is driven by a remotely controlled stepper motor. A lens holding fixture is located in front of the filter wheel, though no lens was installed during the three-color experiment. A chopper wheel is located in front of the lens holder, providing a square wave chopping function at 15 Hz. The front end of the radiometer has a removable cover with a rectangular aperture measuring 1 by 1.75 in.

The field of view (FOV) of the radiometer as configured for the experiment was determined to be approximately 20 deg. in the horizontal direction. The vertical FOV was not measured, but because the bolometer lens is spherical, and the filters are circular, the vertical FOV is assumed to be approximately equal to the horizontal FOV. The radiometer cover plate does not restrict the FOV. The FOV is important primarily to help deter-
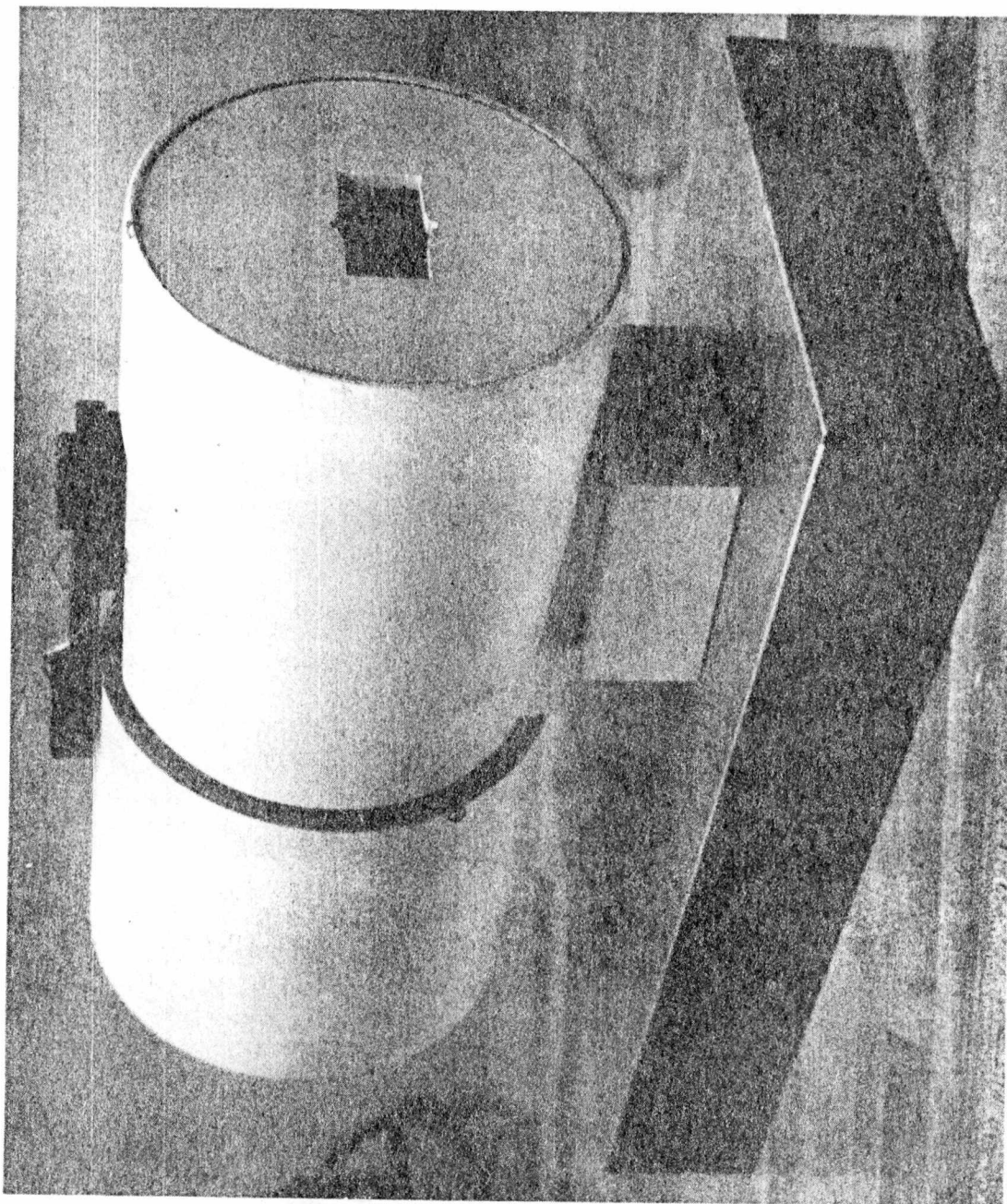
Figure 4.1 Barnes ® Spectral Master Radiometer.
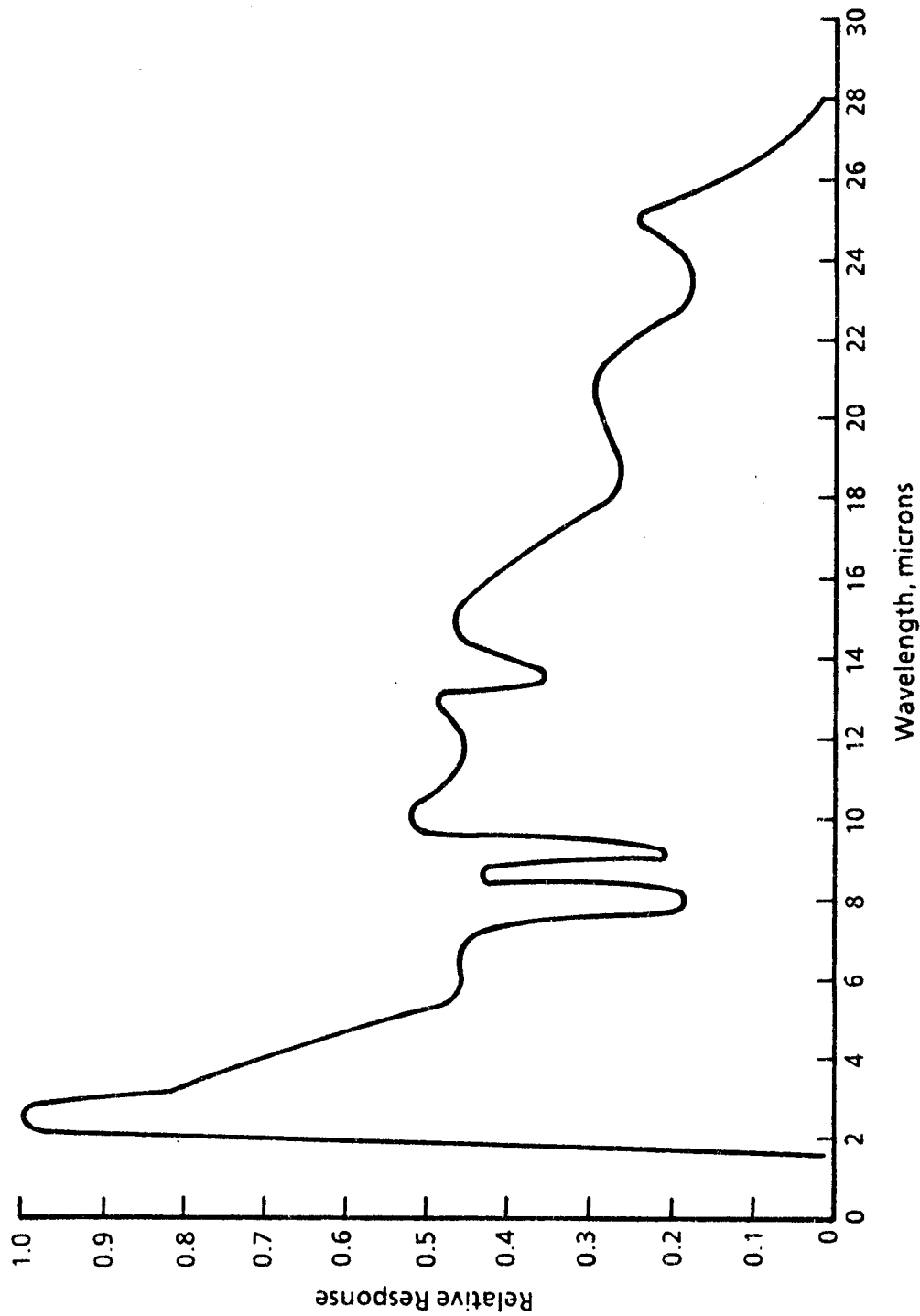
Figure 4.2   Radiometer Detector Spectral Response.

71
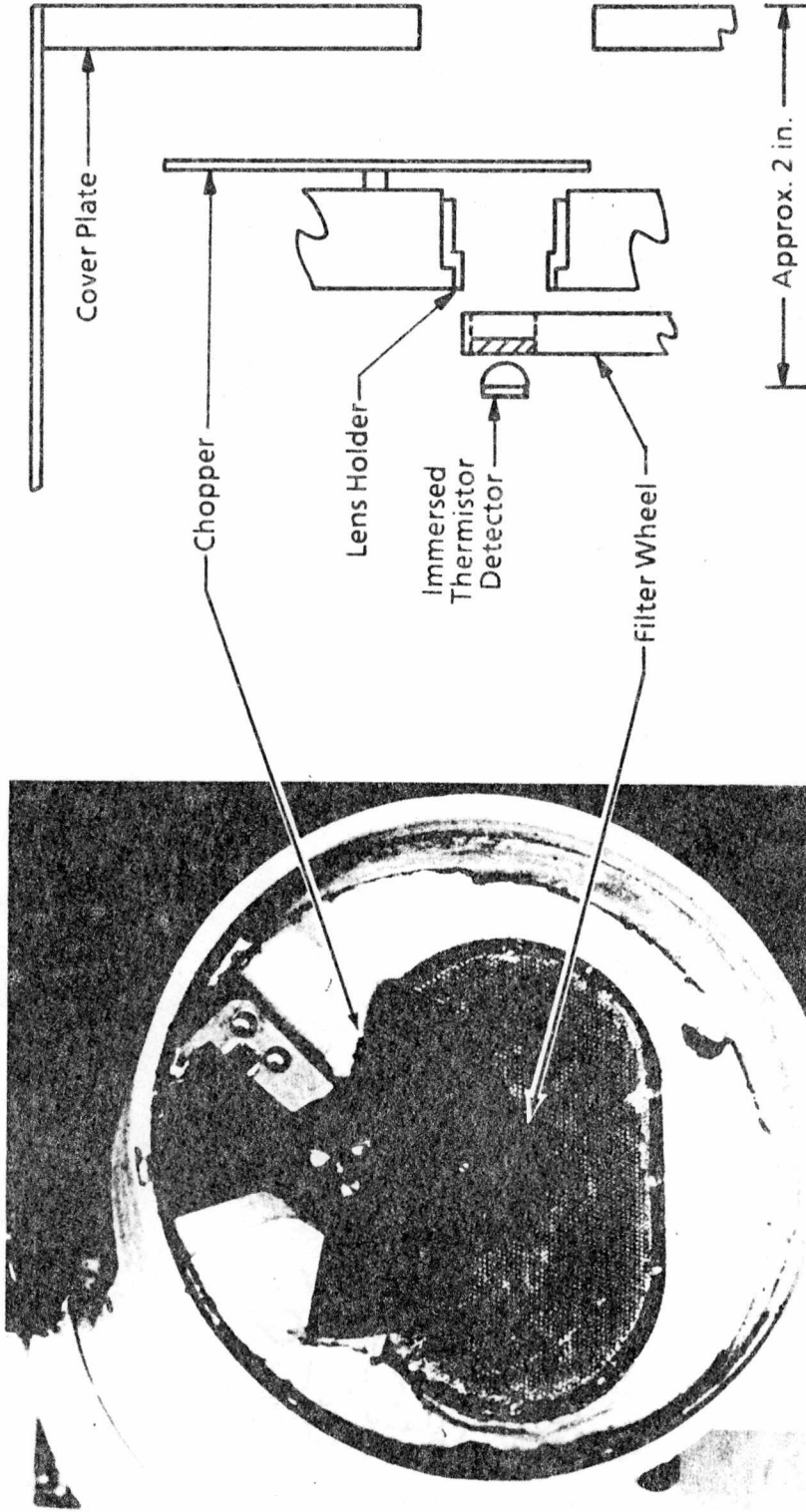
Figure 4.3 Internal View of Barnes ® Spectral Master Radiometer.

Cover Plate

Chopper

Lens Holder

Immersed
Thermistor
Detector

Filter Wheel

Approx. 2 in.

72

mine target spot size, and to ensure that the FOV is filled during portions of the radiometer calibration process.

Filters

The Barnes radiometer filter wheel can accommodate up to eight 0.35 in. dia. filters. Seven filters were installed leaving one filter position open. The choice of filters for this experiment was influenced by filter suitability and availability.

Filter suitability is a function of the temperature of the surface that is being measured, the response of the instrument, and the requirement to avoid the atmospheric CO_2 and H_2O emission and absorption bands (Figure 4.4). For this investigation, the surface temperature range was limited to 300 to 600° C by the capabilities of the heated target surface. The three-color temperature measurement technique requires the measurement of radiant energy at three discrete wavelengths that will result in three distinct and usable radiance ratios. If the center wavelength and the bandwidth of each filter are selected such that the energy collected in each wavelength band is of the same order of magnitude, the radiance ratios can be computed directly from the measured radiometer response (millivolts). Energy levels that are not of the same order of magnitude may

73
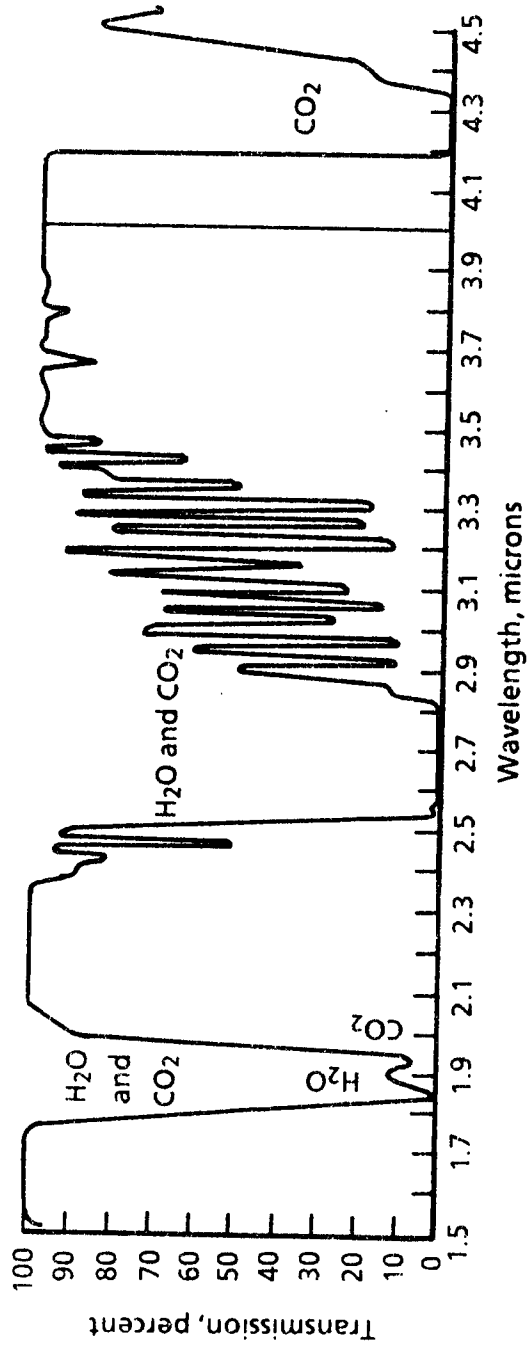
Figure 4.4   Water Vapor and Carbon Dioxide Absorption and Emission Bands in the 1.5 to 4.5 μm Range.

74

lead to radiance ratios with significant round off errors. Using calculated in-band radiance to determine radiance ratio may obviate the requirement to select filters with similar total bandpass energy levels, but for the sake of simpler data reduction, comparable total bandpass energy levels were considered a requirement for the filters selected.

Filter availability was also a factor considered, since the selection of filters sized to fit the filter wheel (0.35 in dia.) was limited. Fabrication of filters to match the optimum specifications for the experiment was not economically feasible. Filters were chosen from among those already available through commercial suppliers. They were installed in the filter wheel as shown in Table 4.1. The spectral response of the filters (as supplied by the filter manufacturer) is shown in Figure 4.5.

Target Surface

The target surface for this experiment was chosen to produce the best experimental results possible using readily available materials. The primary features that were considered important for the target surface were stable temperature control, uniform surface temperature, independent temperature verification, diffuse surface behavior, and an emissivity level significantly less

75

Table 4.1 List of Filters Installed in Barnes ® Radiometer.

Wheel Position	Lower Half-Power Point, μm	Upper Half-Power Point, μm	Bandwidth, μm	Center Wavelength, μm
1	1.987	2.063	0.076	2.025
2	2.033	2.385	0.352	2.209
3	3.398	3.599	0.201	3.4985
4	3.398	3.670	0.272	3.534
5	3.807	3.969	0.161	3.888
6	3.939	4.105	0.166	4.022
7	9.948	11.428	1.480	10.688
8		No filter		
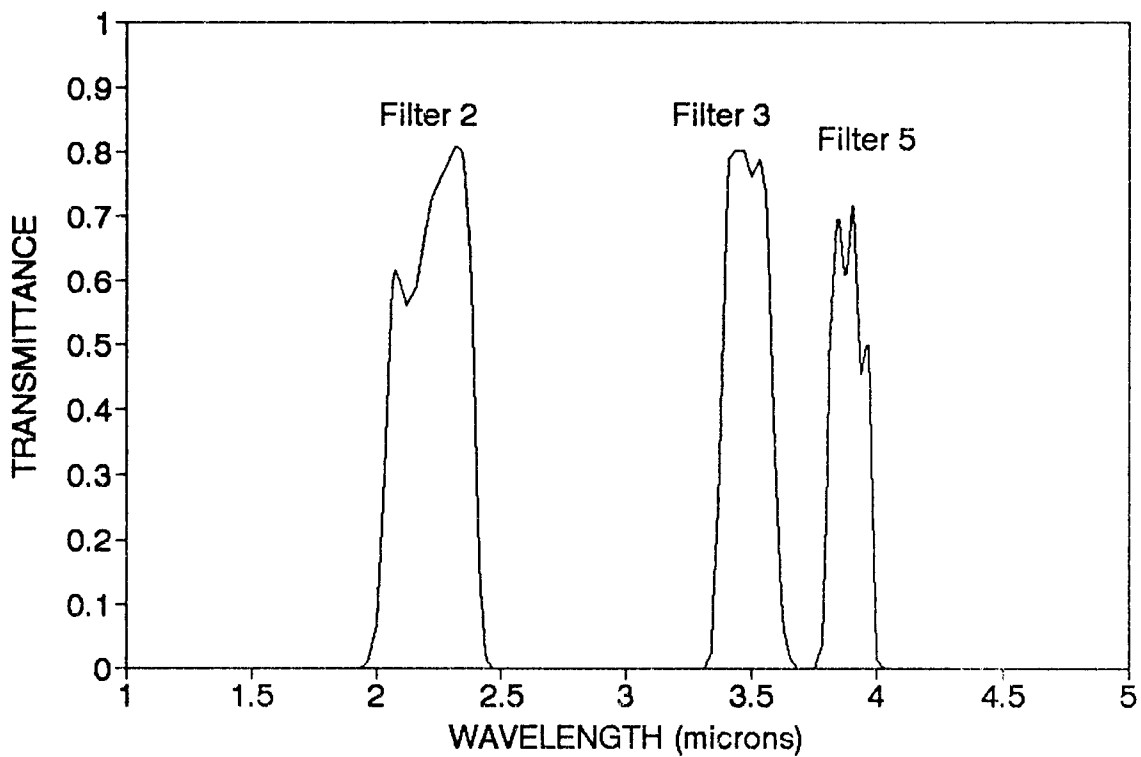
Figure 4.5   Spectral Response of Radiometer Filters
2, 3, and 5.

than 1.0. An electrically heated aluminum plate was chosen for the target surface. The properties of the aluminum plate did not meet the specifications in all cases, but were believed to provide a reasonable approximation within the available resources. A sketch of the target is shown in Figure 4.6. The properties of the target are discussed below.

Target Temperature Control

Target temperature was controlled using an electric hotplate with a variable power supply. Supply voltage could be varied between 30 and 120 volts AC. The hot plate was made of cast iron with resistance heater coils located behind the cast iron plate. The hotplate temperature at 120 volts stabilized at approximately 500 °C. The cast iron surface of the hotplate exhibited an emittance very close to 1.0 and was therefore considered unsuitable for this experiment. An aluminum plate was bolted to the hotplate to serve as the target surface. The high thermal conductivity of the aluminum provided good heat transfer from the hotplate.

Uniform Surface Temperature

Uniform target surface temperatures were important to the successful completion of this experiment. It was expected that the edges of the target would be slightly

78
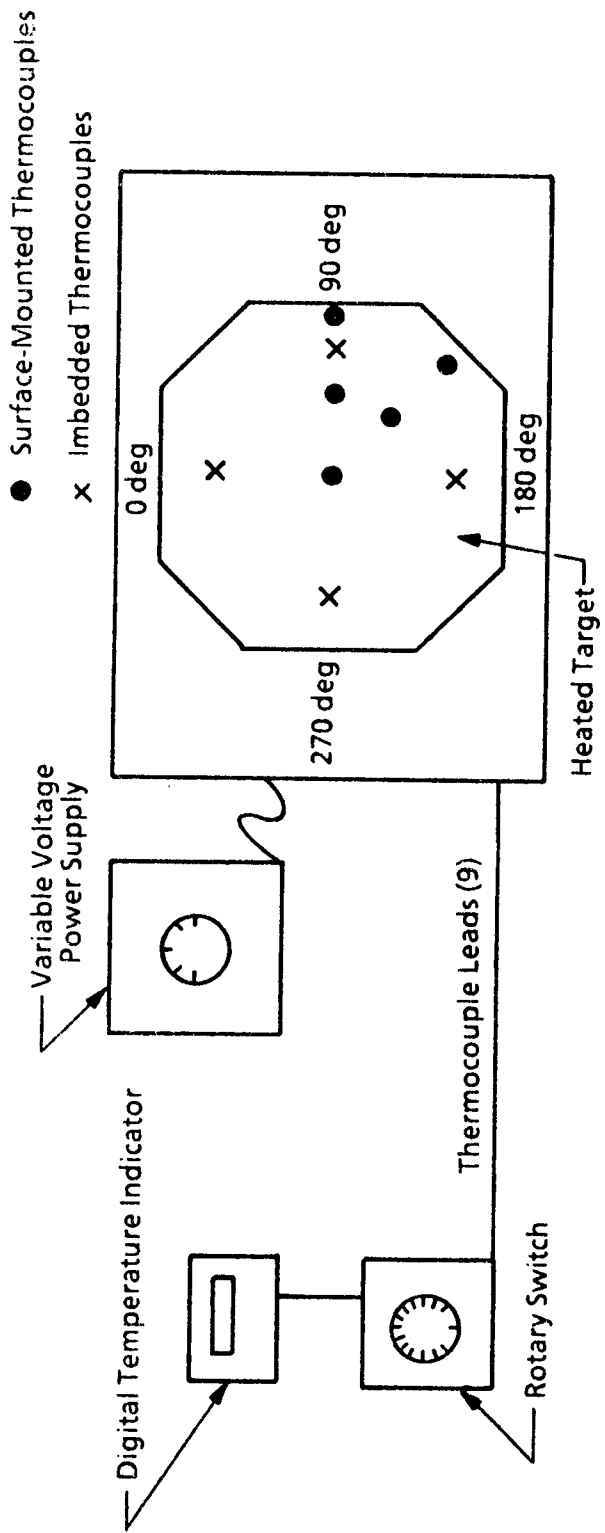
Figure 4.6 Electrically Heated Target Surface.

79

79

cooler than the center. Aluminum was chosen for the target surface partly for its high thermal conductivity, which was expected to minimize radial temperature gradients. A circular shaped target would be preferred to a square or rectangular target from the standpoint of minimizing circumferential temperature gradients attributable to radiation from the four corners, but for ease of fabrication, an octagonal shape was chosen. A Hughes [R] Probeye infrared scanning camera was used to check the radial and circumferential temperature profiles. Surface mounted thermocouples were added to further assess temperature gradients but were not installed when radiance readings were taken. A discussion of the target surface temperature gradients is presented in Chapter V.

Independent Temperature Verification

Independent verification of the target surface temperature is required for the validation of the three-color temperature measurement technique. Installation of thermocouples directly on the target surface helped assess surface temperatures, but was not considered feasible during radiance measurements because the thermocouples and lead wires would interfere with the radiance readings. Internal thermocouples were imbedded at four locations around the plate (see Figure 4.6).

80

Digital readout of the thermocouples was used to provide an indication of the surface temperature. The Hughes Probeye data and the surface mounted thermocouple data were used to formulate an adjustment to the indicated temperature (from the imbedded thermocouples) to provide the best possible estimate of target true surface temperature (hereafter referred to as T_{true}). (Further discussion of this temperature adjustment is found in Chapter V). It must be emphasized that throughout this discussion references to T_{true} are used for convenience in making comparisons. In reality, T_{true} cannot be represented by a single number but as a temperature band within which the true target surface temperature is believed to fall. This temperature band (uncertainty) is estimated to be ± 4° C.

Diffuse surface behavior

The three-color surface temperature measurement technique assumes but does not require diffuse behavior. Most surfaces of interest are probably more diffuse than specular. In a specular reflector, the angle of incidence is equal to the angle of reflection. A diffuse reflector reflects equally in all directions (see Figure 2.7). Any real surface will have some diffuse and some specular reflection. A polished surface is usually predominantly specular, while a dull, rough, or oxidized

surface will generally be more diffuse. The intent of
this experiment is to develop a temperature measurement
technique that might be used with predominantly diffuse
surfaces; a predominantly diffuse target was therefore
desired. The target surface was made from smooth unpol-
ished aluminum. An experiment was conducted with the
aluminum plate to estimate how specular the surface was.
Incident radiation was directed at the surface at an
angle of 50 deg. from the surface. Radiance readings
were made from the target at angles from 30 to 90 deg.
The untreated surface showed a high specular reflection
contribution as indicated by high readings at 50 deg
(Figure 4.7). The surface was roughened using No. 150
emery paper and the readings were repeated. The specu-
lar reflection of the surface was significantly lower
after the surface was roughened. A surface dimpling
technique was used to introduce a pattern of dimples
approximately 1 millimeter in diameter and one half mil-
limeter deep in the target surface (Figure 4.8). The
dimples act as many small cavity radiators on the sur-
face and have the effect of reducing the specular compo-
nent of the reflection. The reflection experiment
showed that the specular reflection after dimpling was
sharply reduced from that of the untreated surface (Fig-
ure 4.8).
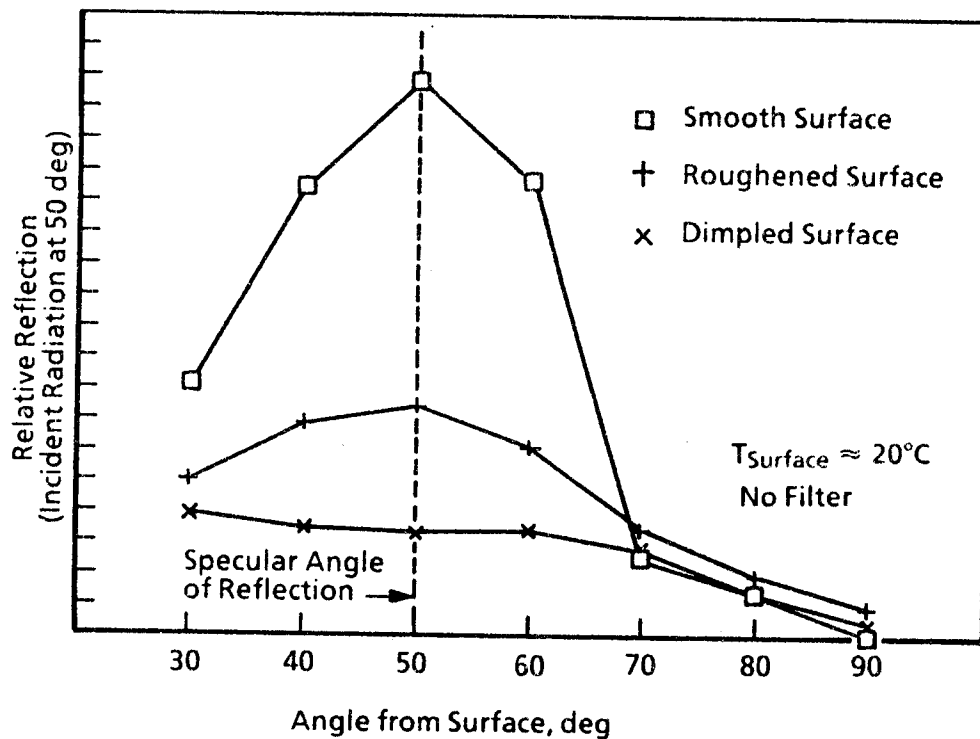
Figure 4.7 Target Surface Reflection Characteristics Before and After Surface Treatments.
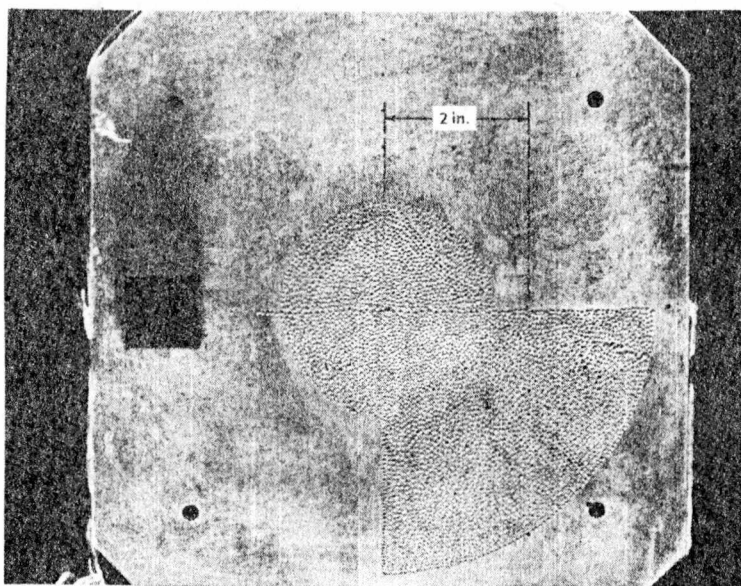
a.   Target
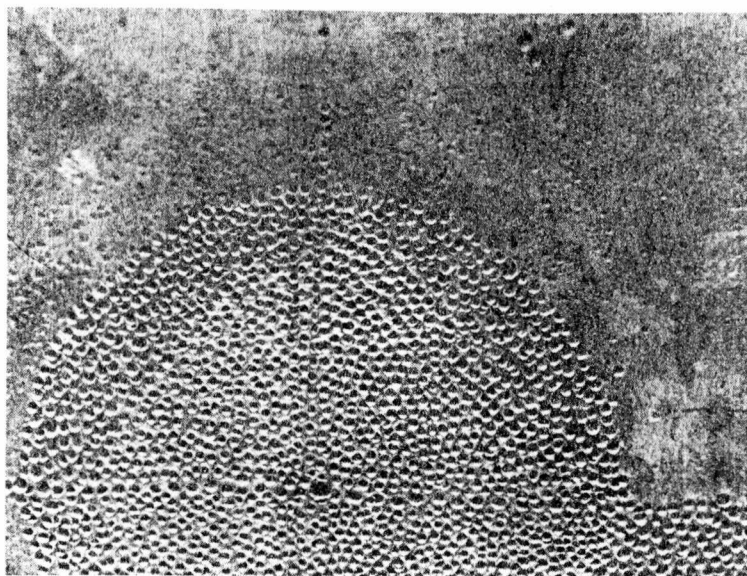
b.   Close-up view of dimples

Figure 4.8   Aluminum Target Surface with Dimples

Emissivity Level

An emissivity level between 0.5 and 0.8 was desired for this experiment. An estimate of the emissivity of a smooth unpolished aluminum surface obtained from published sources (Gubareff p. 263) is shown in Figure 4.9. Notice that the total emissivity of aluminum increases slightly with surface temperature. The change of emissivity with a change in surface temperature introduces an error in a single-color radiance measurement, but if the emissivity ratio remains constant, emissivity changes with temperature should not be a source of error in multi-color measurements (two-color and three-color methods). Note however, that at a temperature near 500 °C, the total emissivity is estimated to be approximately 0.1, far below the desired level for this experiment.

An estimate of the spectral emissivity for aluminum at room temperature is shown in Figure 4.10. Notice that emissivity varies with wavelength. This represents a source of error for the multi-color measurement. For this experiment, the emissivity is desired to be constant at wavelengths from 2 to 4 microns. A discussion of ways to account for errors due to emissivity variation with wavelength (non-gray behavior) is presented in Chapter V.

85
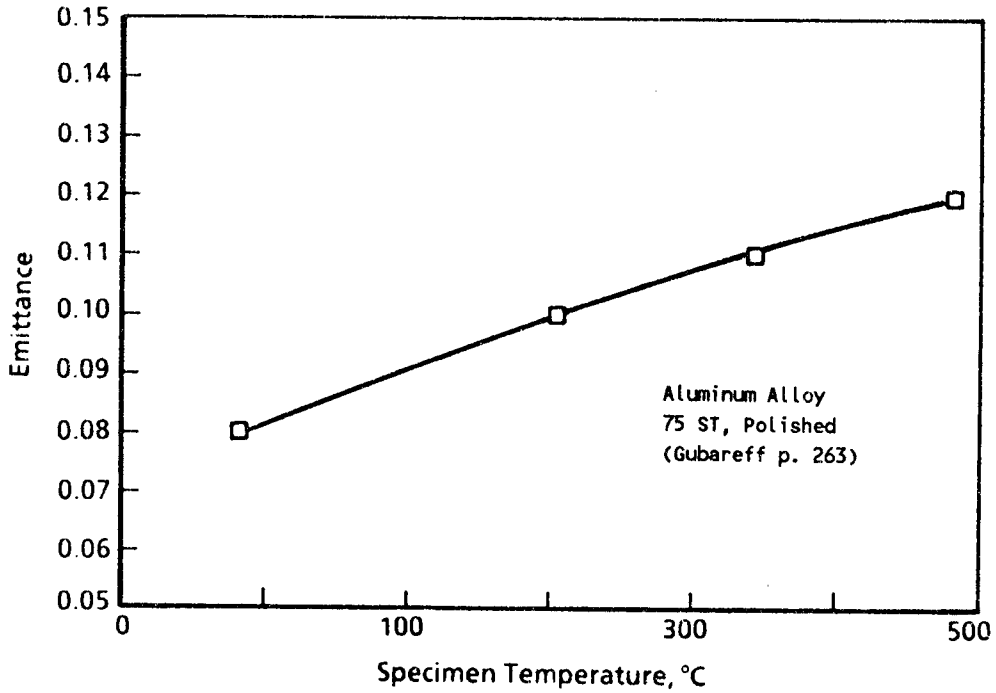
Figure 4.9.   Total Emissivity of an Aluminum Plate
               (Typical Published Values).
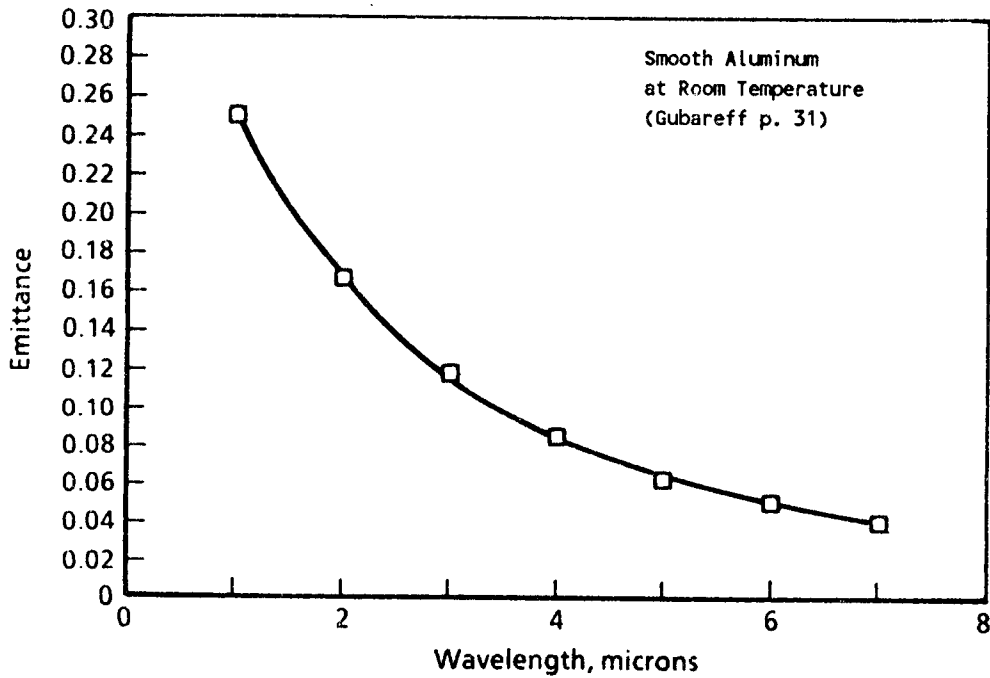
Figure 4.10.   Spectral Emissivity of Aluminum at Room
               Temperature (Typical Published Values).

86

High Temperature Radiation Source

A high temperature source of radiation is required to provide reflected energy for the demonstration of the three-color temperature measurement technique. The high temperature source provides radiation incident on the target surface. Such incident radiation on the target surface, reflected into the radiometer, can cause temperature errors in the single-color and two-color measurements and motivated the proposal of the three-color method. The source of the incident radiation for this experiment does not need to be diffuse or gray if direct readings can be taken with the radiometer. To simplify the experiment, a pair of one inch black bodies were selected as the source of the high temperature radiation (Figure 4.11). The use of black bodies for the source of high temperature incident radiation in this experiment eliminated the need to take direct measurements from the high temperature surface.
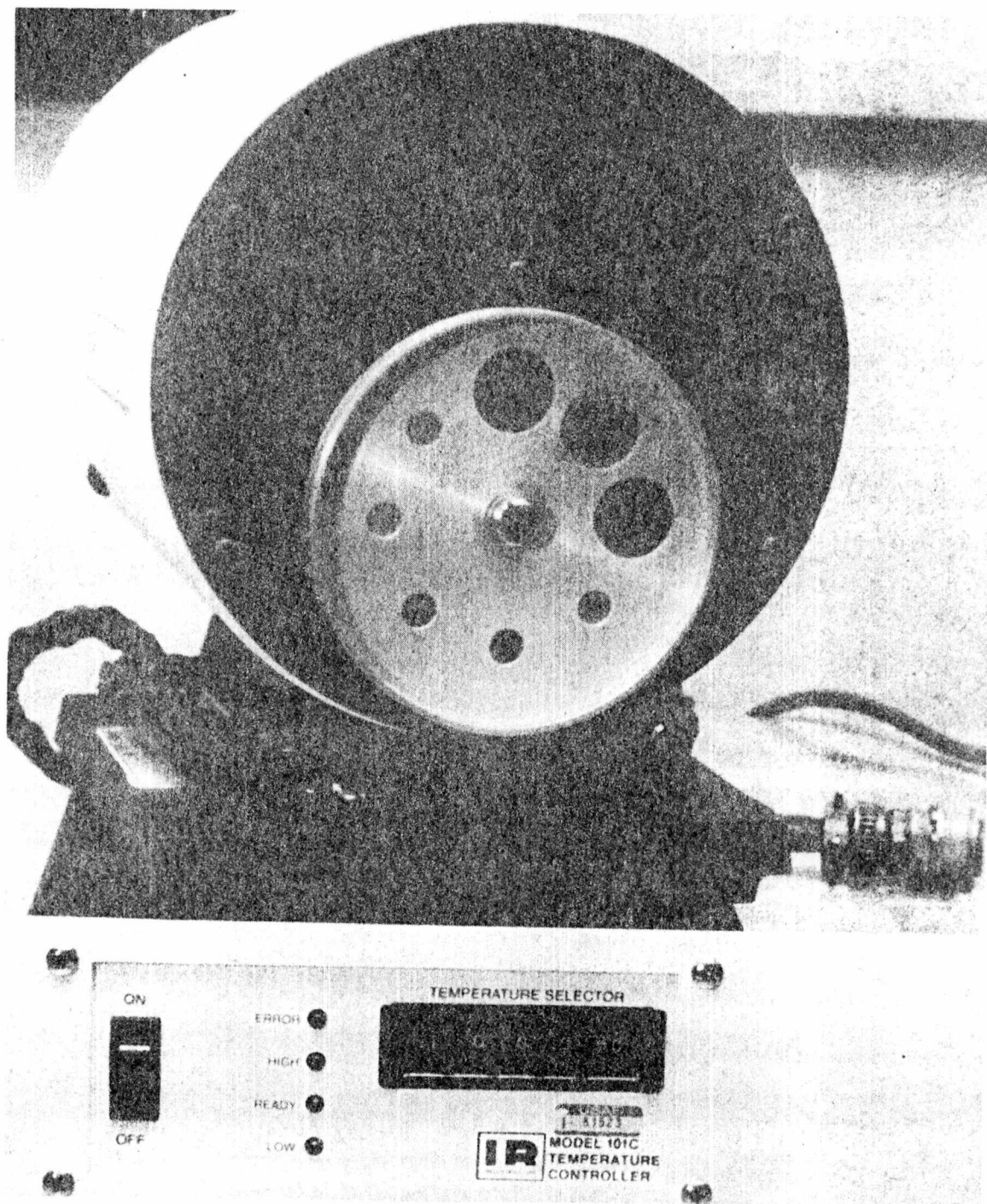
Figure 4.11   Photograph of 1 inch Blackbody Radiator.

88

CHAPTER V

PROCEDURE

Radiometer and Surface Calibrations

Radiometer Calibration

The Barnes radiometer was calibrated for all eight filter positions using a 6 inch blackbody (B.B.) source operated from 200 to 500° C (the maximum temperature achievable). The 6 inch B.B. was chosen to ensure that the radiometer FOV would be filled. A filled FOV is a requirement for single-color calibration. The single-color calibration consisted of establishing a millivolt versus B.B. temperature relationship at 6 points for the radiometer at each filter setting (Figure 5.1). The six calibration points were used to produce calibration curves of the form millivolts $= a(T)^X$.

Radiance ratio (two-color) calibrations were determined by calculating the ratio of the single-color readings in different wavelength bands (filter settings). With radiometer readings using 8 different filters (the open position with no filter can be treated as a filter with 100 percent bandpass over the total range of the radiometer spectral response), 28 unique ratio combinations may be formed. Of these ratio combinations, the three that appeared to be best suited to the three-color

89
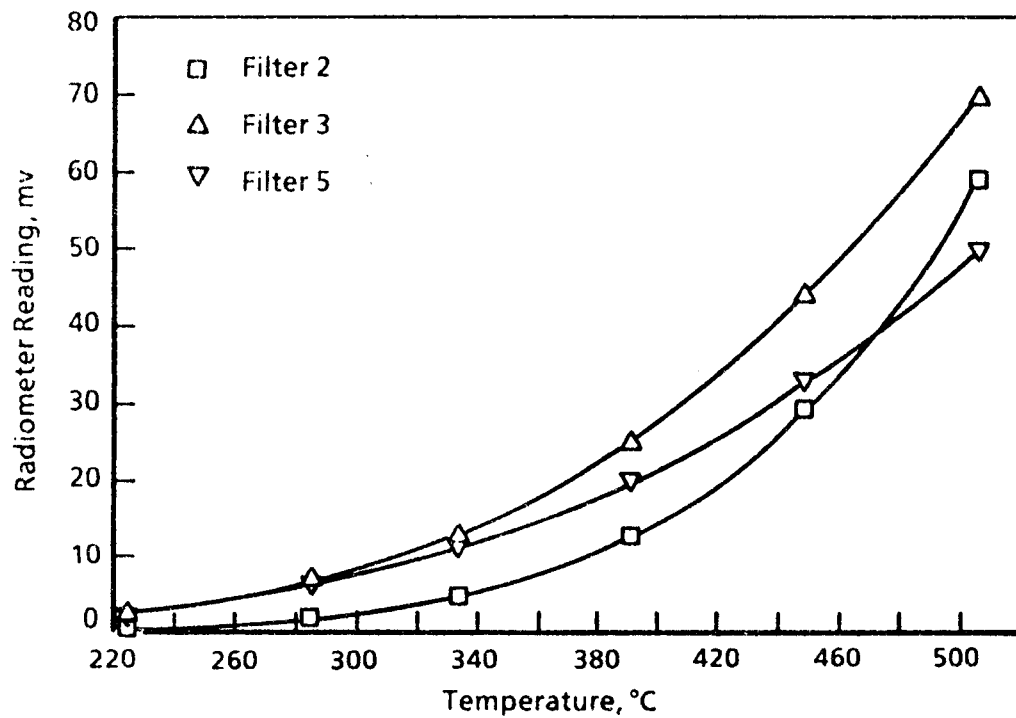
Figure 5.1   Single-color Temperature Calibrations for
Filters 2, 3, and 5.

90

method in the temperature range of this experiment were
from filter 2 (2.0 - 2.4 μm), filter 3 (3.4 - 3.6 μm),
and filter 5 (3.8 - 4.0 μm). These three filters were
then chosen for the three-color experiment and are
designated as $\lambda 1$, $\lambda 2$, and $\lambda 3$ throughout the rest of this
discussion . The radiance ratios with these three fil-
ters (Figure 5.2) are calculated directly from millivolt
readings:

$$R_{12}(T) \quad = \quad \frac{mv_{\lambda 1}}{mv_{\lambda 2}} \qquad\qquad \text{eq. 5.1}$$

$$R_{13}(T) \quad = \quad \frac{mv_{\lambda 1}}{mv_{\lambda 3}} \qquad\qquad \text{eq. 5.2}$$

$$R_{23}(T) \quad = \quad \frac{mv_{\lambda 2}}{mv_{\lambda 3}} \qquad\qquad \text{eq. 5.3}$$

Second order curve fits of the six calibration
points were used to generate radiance ratio tables from
200° to 500° C (Appendix E).

Target Surface Calibration

Four thermocouples were imbedded in the aluminum
target to provide an independent indication of surface
temperature (see Figure 4.6). Surface mounted thermo-
couples were also added to help determine the magnitude
of radial surface temperature profiles and to derive an

91
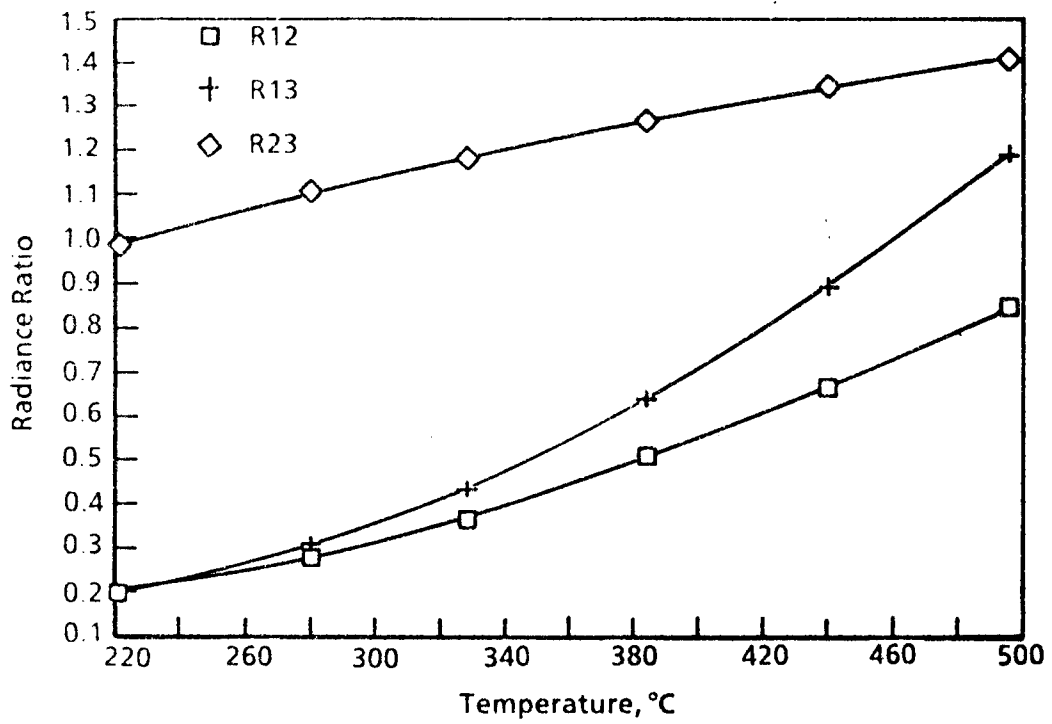
Figure 5.2   Radiance Ratios with Lambda 1, Lambda 2, and
            Lambda 3 from 220 to 500° C.

adjustment to the imbedded thermocouple readings to pro-
vide the most accurate surface temperature indication
that was possible. High emissivity black paint was
applied to a one inch spot located away from the target
area. A Hughes Probeye camera temperature determination
of black spot temperature agreed within 2 percent of the
surface mounted thermocouple at the center of the target
with the target heated to 500° C. Radial surface tem-
perature profiles are shown in Figure 5.3a. The
radiometer FOV produced a target spot size with a radius
of approximately 1.5 in. The radial profile within this
radius was estimated to be small enough ($\leq$ 1° C) to be
ignored in the calculation of target surface tempera-
ture. A correlation between the indicated black spot
temperature internal thermocouple reading at 0 deg. (12
o'clock position) was used to formulate a calculation of
the surface temperature based on the internal thermo-
couple reading. An adjustment of 3° C was applied to
this thermocouple reading to give an estimate of the
surface temperature in the center of the target (see
Figure 5.3b). The indicated target surface temperature
remained stable within ± 1° C throughout the experiment
(Figure 5.4). A list of anticipated contributors to
surface temperature uncertainty are listed in Table 5.1.
The total surface temperature uncertainty was estimated
to be ± 4° C.

a. Target radial profiles

b. Imbedded thermocouple correction
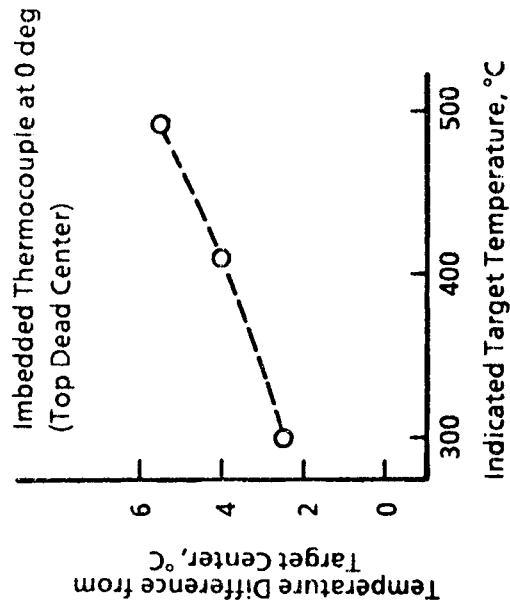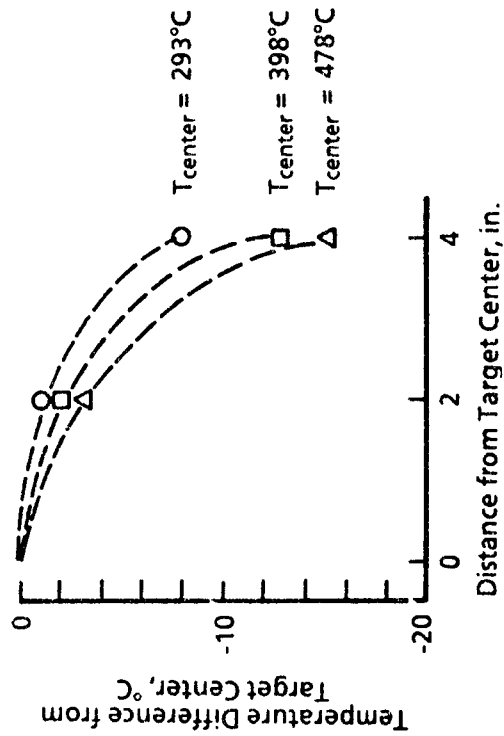
Figure 5.3 Target Surface Temperature Profiles and Correction to Imbedded Thermocouple Readings.
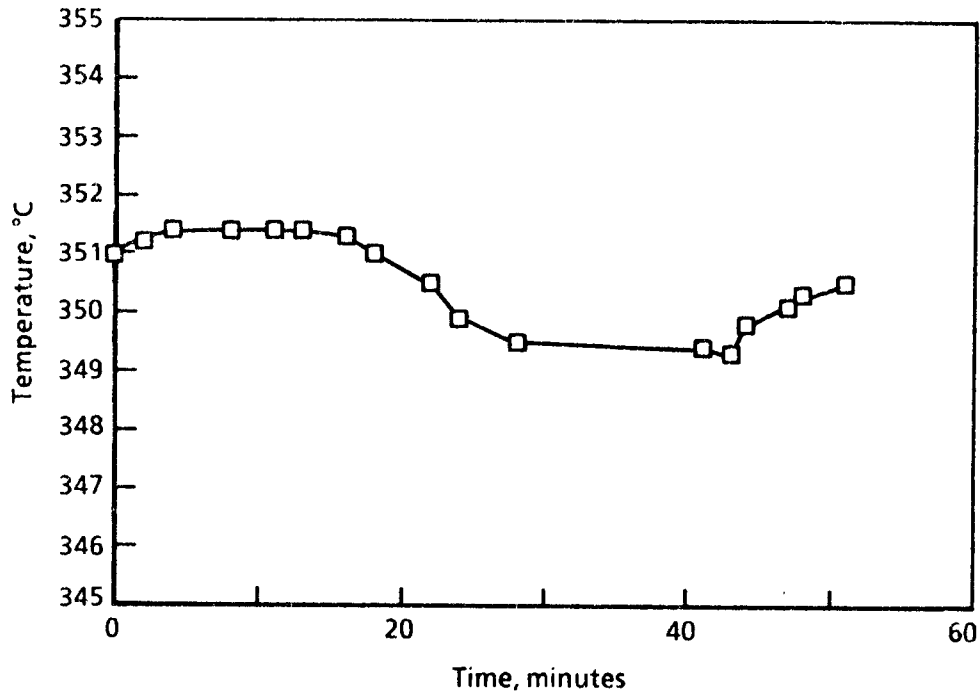
Figure 5.4.   Target Temperature Stability During Three-
color Experiment.

95

Table 5.1   Estimated Contributors to Target Surface
            Temperature Uncertainty.

Source of Uncertainty	Estimated Contribution (less than or equal to)
Thermocouple Reading	± 2 °C
Radiation Error on Thermocouple	± 2 °C
Radial Temperature Profile	± 1 °C
Circumferential Temperature Profile	± 2 °C
Temperature Fluctuation with Time	± 1 °C
Cumulative (Root Sum of Squares)	± 4 °C

Set up and Data Acquisition

The set up for the three-color experiment is shown in Figure 5.5. The radiometer was positioned six inches from the target surface. The small distance between the radiometer and the target was required in order to keep the target spot size to a minimum ($\approx$ 3 in. dia.). The two blackbody radiators were also located about six inches from the target surface at an angle of about 45 deg. on each side of the radiometer. One of the black-bodies produced a lower intensity reflection than the other one despite the fact that they were set to the same temperature. This difference in reflected energy is attributed to slight differences in alignment of the blackbodies or to surface irregularities. This resulted in three different reflected energy levels when the blackbodies were opened and closed in combination. Blackbody A yielded the lowest level of reflected energy ($\approx$ 5 percent @ 1000° C). Blackbody B yielded a level nearly double that for Blackbody A ($\approx$ 10 percent @ 1000° C). The levels were additive when both Blackbodies were open ($\approx$ 15 percent @ 1000 ° C). The percent reflected energy (percent reflection) was calculated as shown below:

$$pH\% = \left[\frac{N_r}{N_o} - 1 \right] \times 100\% \qquad \text{eq. 5.4}$$

97
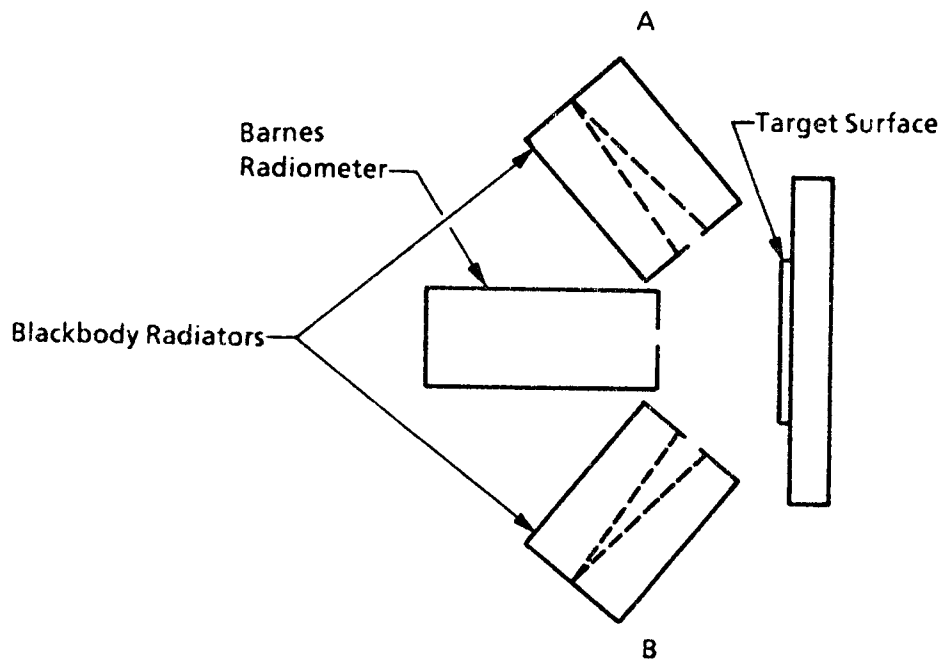
Figure 5.5. Hardware Setup for Three-color Experiment.

where:

$$pH\% = \text{percent reflection}$$
$$N_r = \text{radiance measured with reflection}$$
$$N_o = \text{radiance without reflection}$$

Data Reduction

Reduction of the experimental data was accomplished using a simple computer program. Raw millivolt readings and corresponding gain values were combined with the appropriate zero offset to yield adjusted millivolt readings for each wavelength band (filter position) where data were collected. The adjusted millivolt values were divided by the assumed value for emissivity and compared to the single-color calibration curves to determine single-color temperature solutions.

Radiance ratios calculated from the adjusted millivolt values were compared to tabulated radiance ratio versus temperature data from the radiometer calibration to compute two-color temperatures. The two-color temperature solutions are denoted T_{12}, T_{13}, and T_{23} calculated from R_{12}, R_{13}, and R_{23} respectively.

Values for the geometry factor (g) were calculated for R_{12}, R_{13}, and R_{23} as outlined in Chapter III (equations 3.7, 3.8, and 3.9). An example of these solutions was shown graphically in Figure 3.1.

The single-color, two-color and three-color tem-

perature measurement techniques each yield 3 solutions when the data from 3 wavelength bands is used. Unless otherwise noted in the discussion that follows, an average of the three solutions resulting from the three wavelengths will be used to represent the solution for each of the measurement techniques.

Radiance ratio correction for non-gray behavior

The two-color and three-color solutions are based on the assumption that the surface being measured behaves as a graybody. If graybody behavior is not assumed, a correction to the radiance ratios can be made:

$$R_{12} \text{ calibration} \quad = \quad \frac{N_b(\lambda 1, T)}{N_b(\lambda 2, T)} \qquad \text{eq. 5.5}$$

$$R_{12} \text{ measured} \quad = \quad \frac{\epsilon_{\lambda 1} N_b(\lambda 1, T)}{\epsilon_{\lambda 2} N_b(\lambda 2, T)} \qquad \text{eq. 5.6}$$

$$R_{12} \text{ calibration} \quad = \quad R_{12} \text{ measured} \quad x \quad \frac{\epsilon_{\lambda 2}}{\epsilon_{\lambda 1}} \qquad \text{eq. 5.7}$$

Correction for reflectance

For non-gray behavior equations 3.4, 3.5, and 3.6 become:

100

$$\frac{\epsilon_{\lambda 1}}{\epsilon_{\lambda 2}} \ R_{12} = \frac{B1_{\lambda 1} \ - \ p_{\lambda 1}F_{1-2}B2_{\lambda 1}}{B1_{\lambda 2} \ - \ p_{\lambda 2}F_{1-2}B2_{\lambda 2}} \qquad \text{eq. 5.8}$$

$$\frac{\epsilon_{\lambda 1}}{\epsilon_{\lambda 3}} \ R_{13} = \frac{B1_{\lambda 1} \ - \ p_{\lambda 1}F_{1-2}B2_{\lambda 1}}{B1_{\lambda 3} \ - \ p_{\lambda 3}F_{1-2}B2_{\lambda 3}} \qquad \text{eq. 5.9}$$

$$\frac{\epsilon_{\lambda 2}}{\epsilon_{\lambda 3}} \ R_{23} = \frac{B1_{\lambda 2} \ - \ p_{\lambda 2}F_{1-2}B2_{\lambda 2}}{B1_{\lambda 3} \ - \ p_{\lambda 3}F_{1-2}B2_{\lambda 3}} \qquad \text{eq. 5.10}$$

or once the correction for emissivity ratio is made:

$$R_{12}' = \frac{B1_{\lambda 1} \ - \ p_{\lambda 1}F_{1-2}B2_{\lambda 1}}{B1_{\lambda 2} \ - \ p_{\lambda 2}F_{1-2}B2_{\lambda 2}} \qquad \text{eq. 5.11}$$

$$R_{13}' = \frac{B1_{\lambda 1} \ - \ p_{\lambda 1}F_{1-2}B2_{\lambda 1}}{B1_{\lambda 3} \ - \ p_{\lambda 3}F_{1-2}B2_{\lambda 3}} \qquad \text{eq. 5.12}$$

$$R_{23}' = \frac{B1_{\lambda 2} \ - \ p_{\lambda 2}F_{1-2}B2_{\lambda 2}}{B1_{\lambda 3} \ - \ p_{\lambda 3}F_{1-2}B2_{\lambda 3}} \qquad \text{eq. 5.13}$$

solving for the shape factor:

$$F_{1-2} = \frac{R_{12}B1_{\lambda 2} \ - \ B1_{\lambda 1}}{p_{\lambda 2}R_{12}B2_{\lambda 2} \ - \ p_{\lambda 1}B2_{\lambda 1}} \qquad \text{eq. 5.14}$$

$$F_{1-2} = \frac{R_{13}B1_{\lambda 3} \ - \ B1_{\lambda 1}}{p_{\lambda 3}R_{13}B2_{\lambda 3} \ - \ p_{\lambda 1}B2_{\lambda 1}} \qquad \text{eq. 5.15}$$

$$F_{1-2} = \frac{R_{23}B1_{\lambda 3} \ - \ B1_{\lambda 2}}{p_{\lambda 3}R_{23}B2_{\lambda 3} \ - \ p_{\lambda 2}B2_{\lambda 2}} \qquad \text{eq. 5.16}$$

multiply both sides of the equations by $p_{\lambda 1}$:

$$p_{\lambda 1}F_{1-2} = \frac{R_{12}B1_{\lambda 2} - B1_{\lambda 1}}{\dfrac{p_{\lambda 2}}{p_{\lambda 1}} R_{12}B2_{\lambda 2} - B2_{\lambda 1}} \qquad \text{eq. 5.17}$$

$$p_{\lambda 1}F_{1-2} = \frac{R_{13}B1_{\lambda 3} - B1_{\lambda 1}}{\dfrac{p_{\lambda 3}}{p_{\lambda 1}} R_{13}B2_{\lambda 3} - B2_{\lambda 1}} \qquad \text{eq. 5.18}$$

$$p_{\lambda 1}F_{1-2} = \frac{R_{23}B1_{\lambda 3} - B1_{\lambda 2}}{\dfrac{p_{\lambda 3}}{p_{\lambda 1}} R_{23}B2_{\backslash 3} - \dfrac{p_{\lambda 2}}{p_{\lambda 1}} B2_{\lambda 2}} \qquad \text{eq. 5.19}$$

The three-color solution now depends on the reflectance ratios rather than absolute reflectance levels.

If surface 1 is truly a diffuse emitter and a diffuse reflector, then Kirchoff's law holds for the spectral properties:

$$\alpha_\lambda = \epsilon_\lambda \qquad \text{(eq. 2.14)}$$

and we can say that:

$$p_{\lambda 1} = (1 - \epsilon_{\lambda 1}) \qquad \text{eq. 5.20}$$

Reflectance ratios required to correct for non-gray behavior can then be calculated using the emissivity estimates used in the radiance ratio correction.

For a non-diffuse surface we must concern ourselves

102

with the directional properties. The directional reflectance has both a specular and a diffuse component and cannot be related to emissivity by the simple relation in equation 5.20. In such instances, the only reliable method of characterizing the reflectance is to take detailed measurements of the bidirectional reflectance with respect to the incident and viewing angles. Such measurements are commonly referred to as bidirectional distribution function (BRDF) measurements.

While the BRDF can be characterized for the target surface (with the appropriate instruments), the correction for reflectance ratios for a non-diffuse surface would require the accurate knowledge of the incident angle and the viewing angle. Unless surface 2 (the source of the incident radiation) is a point source, there will be many incident angles involved. The problem of assessing the bidirectional reflectance becomes very tedious and is beyond the scope of this investigation.

CHAPTER VI

RESULTS

Results With Graybody Assumption

The objective of the three-color measurement tech-
nique is the determination of surface temperature in the
presence of reflected radiation without _a priori_ infor-
mation about surface properties. The two-color and
three-color methods do not require knowledge of emit-
tance values, but emissivity ratios must be known. This
is not a problem if the target surface properties
approximate those of a graybody, for then the emissivity
ratios are known to be approximately 1.0. The assump-
tion of graybody behavior does not stipulate specific
values for $\epsilon_{\lambda 1}$, $\epsilon_{\lambda 2}$, or $\epsilon_{\lambda 3}$. To illustrate data
reduction with no _a priori_ surface property information,
the single-color solutions are computed with
$\epsilon_{\lambda 1} = \epsilon_{\lambda 2} = \epsilon_{\lambda 3} = 1.0$. The two-color and three-color
solutions were computed with the emissivity ratios
assumed to be 1.0. The temperature solutions for each
of the three methods discussed are presented in Table
6.1. The estimated temperature errors of each of the
three methods are shown in Figure 6.1 plotted as a func-
tion of percent reflected energy which is a measure of

104

Table 6.1 Summary of Single-color, Two-color, and Three-color
Solutions with no A Priori Surface Property Information

a. Summary of Single-color Solutions

Blackbody A (° C)	Blackbody B (° C)	Percent Reflected Energy	Single-color solutions (Ttrue = 348° C)							
			T1	T1 error	T2	T2 error	T3	T3 error	Tavg	avg error
---	---	0	325	-23	289	-59	278	-70	297	-51
900	---	4	335	-13	293	-55	282	-66	303	-45
---	900	8	341	-7	295	-53	284	-64	307	-41
900	900	12	348	0	298	-50	285	-63	310	-38
1000	---	5	341	-7	295	-53	284	-64	307	-41
---	1000	10	349	1	298	-50	286	-62	311	-37
1000	1000	15	359	11	301	-47	289	-59	316	-32

105

Table 6.1   Summary of Single-color, Two-color, and Three-color Solutions with Estimated Emissivities from Published Source

b.   Summary of Two-color Solutions

Blackbody A (°C)	Blackbody B (°C)	Percent Reflected Energy	single-color solutions (Ttrue = 348 C)							
			T12	T12 error	T13	T13 error	T23	T23 error	Tavg	avg error
--	--	0	412	64	410	62	408	60	410	62
900	--	4	440	92	434	86	415	67	430	82
--	900	8	454	106	447	99	421	73	441	93
900	900	12	475	127	466	118	426	78	456	108
1000	--	5	455	107	448	100	423	75	442	94
--	1000	10	476	128	468	120	432	84	459	111
1000	1000	15	507	159	494	146	434	86	478	130

Table 6.1   Summary of Single-color, Two-color, and Three-color
Solutions with no A Priori Surface Property Information

c.   Summary of Three-color Solutions

Blackbody A (°C)	Blackbody B (°C)	Percent Reflected Energy	Single-color solutions (Ttrue = 348° C)										
			T12	T12 error	T13	T13 error	T23	T23 error	Tavg	avg error
---	---	0	397	49	411	63	412	64	407	59
900	---	4	384	36	398	50	399	51	394	46
---	900	8	384	36	397	49	398	50	393	45
900	900	12	375	27	388	40	389	41	384	36
1000	---	5	391	43	404	56	405	57	400	52
---	1000	10	391	43	404	56	405	57	400	52
1000	1000	15	372	24	383	35	384	36	380	32
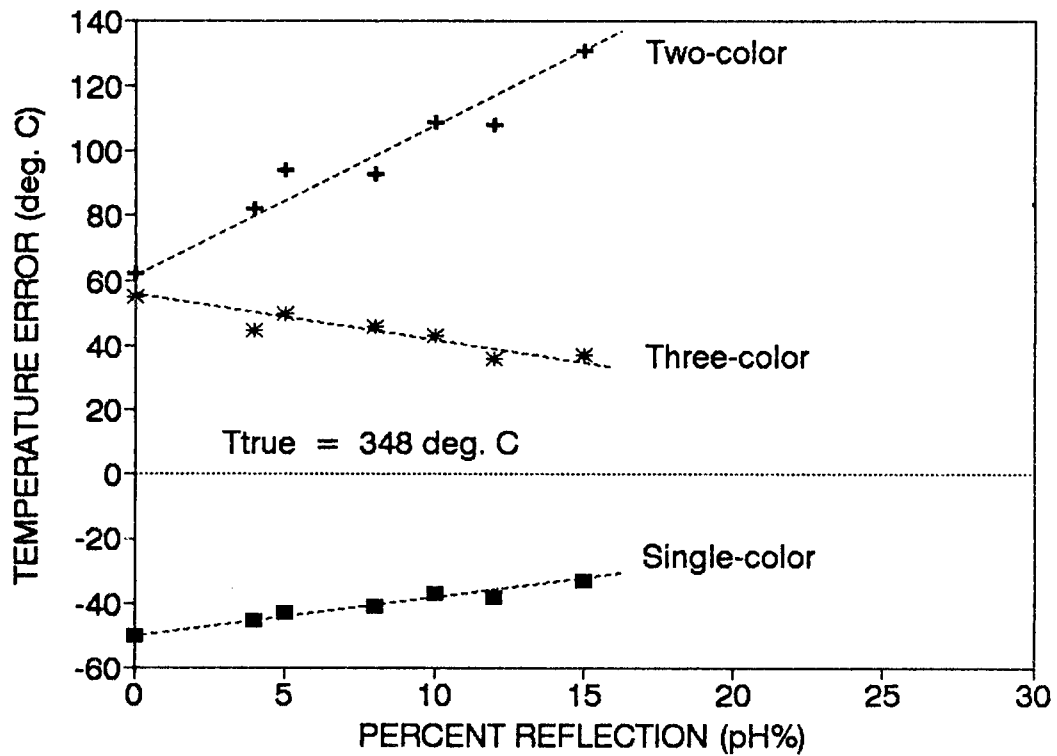
Figure 6.1   Comparison of Calculated Temperature Errors
with Increasing Reflected Radiant Energy
(Data Reduced with No A Priori Surface
Property Information).

the relative amount of sensed energy that is due to reflected energy. This was defined in chapter V as:

$$pH\% = \left[\frac{N_r}{N_o} - 1 \right] \times 100\% \qquad eq. \ 5.4$$

where:

pH% = percent reflected energy
N_r = radiance measured with reflected energy
N_o = radiance without reflected energy

Single-Color Solutions with ε = 1.0

The estimated error of the single-color solution (with $\epsilon = 1.0$) without reflected energy is substantial (-50° C). This is, of course, due to the fact that the actual values of ϵ were not used in the data reduction. (No a priori information is assumed other than graybody behavior.) Note however that as reflected energy (percent reflected energy) increases, the single-color error decreases. This result could have been anticipated since the effect of incident radiation is to increase the indicated single color temperature and the assumption $\epsilon = 1.0$ causes indicated single-color temperature to err on the low side of T_{true}. However, it must be noted that at some level of reflected energy, the indicated single-color temperature will reach T_{true} and at that point further increases in reflected energy will

109

increase the single-color temperature errors. Since the reflected energy in the typical experiment is neither controlled or known, it would be difficult to assess from single-color data whether or not this point has been reached. Still, it is important to observe that the single-color errors in this experiment decrease as reflected energy increases.

Two-color solutions with graybody assumption

The two-color solutions errors are also presented in Figure 6.1. Note that the two-color error is over 60° C with no reflected energy. This is no doubt a result of the incorrect assumption of graybody behavior. As with the single-color solutions, the two-color solutions increase with increasing reflected energy. But since the two-color solution initially errs on the high side of T_{true}, the two-color temperature errors increase with increasing reflected energy. Notice also that the slope of the line through the two color solution errors is greater than that through the single color errors. This indicates that the two-color solution is more sensitive to error from reflected energy than the single-color solution as predicted in Chapter II.

110

Three-color solution with graybody assumption

The three-color solution with no reflected energy
yields the same error as the two-color solution. This
is expected since the three-color solution with no
reflected radiation reduces to the two-color solution.
(No reflected energy implies that $pF_{1-2} = g = 0$.) The
three-color solution errors decrease with increasing
reflected energy. This also must be viewed as a for-
tuitous result arising from the fact that the solution
with no reflected energy errs on the high side of T_{true}.
The magnitude of the three-color temperature errors are
significantly higher than those proposed for this demon-
stration of the three-color method. The data suggests
that the gray body assumption is not valid for this
experiment.

Results with estimated values for emissivity

The assumption that the target surface was a good
approximation of a gray surface was questioned after
reviewing the properties of aluminum in published
sources. However, the surface properties of aluminum
are so highly variable (dependent on surface prepara-
tion, smoothness, oxidation, etc.) that a reasonable
estimate for the spectral emissivity of the target sur-

111

face was difficult to obtain. Additionally, the target surface in this experiment has a unique surface treatment (dimples) that has been shown to have a dramatic effect on the room temperature surface properties. The two-color method and the three-color method do not require specific values for spectral emissivity, but the ratio of emissivity in the wavelength bands of interest must either be known or assumed. Emittance estimates of $\epsilon_{\lambda 1} = 0.166$, $\epsilon_{\lambda 2} = 0.099$, and $\epsilon_{\lambda 3} = 0.088$ were obtained by interpolation of Figure 4.10. The results of data reduction using these emissivity values are presented in Table 6.2. The single-color, two-color, and three-color measurement errors are compared in Figure 6.2.

Single-color solutions with estimated values for emissivity

The single-color solutions with the estimated emittances from Gubareff yield temperatures on the high side of T_{true}. The estimated emissivities are no doubt too low for this target surface as anticipated. Note that the single-color temperature errors using the published emissivity estimates increase with increasing reflected energy. The sensitivity of the single-color temperature solutions to the percent reflected energy is about the same using the estimated values for emissivity as for

112

Table 6.2 Summary of Single-color, Two-color, and Three-color Solutions with Estimated Emissivities from Published Source.

a. Summary of Single-color Solutions

Blackbody A (° C)	Blackbody B (° C)	Percent Reflected Energy	Single-color solutions (Ttrue = 348° C)							
			T1	T1 error	T2	T2 error	T3	T3 error	Tavg	avg error
---	---	0	440	92	513	165	546	198	500	152
900	---	4	454	106	519	171	552	204	508	160
---	900	8	462	114	524	176	556	208	514	166
900	900	12	472	124	528	180	560	212	520	172
1000	---	5	462	114	523	175	556	208	514	166
---	1000	10	473	125	529	181	561	213	521	173
1000	1000	15	488	140	535	187	567	219	530	182

Table 6.2 Summary of Single-color, Two-color, and Three-color Solutions with Estimated Emissivities from Published Source.

b. Summary of Two-color Solutions

Blackbody A (° C)	Blackbody B (° C)	Percent Reflected Energy	Single-color solutions (Ttrue = 348° C)							
			T12	T12 error	T13	T13 error	T23	T23 error	Tavg	avg error
---	---	0	327	-21	324	-24	313	-35	321	-27
900	---	4	364	16	344	-4	319	-29	342	-6
---	900	8	364	16	355	7	324	-24	348	0
900	900	12	382	34	370	22	328	-20	360	12
1000	---	5	364	16	356	8	325	-23	348	0
---	1000	10	383	35	372	24	333	-15	363	15
1000	1000	15	409	61	393	45	334	-14	379	31

Table 6.2 Summary of Single-color, Two-color, and Three-color Solutions with Calculate Values for Emissivities.

c. Summary of Three-color Solutions

| Blackbody A (°C)	Blackbody B (°C)	Percent Reflected Energy	Single-color solutions (Ttrue = 348°C)							
			T12	T12 error	T13	T13 error	T23	T23 error	Tavg	avg error
---	---	0	305	-43	305	-43	304	-44	304	-44
900	---	4	300	-48	299	-49	298	-50	299	-49
---	900	8	300	-48	298	-50	298	-50	299	-49
900	900	12	294	-54	291	-57	291	-57	292	-56
1000	---	5	304	-44	304	-44	304	-44	304	-44
---	1000	10	304	-44	304	-44	304	-44	304	-44
1000	1000	15	291	-57	288	-60	288	-60	289	-59
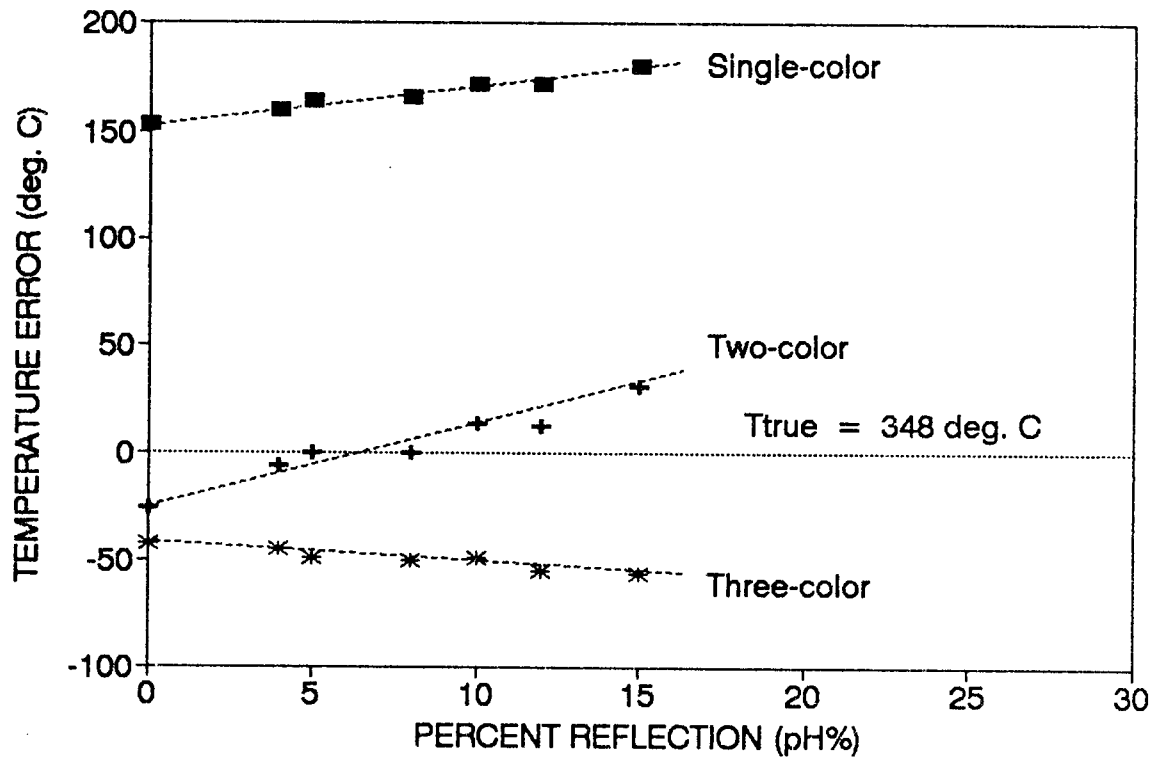
Figure 6.2   Comparison of Calculated Temperature Errors
with Increasing Reflected Radiant Energy
(Data Reduced Using Estimated Emissivities
from Published Source).

the solutions with graybody assumption, but the magnitude of the errors is much greater.

Two-color solution with estimated values for emissivity

The use of published emissivity estimates in the two-color solution reduces the errors dramatically when compared with the solution with graybody assumption. The error with no reflected energy is about -25° C and decreases to 0° C at 8 percent reflected energy before increasing to +30° C at 15 percent reflected energy. The two-color solution using the published emissivity estimates remains sensitive to reflected energy.

Three-color solutions with estimated value for emissivity

The three-color method was applied with radiance ratios corrected using emissivity ratios derived from the published emissivity estimates. Bidirectional reflectance estimates were not available. An attempt was made to use the estimated emissivity values to estimate the reflectance ratios as outlined in Chapter V. Use of these radiance ratio estimates cause the three-color solution to fail to converge. It is recognized that the target surface has a strong component of

117

specular reflectance, which makes corrections for non-gray reflectance very difficult. Corrections for non-gray behavior in this experiment were restricted to radiance ratio corrections with emissivity ratios.

The three-color solution errors after correcting the data with the published emissivity estimates range from -40° C with no reflected energy to over -50° C with 15 percent reflected energy. This is not a significant improvement over the three-color solutions with the gray body assumption. Note that in this case the measurement error is increasing with increasing reflected energy.

The magnitude of the three-color temperature errors remain significantly higher than those desired. The data suggest that the three-color method for this experiment using estimated values of emissivity obtained from Figure 4.10, while superior to the two-color method, is inferior to the single color method.

Results with measured emissivity values

Estimates for the spectral emissivity of the aluminum target can be made using the single-color data with no reflected energy. These estimates of emissivity using experimental data will be referred to as measured emissivity values. They are calculated by dividing the measured millivolt reading by the calibration millivolt

reading at T_{true}:

$$\epsilon_{\lambda 1} = \frac{mv_{\lambda 1} \text{ (measured with no reflected energy)}}{mv_{\lambda 1} \text{ (from calibration curve at } T_{true})}$$

Measured values for $\epsilon_{\lambda 2}$ and $\epsilon_{\lambda 3}$ are calculated similarly. Temperature solutions shown in Table 6.3 and Figure 6.3 were computed using these measured values for emissivity ($\epsilon_{\lambda 1} = 0.685$, $\epsilon_{\lambda 2} = 0.483$, and $\epsilon_{\lambda 3} = 0.452$) to make radiance ratio corrections. A comparison of the temperature measurement errors for the three methods using measured emissivity is presented in Figure 6.3.

Single-color solutions with measured emissivity

These estimates for emissivity by nature of their derivation from the data with no reflected energy and T_{true}, will cause the single-color measurement error with no reflected energy to approach zero. The single-color measurements are still subject to increasing error with increasing reflected energy; however, the errors remain $\leq 10^\circ$ C.

Two-color solutions with measured emissivity

Use of the measured spectral emissivity values also causes the two-color measurement error (with no reflec-

119

Table 6.3   Summary of Single-color, Two-color, and Three-color Solutions with Calculated Values for Emissivities.

a.   Summary of Single-color solutions

Blackbody A (°C)	Blackbody B (°C)	Percent Reflected Energy	Single-color solutions (Ttrue = 348° C)							
			T1	T1 error	T2	T2 error	T3	T3 error	Tavg	avg error
--	--	0	348	0	348	0	348	0	348	0
900	--	4	357	9	350	2	350	2	350	2
--	900	8	362	14	353	5	352	4	352	4
900	900	12	370	22	355	7	354	6	354	6
1000	--	5	362	14	353	5	352	4	352	4
--	1000	10	370	22	356	8	355	7	355	7
1000	1000	15	381	33	360	12	359	11	359	11

Table 6.3   Summary of Single-color, Two-color, and Three-color Solutions with Calculated Values for Emissivities.

b.   Summary of Two-color Solutions

Blackbody A (°C)	Blackbody B (°C)	Percent Reflected Energy	Single-color solutions (Ttrue = 348° C)							
			T12	T1 error	T13	T2 error	T23	T3 error	Tavg	avg error
---	---	0	345	-3	345	-3	352	4	347	-1
900	---	4	369	21	366	18	358	10	364	16
---	900	8	382	34	377	29	364	16	374	26
900	900	12	401	53	393	45	368	20	387	39
1000	---	5	383	35	378	30	365	17	375	27
---	1000	10	401	53	394	46	373	25	389	41
1000	1000	15	429	81	417	69	375	27	407	59

Table 6.3   Summary of Single-color, Two-color, and Three-color
            Solutions with Calculated Values for Emissivities.

c. Summary of Three-color Solutions

| Blackbody A (° C)	Blackbody B (° C)	Percent Reflected Energy	Three-color solutions (Ttrue = 348° C)								
			T1	T1 error	T2	T2 error	T3	T3 error	Tavg	avg error
---	---	0	348	0	358	10	359	11	355	7
900	---	4	342	-6	350	2	351	3	348	0
---	900	8	341	-7	350	2	351	3	347	-1
900	900	12	334	-14	341	-7	342	-6	339	-9
1000	---	5	345	-3	354	6	355	7	351	3
---	1000	10	342	-6	351	3	352	4	348	0
1000	1000	15	332	-16	338	-10	338	-10	336	-12
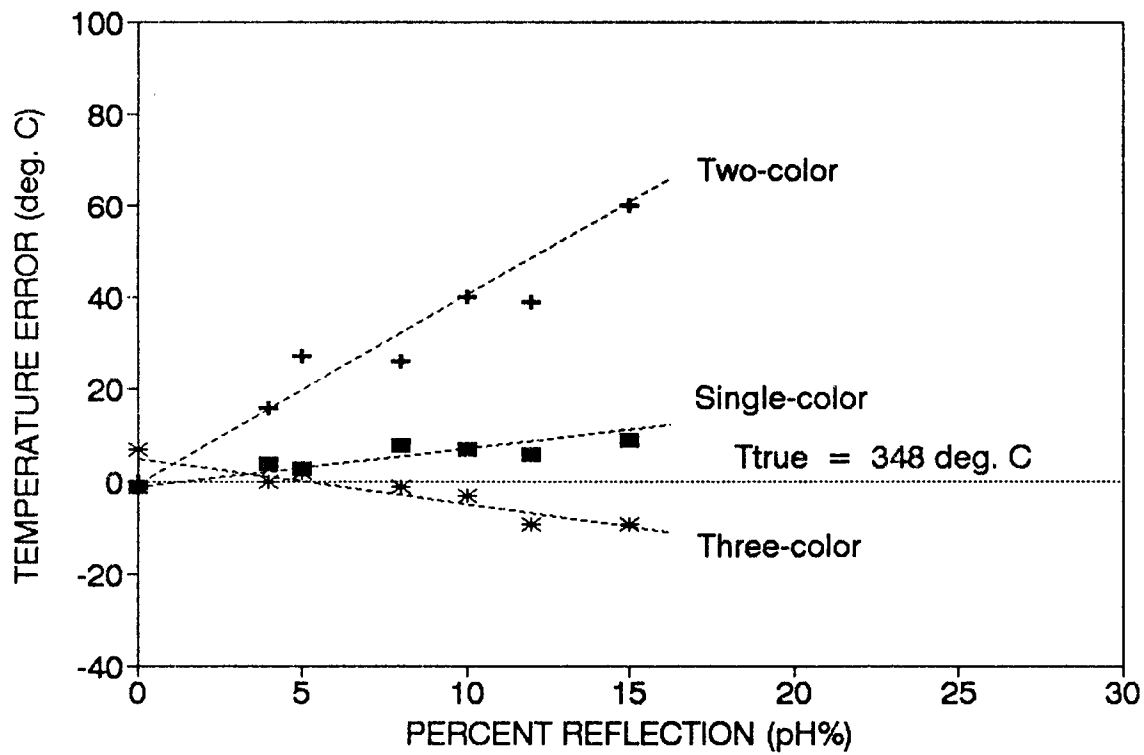
Figure 6.3 Comparison of Calculated Temperature Errors
with Increasing Reflected Radiant Energy
(Data Reduced Using Calculated Emissivi-
ties).

tion) to approach zero as would be expected if the emit-tances were precisely known. The two-color method how-ever, remains highly sensitive to the effects of reflected radiation with errors increasing to 60° C at 15 percent reflected energy.

Three-color solutions with measured emissivity

Errors in the three-color solution using measured emissivity values should also approach zero but were 7° C without reflected energy. This illustrates that the two-color method (by virtue of its simplicity) is supe-rior to the three-color method for the case where emit-tance ratios are precisely known, and where no incident radiation is present. The three-color measurement errors increased with increasing reflected energy as did the two-color and the single-color errors. The three-color measurement errors with incident radiation are about the same order of magnitude as those for the sin-gle-color solution. But note that the three-color errors are dramatically reduced over the two-color errors. This indicates that the fundamental concept of the three-color solution is valid, provided that the necessary assumptions are met. While the three-color method does not appear to yield significantly better results than the single-color method in this experiment,

one should remember that the single-color solutions represented in Figure 6.3 require precise values of $\epsilon_{\lambda 1}$, $\epsilon_{\lambda 2}$, and $\epsilon_{\lambda 3}$, while the three-color solution requires only that the emissivity ratios are known. This means that if a truly gray target surface were used, the three-color method would yield good results without detailed information about spectral emissivity.

CHAPTER VII

CONCLUSIONS AND RECOMMENDATIONS

Conclusions

The objective of the experiment was to investigate an infrared surface temperature measurement technique that could be used without detailed prior knowledge of surface properties and could correct for errors that might be caused by incident radiation. The results discussed herein lead to the following conclusions:

1. For the aluminum target in this experiment, the three-color technique does not meet the goal of less than ± 30° C temperature error when incident radiation is present and when graybody behavior is assumed.

2. The three-color solution errors did not decrease significantly with the use of emissivity estimates from published sources.

3. The three-color solution errors were less than 10° C (less than 2 percent) when measured values of emissivity were used to adjust the data. The measured values were derived from data collected with no incident radiation on the target surface. The requirement to collect data with-

126

out incident radiation does not meet the objective of the three-color method. However, the positive results with the measured emissivity values suggest that the three-color method may provide acceptable results on surfaces that more closely approximate graybody behavior.

4. The two-color solution is highly sensitive to reflection of incident radiation. Measurement errors with measured values of emissivity increased from less than 1° C with no reflection, to 60° C at 15 percent reflected energy (the maximum level of incident radiation that was experienced during the experiment.)

5. The single-color solution is less sensitive to errors due to incident radiation than the two-color solution. The single-color solution errors with measured values of emissivity are the same order of magnitude (less than 10° C) as the three-color solution errors. However, while the successful three-color results depend on precise emissivity ratios, the successful single-color results require precise values of emissivity. Such precise values for emissivity are rarely available a priori even if the surface approximates graybody behavior. More-

127

over, certain circumstances (such as IR attenuation or non-filled field of view) dictate two-color measurements. The three-color results show a clear improvement over the conventional two-color results.

Recommendations

Further Investigations

Further investigations should include the following:

1. Investigate optimum wavelength separation for radiance ratios used in the three-color technique.

2. The use of a circular variable filter in future experiments will allow the flexibility to select optimum radiance ratios for a given situation and may allow extension of the three-color technique to n-colors.

3. Further corrections to the data reported herein may be possible if bidirectional reflectance function (BDRF) measurements are made of the target at room temperature.

Future Applications

Possible future applications in turbine engines might include:

1. Turbine engine hotparts--The internal surfaces of a typical turbine engine exhaust system (designated "hotparts") are much more complex than the geometry used for the demonstration of the three-color technique. Further study will be required to determine the suitability of the three-color technique to complex geometries with multiple sources of incident radiation.

2. Turbine blade pyrometry--The first row of turbine blades downstream of an annular combustor are subject to significant incident radiation. The turbine blade geometry is not a great deal more complex than the simple geometry used in this experiment. The rotational speeds of the turbine blades will require pyrometer response times on the order of a micro-second (10^{-6} sec.) (Beynon p. 473). Further study will be required to determine if such a high response three-color pyrometer is feasible.

129

BIBLIOGRAPHY

BIBLIOGRAPHY

Atkinson, W. H. and Strange, R. R. "Pyrometer Temperature Measurements in the Presence of Reflected Radiation." Presented at the ASME-AIChE Heat Transfer Conference, St. Louis, MO, August 1976.

Atkinson, W. H. and Strange, R. R. "Turbine Pyrometry for Advanced Engines." Presented at the AIAA/SAE/ASME/ASEE 23rd Joint Propulsion Conference, San Diego, CA, June 29-July 2, 1987.

Beynon, T.G.R., Temperature, Its Measurement and Control in Science and Industry, (American Institute of Physics, 1982), Vol. 5, Part 1, pp. 473.

DeWitt, D.P. and Kunz H., Temperature, Its Measurement and Control in Science and Industry, (Instrument Society of America, 1972), Vol. 4, Part 1, pp. 600.

Gardner, J.L., Jones, T.P., et al. "A broadband ratio pyrometer", Temperature: Its Measurement and Control in Science and Industry, (American Institute of Physics, 1982), Vol. 5, Part 1, pp. 409.

Gubareff, G.G., et al. Thermal Radiation Properties Survey, MN: Honeywell Research Center, 1960.

Halliday, David, and Resnick, Robert, Fundamentals of Physics. NY: Wiley, 1970.

Holman, J.P., Experimental Methods for Engineers, NY: McGraw-Hill, 1978.

Horman, M.H., "Temperature Analysis from Multispectral Infrared Data", Applied Optics, Vol. 15, No. 9, 1976, 2099-2104.

Hunter, G. B. , Allemand, C. D., and Edgar, T. W. "Multiwavelength Pyrometry: An Improved Method." Optical Engineering, Vol. 24, No. 6, November/December 1985, pp. 1081-1085.

Nutter, G.D., "Radiation Thermometry -- The Measurement Problem", Noncontact Temperature Measurement; Proceedings of the NASA workshop, Washington, DC: 1987, pp. 3-63.

131

BIBLIOGRAPHY (Concluded)

Sparrow, E.M., and Cess, R.D., Radiation Heat Transfer. Belmont CA: Brooks/Cole, 1970.

Spjut, R.E., "Common But Unappreciated Sources of Error in One, Two, and Multiple-color Pyrometry", Noncontact Temperature Measurement; Proceedings of the NASA workshop, Washington, DC: 1987.

APPENDICES

APPENDIX A

<u>TEMPERATURE ERROR DUE TO UNKNOWN EMISSIVITY</u>

<u>IN SINGLE-COLOR MEASUREMENTS</u>

As described in Chapter II (page 32) the relation-
ship of radiance to temperature is:

$$\frac{dT}{T} = \left[\frac{\lambda T}{c2} \right] \frac{dN}{N}$$

eq. 2.26

from which the influence coefficient is:

$$\text{I.C.} = \left[\frac{\lambda T}{c2} \right]$$

eq. 2.29

The influence coefficient of emissivity to radiance can
be shown to be 1.0:

$$N = \epsilon Nb$$

eq. A.1

if Nb is held constant (neglecting for the moment any
other source of error other than ϵ):

$$\frac{dN}{d\epsilon} = Nb = \frac{N}{\epsilon}$$

eq. A.2

$$\frac{dN}{N} = \frac{d\epsilon}{\epsilon}$$

eq. A.3

substituting A.3 into 2.26 we have:

$$\frac{dT}{T} = \left[\frac{\lambda T}{c2} \right] \frac{d\epsilon}{\epsilon}$$

eq. A.4

The error in emissivity is given by the relation:

$$\frac{d\epsilon}{\epsilon} = \frac{\epsilon_{true} - \epsilon_{assumed}}{\epsilon_{true}} \qquad \text{eq. A.5}$$

If the value of $\epsilon_{assumed}$ is 1:

$$\frac{d\epsilon}{\epsilon} = \frac{\epsilon - 1}{\epsilon} \qquad \text{eq. A.6}$$

where ϵ now represents ϵ_{true}, and:

$$\frac{dT}{T} = \left[\frac{\lambda T}{c2} \right] \frac{\epsilon - 1}{\epsilon} \qquad \text{eq. A.7}$$

Equation A.7 represents the error in the temperature measurement due to emissivity error.

APPENDIX B

ERRORS IN RADIANCE MEASUREMENTS

DUE TO

DETECTOR NOISE

A typical blackbody receiver will have a uniform response to spectral radiant power. A thermistor bolometer can be thought of as a blackbody receiver. The bolometer detectivity is shown to be independent of wavelength in Figure 2.9 (page 25).

Detectivity (D) is defined as (Holman p. 160):

$$D = \frac{R_V}{\text{rms noise-voltage output}} = \frac{1}{\text{NEP}} \qquad \text{eq. B.1}$$

where R_V is the responsivity defined as:

$$R_V = \frac{\text{rms output voltage}}{\text{rms power incident on detector}} \qquad \text{eq. B.2}$$

The noise equivalent power (NEP) is defined as the minimum incident radiant power required to produce a signal to noise (S/N) ratio of unity. A normalized detectivity (D^*) is defined as:

$$D^* = (A\ df)^{\frac{1}{2}} D \qquad \text{eq. B.3}$$

where:

    A = detector area
    df = noise bandwidth

The performance of IR detectors is typically specified in terms of D^*.

The radiance error due to detector noise can be described by:

$$\frac{dN}{N} \text{ (noise)} = \frac{\text{noise voltage}}{\text{signal voltage}} = \frac{1}{S/N} \qquad \text{eq. B.4}$$

From equation B.1 we have:

$$NEP = \frac{\text{rms noise-voltage output}}{R_V} \qquad \text{eq. B.5}$$

multiplying equation B.5 by B.2:

$$NEP = \frac{\text{rms noise-voltage output} * \text{rms power}}{\text{rms output voltage}}$$

or:

$$NEP = \frac{N}{S/N} \qquad \text{eq. B.6}$$

divide equation B.6 by radiance (N):

$$\frac{NEP}{N} = \frac{1}{S/N} \qquad \text{eq. B.7}$$

substituting equation B.7 into B.4:

$$\frac{dN}{N} \text{ (noise)} = \frac{NEP}{N} = \frac{1}{D \cdot N} \qquad \text{eq. B.8}$$

139

From equation B.8 we can compute the error in

radiant power due to detector noise. A detectivity

of 0.02 was assumed for a sample case referred to

herein as a typical blackbody receiver. The resulting

error in the radiance measured from a blackbody at 1000

K due to detector noise for this case is shown in

Figure 2.14 (page 36).

APPENDIX C

ERRORS IN TWO-COLOR TEMPERATURE MEASUREMENTS

DUE TO A NON-FILLED FIELD OF VIEW

The two-color pyrometer does not require that the field of view be filled to if the effects of background radiation can be neglected. The two-color pyrometer measures the radiance at two given wavelengths. The ratio of the radiance measurements will be independent of the portion of the field of view that is filled if there is no background radiation. The errors that might be present in the ratio measurement by overlooking the background radiation can be illustrated in the following example.

Assume that a target surface at 1000 K is to be viewed by the ratio pyrometer with $\lambda 1$ being a very narrow band centered at 2 microns, and $\lambda 2$ likewise centered at 3 microns. Assume that the target and the background both have emissivities of 0.9. The measured radiance ratio will be:

$$R_{12} = \frac{\epsilon_{t\lambda 1} Nb(Tt)(\%FOV) + \epsilon_{bk\lambda 1} Nb(Tbk)(1-\%FOV)}{\epsilon_{t\lambda 2} Nb(Tt)(\%FOV) + \epsilon_{bk\lambda 2} Nb(Tbk)(1-\%FOV)}$$

eq. C.1

where:

ϵ_t	=	emissivity of the target
ϵ_{bk}	=	emissivity of the background
Nb(Tt)	=	radiance of the target
Nb(Tbk)	=	radiance of the background
%FOV	=	fraction of the field of view that is filled

142

Equation C.1 is evaluated for the sample case given above. The error in the radiance ratio (R_{12}) due to a non-filled FOV is computed as:

$$\frac{dR_{12}}{R_{12}} = \frac{R_{12} \text{ (filled FOV)} - R_{12} \text{ (\%FOV)}}{R_{12} \text{ (filled FOV)}} \qquad \text{eq. C.2}$$

and is shown in Figure 2.19 (page 45). At room temperature ($\approx$300 K) there is so little radiant energy relative to the energy at the target temperature that the error in the radiance ratio for a FOV that is more than ten percent filled is less than 0.1 percent. Even for a background at 400 K the ratio error is less than one percent for a FOV that is more than 10 percent filled. This analysis suggests that the effects of background emitted radiation will have little impact on the ratio measurement. Of course the ratio measurement is also subject to error if significant amounts of solar or incandescent radiation are reflected into the instrument from the background. Reflections from the target itself can also introduce errors in the ratio measurement; reduction of such errors is in fact the primary subject of this investigation. Reflections from the target do not contribute to the error associated with a non-filled FOV.

APPENDIX D

<u>DETERMINATION OF MINIMUM FEASIBLE WAVELENGTH SEPARATION</u>

<u>FOR A RATIO PYROMETER</u>

Influence Coefficient of Ratio Pyrometers

In Chapter II, Wein's approximation was used to arrive at an approximation of radiance in the form:

$$Nb(T) = aT^b \qquad \text{eq. 2.27}$$

where:

$$b = \frac{c2}{\lambda T} \qquad \text{eq. 2.28}$$

which led to the calculation of the influence coefficient of radiance to temperature:

$$\frac{dT}{T} = \left[\frac{\lambda T}{c2} \right] \frac{dN}{N} \qquad \text{eq. D.1}$$

In a similar way, the influence coefficient for a ratio pyrometer can be determined:

$$R_{12} = \frac{Nb(\lambda 1,T)}{Nb(\lambda 2,T)} \approx \frac{a_1 T^{b_1}}{a_2 T^{b_2}} \qquad \text{eq. D.2}$$

$$R_{12} = a_3 T^{(b_1 - b_2)} \qquad \text{eq. D.3}$$

$$\frac{dR_{12}}{dT} = (b_1 - b_2) a_3 \frac{T^{(b_1 - b_2)}}{T} \qquad \text{eq. D.4}$$

by substituting eq. D.3 into D.4 we have:

$$\frac{dR_{12}}{R_{12}} = (b_1 - b_2) \frac{dT}{T} \qquad \text{eq. D.5}$$

or:

$$\frac{dT}{T} = \frac{1}{(b_1 - b_2)} \frac{dR_{12}}{R_{12}} \qquad \text{eq. D.6}$$

since $b_1 = c2/(\lambda 1 T)$ and $b_2 = c2/(\lambda 2 T)$:

$$\frac{dT}{T} = \frac{\lambda 1 \lambda 2}{(\lambda 1 - \lambda 2)} \frac{T}{c2} \frac{dR_{12}}{R_{12}} \qquad \text{eq. D.7}$$

We define wavelength separation (δ) as:

$$\delta = \frac{\lambda 2 - \lambda 1}{\lambda 1} \qquad \text{eq. D.8}$$

and equation D.7 becomes:

$$\frac{dT}{T} = \frac{\delta + 1}{\delta} \frac{\lambda 1 T}{c2} \frac{dR_{12}}{R_{12}} \qquad \text{eq. D.9}$$

The influence coefficient of radiance to temperature in a ratio pyrometer is therefore:

$$I.C. = \frac{\delta + 1}{\delta} \frac{\lambda 1 T}{c2} \qquad \text{eq. D.10}$$

146

Note that the influence coefficient is a function
of δ, $\lambda 1$, and T. A generalized presentation of the
influence coefficient (see Figure 2.22, page 51)
can be made in the form:

$$\frac{I.C.}{\lambda 1 T} = \frac{\delta + 1}{\delta} \quad \frac{1}{c2} \qquad \text{eq. D.11}$$

Influence coefficient curves for specific values of
temperature can be easily generated for specific cases
as shown in Figure 2.23.

Noise induced radiance ratio errors

In Appendix B we examined how detector noise con-
tributes to the error in measured radiance. Now let us
examine how detector noise influences the errors in the
measured radiance ratios. Detector noise can be esti-
mated in advance by using published values of detecti-
vity (D*) for the detector used (Holman p. 161) and by
knowing the geometry of the instrument. For this dis-
cussion, let us again use a hypothetical "blackbody
receiver" to illustrate the effects of detector noise.
Noise induced radiance error for this blackbody receiver
is shown in Figure 2.14 (page 36). Since noise is a
random phenomenon, the effects of noise in the radiance
ratio are determined statistically by combining the

147

noise induced radiance errors at the two wavelength
bands ($\lambda 1$ and $\lambda 2$).

$$\frac{dR_{12}}{R_{12}} \text{ (noise)} = \left[\left(\frac{dN_{\lambda 1}}{N_{\lambda 1}}\right)^2 + \left(\frac{dN_{\lambda 2}}{N_{\lambda 2}}\right)^2\right]^{\frac{1}{2}} \quad \text{eq. D.12}$$

where:

$$\frac{dN_{\lambda 1}}{N_{\lambda 1}} = \text{ noise induced error in radiance at } \lambda 1$$

$$\frac{dN_{\lambda 2}}{N_{\lambda 2}} = \text{ noise induced error in radiance at } \lambda 2$$

For the above described detector viewing a target
at 1000 K, the noise induced ratio error is shown in
Figure 2.24 (page 54). The effect of detector noise on
the temperature error is obtained by multiplying the
noise induced ratio error by the influence coefficient.
(see Figure 2.25).

$$\frac{dT}{T} = \frac{\delta + 1}{\delta} \quad \frac{\lambda 1 T}{c2} \left[\left(\frac{dN_{\lambda 1}}{N_{\lambda 1}}\right)^2 + \left(\frac{dN_{\lambda 2}}{N_{\lambda 2}}\right)^2\right]^{\frac{1}{2}} \quad \text{eq. D.13}$$

<u>Ratio Pyrometry errors due to Non-gray Behavior</u>

A method of characterizing the error in the ratio
measurement due to non-gray behavior of a surface is

148

outlined by Gardner (p. 409). The variation of the
spectral emissivity with wavelength can be represented
by a straight line through $\epsilon\lambda 1$ and $\epsilon\lambda 2$. The slope of
this line is:

$$m = \frac{\epsilon\lambda 2 - \epsilon\lambda 1}{\lambda 2 - \lambda 1} \qquad \text{eq. D.14}$$

The ratio of the spectral emissivity can be represented
as:

$$\frac{\epsilon\lambda 2}{\epsilon\lambda 1} = \frac{\epsilon\lambda 1 + m\left(\lambda 2 - \lambda 1\right)}{\epsilon\lambda 1} \qquad \text{eq. D.15}$$

$$\frac{\epsilon\backslash 2}{\epsilon\backslash 1} = 1 + \frac{m}{\epsilon\backslash 1}\left(\lambda 2 - \lambda 1\right) \qquad \text{eq. D.16}$$

Since the ratio technique assumes:

$$\frac{\epsilon\lambda 2}{\epsilon\lambda 1} = 1$$

the term:

$$\frac{m}{\epsilon\lambda 1}\ \lambda 2 - \lambda 1$$

represents the error in the ratio measurement due to
non-gray behavior:

149

$$\frac{dR_{12}}{R_{12}} = \frac{m}{\epsilon \lambda 1} \left(\lambda 2 - \lambda 1 \right) \qquad\qquad \text{eq. D.17}$$

Recalling our definition of wavelength separation, δ, from equation D.7 we can rewrite equation D.17 in terms of wavelength separation:

$$\frac{dR_{12}}{R_{12}} = \frac{m}{\epsilon \lambda 1} \delta \lambda 1 \qquad\qquad \text{eq. D.18}$$

The term $(m/\epsilon \lambda 1)$ will be referred to as the non-gray index (N.G.I.) of the surface. (A non-gray index of zero would imply graybody behavior).

$$\frac{m}{\epsilon \lambda 1} = \text{non-gray index (N.G.I.)}$$

Substituting equation D.18 into D.9 gives the temperature error due to non-gray behavior for a ratio pyrometer:

$$\frac{dT}{T} = \frac{m}{\epsilon \lambda 1} \delta + 1 \lambda 1^2 \frac{T}{c2} \qquad\qquad \text{eq. D.19}$$

This error is shown in Figure 2.21 (page 49) for a surface at 1000 K, and N.G.I. = 0.1.

It can readily be seen from equation D.18 that the radiance error is reduced by reducing δ. In fact, as δ

approaches zero the radiance error due to non-gray behavior approaches zero. This is where Gardner's analysis seems to stop. But as implied in Figure 2.23 (page 52), as δ approaches zero the radiance to temperature influence coefficient approaches infinity! An even more important observation is that noise induced temperature error in the ratio measurement _increases_ (Figure 2.25 page 55) as δ decreases below a certain point. The error due to non-gray behavior is not a random error and therefor a statistical combination of errors is not appropriate. A sum of the two errors is suggested.

$$\frac{dT}{T} = \frac{dT}{T}\text{(noise)} + \frac{dT}{T}\text{(non-gray)}$$

$$\frac{dT}{T} = \frac{\delta+1}{\delta}\frac{\lambda 1 T}{c2}\left[\left(\frac{dN_{\lambda 1}}{N_{\lambda 1}}\right)^2 + \left(\frac{dN_{\lambda 2}}{N_{\lambda 2}}\right)^2\right]^{\frac{1}{2}} + \frac{m}{\epsilon \lambda 1}\,\delta+1\,\lambda 1^2\,\frac{T}{c2}$$

eq. D.19

An example of this error for a surface at 1000 K and N.G.I. = 0.1 is shown in Figure 2.26 (page 56). The minimum in the temperature error curve suggests a "minimum feasible wavelength separation" for the ratio pyrometer.

Note that the determination of the minimum feasible wavelength separation requires _a priori_ knowledge of:

151

a) $\lambda 1$, the shorter of the two ratio wavelengths

b) the noise characteristics of the detector

c) the temperature of the surface of interest

d) the nature of the spectral emittance variation or non-gray index of the surface of interest

Determination of $\lambda 1$

Determining the best value for $\lambda 1$ (the shorter of the two wavelengths in the ratio measurement) is the same as determining the "shortest feasible wavelength" for a single color instrument as outlined in Chapter II. Note that if atmospheric attenuation is a concern, the choices for $\lambda 1$ and $\lambda 2$ are constrained to the available atmospheric "windows" (see Figure 4.4).

Surface Temperature

The accurate determination of surface temperature is the goal of ratio pyrometry. To require that the answer be known in advance is somewhat of a paradox. However, if the approximate temperature of the surface to be measured is known in advance, the ratio pyrometer can be designed to operate optimally and reduce the errors associated with the ratio measurement.

152

Non-gray index

It is not clear to the author that a reliable
method exists for predicting the non-gray index of a
particular surface without detailed measurements. Spec-
tral emissivity variations are so widespread that pub-
lished values are rarely of great benefit. However, it
does seem possible that for a given material, the non-
gray index may be less sensitive to surface condition
than emissivity. This is an area for further study.

APPENDIX E

TABULATED RADIANCE RATIOS FROM 300 TO 500 C

FOR BARNES RADIOMETER (R_{12}, R_{13}, AND R_{23})

Tabulated Radiance Ratios from 300 to 500°C

Temperature	R12	R13	R23
300	0.3059	0.3419	1.1194
301	0.3076	0.3444	1.1209
302	0.3094	0.3470	1.1225
303	0.3112	0.3495	1.1240
304	0.3130	0.3521	1.1256
305	0.3148	0.3547	1.1271
306	0.3166	0.3573	1.1287
307	0.3184	0.3599	1.1302
308	0.3202	0.3626	1.1318
309	0.3221	0.3652	1.1333
310	0.3239	0.3679	1.1349
311	0.3257	0.3706	1.1364
312	0.3276	0.3733	1.1380
313	0.3295	0.3760	1.1395
314	0.3313	0.3787	1.1410
315	0.3332	0.3815	1.1426
316	0.3351	0.3842	1.1441
317	0.3370	0.3870	1.1457
318	0.3389	0.3898	1.1472
319	0.3408	0.3926	1.1487
320	0.3428	0.3954	1.1503
321	0.3447	0.3983	1.1518
322	0.3466	0.4011	1.1533
323	0.3486	0.4040	1.1549
324	0.3505	0.4069	1.1564
325	0.3525	0.4098	1.1579
326	0.3545	0.4127	1.1595
327	0.3565	0.4156	1.1610
328	0.3585	0.4186	1.1625
329	0.3605	0.4215	1.1640
330	0.3625	0.4245	1.1656
331	0.3645	0.4275	1.1671
332	0.3665	0.4305	1.1686
333	0.3686	0.4336	1.1701
334	0.3706	0.4366	1.1717
335	0.3726	0.4397	1.1732
336	0.3747	0.4427	1.1747
337	0.3768	0.4458	1.1762
338	0.3789	0.4489	1.1777
339	0.3809	0.4521	1.1793
340	0.3830	0.4552	1.1808
341	0.3851	0.4583	1.1823
342	0.3872	0.4615	1.1838
343	0.3894	0.4647	1.1853
344	0.3915	0.4679	1.1868
345	0.3936	0.4711	1.1883
346	0.3958	0.4743	1.1899
347	0.3979	0.4776	1.1914
348	0.4001	0.4809	1.1929
349	0.4023	0.4841	1.1944
350	0.4044	0.4874	1.1959

Temperature	R12	R13	R23
351	0.4066	0.4907	1.1974
352	0.4088	0.4941	1.1989
353	0.4110	0.4974	1.2004
354	0.4132	0.5008	1.2019
355	0.4155	0.5041	1.2034
356	0.4177	0.5075	1.2049
357	0.4199	0.5109	1.2064
358	0.4222	0.5143	1.2079
359	0.4244	0.5178	1.2094
360	0.4267	0.5212	1.2109
361	0.4290	0.5247	1.2124
362	0.4313	0.5282	1.2139
363	0.4335	0.5317	1.2154
364	0.4358	0.5352	1.2169
365	0.4381	0.5387	1.2183
366	0.4405	0.5423	1.2198
367	0.4428	0.5458	1.2213
368	0.4451	0.5494	1.2228
369	0.4475	0.5530	1.2243
370	0.4498	0.5566	1.2258
371	0.4522	0.5602	1.2273
372	0.4545	0.5639	1.2288
373	0.4569	0.5675	1.2302
374	0.4593	0.5712	1.2317
375	0.4617	0.5749	1.2332
376	0.4641	0.5786	1.2347
377	0.4665	0.5823	1.2362
378	0.4689	0.5860	1.2376
379	0.4713	0.5898	1.2391
380	0.4738	0.5935	1.2406
381	0.4762	0.5973	1.2421
382	0.4786	0.6011	1.2435
383	0.4811	0.6049	1.2450
384	0.4836	0.6088	1.2465
385	0.4860	0.6126	1.2480
386	0.4885	0.6165	1.2494
387	0.4910	0.6203	1.2509
388	0.4935	0.6242	1.2524
389	0.4960	0.6281	1.2538
390	0.4986	0.6320	1.2553
391	0.5011	0.6360	1.2568
392	0.5036	0.6399	1.2582
393	0.5062	0.6439	1.2597
394	0.5087	0.6479	1.2611
395	0.5113	0.6519	1.2626
396	0.5138	0.6559	1.2641
397	0.5164	0.6599	1.2655
398	0.5190	0.6640	1.2670
399	0.5216	0.6680	1.2684
400	0.5242	0.6721	1.2699

Temperature	R12	R13	R23
401	0.5268	0.6762	1.2713
402	0.5294	0.6803	1.2728
403	0.5321	0.6844	1.2743
404	0.5347	0.6886	1.2757
405	0.5373	0.6927	1.2772
406	0.5400	0.6969	1.2786
407	0.5427	0.7011	1.2801
408	0.5453	0.7053	1.2815
409	0.5480	0.7095	1.2830
410	0.5507	0.7137	1.2844
411	0.5534	0.7180	1.2858
412	0.5561	0.7223	1.2873
413	0.5588	0.7265	1.2887
414	0.5615	0.7308	1.2902
415	0.5643	0.7352	1.2916
416	0.5670	0.7395	1.2930
417	0.5697	0.7438	1.2945
418	0.5725	0.7482	1.2959
419	0.5753	0.7526	1.2974
420	0.5780	0.7569	1.2988
421	0.5808	0.7614	1.3002
422	0.5836	0.7658	1.3017
423	0.5864	0.7702	1.3031
424	0.5892	0.7747	1.3045
425	0.5920	0.7791	1.3060
426	0.5948	0.7836	1.3074
427	0.5977	0.7881	1.3088
428	0.6005	0.7926	1.3102
429	0.6034	0.7972	1.3117
430	0.6062	0.8017	1.3131
431	0.6091	0.8063	1.3145
432	0.6120	0.8109	1.3159
433	0.6148	0.8155	1.3174
434	0.6177	0.8201	1.3188
435	0.6206	0.8247	1.3202
436	0.6235	0.8293	1.3216
437	0.6265	0.8340	1.3231
438	0.6294	0.8387	1.3245
439	0.6323	0.8433	1.3259
440	0.6353	0.8481	1.3273
441	0.6382	0.8528	1.3287
442	0.6412	0.8575	1.3301
443	0.6441	0.8623	1.3315
444	0.6471	0.8670	1.3330
445	0.6501	0.8718	1.3344
446	0.6531	0.8766	1.3358
447	0.6561	0.8814	1.3372
448	0.6591	0.8862	1.3386
449	0.6621	0.8911	1.3400
450	0.6651	0.8960	1.3414

Temperature	R12	R13	R23
451	0.6682	0.9008	1.3428
452	0.6712	0.9057	1.3442
453	0.6743	0.9106	1.3456
454	0.6773	0.9156	1.3470
455	0.6804	0.9205	1.3484
456	0.6835	0.9254	1.3498
457	0.6866	0.9304	1.3512
458	0.6897	0.9354	1.3526
459	0.6928	0.9404	1.3540
460	0.6959	0.9454	1.3554
461	0.6990	0.9505	1.3568
462	0.7021	0.9555	1.3582
463	0.7053	0.9606	1.3596
464	0.7084	0.9656	1.3610
465	0.7116	0.9707	1.3624
466	0.7147	0.9758	1.3638
467	0.7179	0.9810	1.3651
468	0.7211	0.9861	1.3665
469	0.7243	0.9913	1.3679
470	0.7275	0.9965	1.3693
471	0.7307	1.0016	1.3707
472	0.7339	1.0068	1.3721
473	0.7371	1.0121	1.3735
474	0.7403	1.0173	1.3748
475	0.7436	1.0226	1.3762
476	0.7468	1.0278	1.3776
477	0.7501	1.0331	1.3790
478	0.7533	1.0384	1.3804
479	0.7566	1.0437	1.3817
480	0.7599	1.0490	1.3831
481	0.7632	1.0544	1.3845
482	0.7665	1.0598	1.3859
483	0.7698	1.0651	1.3872
484	0.7731	1.0705	1.3886
485	0.7764	1.0759	1.3900
486	0.7798	1.0814	1.3913
487	0.7831	1.0868	1.3927
488	0.7864	1.0923	1.3941
489	0.7898	1.0977	1.3954
490	0.7932	1.1032	1.3968
491	0.7965	1.1087	1.3982
492	0.7999	1.1142	1.3995
493	0.8033	1.1198	1.4009
494	0.8067	1.1253	1.4023
495	0.8101	1.1309	1.4036
496	0.8135	1.1365	1.4050
497	0.8170	1.1421	1.4063
498	0.8204	1.1477	1.4077
499	0.8238	1.1533	1.4091
500	0.8273	1.1589	1.4104

VITA

Andrew Glen Jackson was born on November 29, 1954 in the back of a Studebaker in Billings, Montana. His parents were Victor Rex Jackson of Belfry, Montana and Naomi Wagstaff of Kamas, Utah. Andrew attended Bridger Public Elementary School from August, 1961 through May, 1969. He was graduated from Bridger High School in 1973 and enrolled at the Brigham Young University in Provo, Utah. He interrupted his studies to prepare and serve as a missionary for the Church of Jesus Christ of Latter-Day Saints in Stockholm, Sweden. Andrew married Linda Shanklin of Columbia, Tennessee on April 21, 1979 and received a Bachelor of Science degree in Mechanical Engineering from Brigham Young University in 1980. He accepted employment with ARO, Inc. (now Sverdrup Technology, Inc.) at the Arnold Engineering Development Center in January 1981. While employed with Sverdrup Technology he enrolled in graduate school at the University of Tennessee Space Institute, and received a Master of Science degree in Mechanical Engineering in December 1990. He is a member of the Tennesse Section of the American Institute of Astronautics and Aeronautics. Andrew and his wife Linda have four children, Shara, Joseph, Benjamin, and Spencer, and are currently living in Estill Springs, Tennessee.